2D INVERSIONS OF MAGNETO TELLURIC DATA FROM HIMALAYAN REGION

A DISSERTATION

Submitted in partial fulfillment of the requirements for the award of the degree of

MASTER OF TECHNOLOGY

in

GEOPHYSICAL TECHNOLOGY

By

MANOJ KUMAR ROUT

DEPARTMENT OF EARTH SCIENCES
INDIAN INSTITUTE OF TECHNOLOGY ROORKEE
ROORKEE - 247 667 (INDIA)

JUNE, 2012

CANDIDATE'S DECLARATION

I hereby declare that the work which is being presented in this dissertation entitled **"2D Inversion of Magnetotelluric data from Himalayan region"** in the partial fulfillment of the requirement for the award of **Master of Technology** in **Geophysical Technology** submitted in **Department of Earth Sciences, Indian Institute of TechnologyRoorkee,** carried out during a period of July 2011 to May 2012 under the supervision of **Dr. M.Israil**, Professor, Department of Earth Sciences, Indian Institute of TechnologyRoorkee.

The matter embodied in this dissertation has not been submitted by me for award of any other degree.

Date: 6.6. 2012

Manoj Kumar Rout

Place: IIT Roorkee **Manoj Kumar Rout**

This is certified that the above statements made by the candidate are correct to the best of my knowledge and belief.

6/6/12

Prof. M.Israil
Professor
Department of Earth Sciences
Indian Institute of Technology Roorkee
Uttarakhand, India

ACKNOWLEDGEMENT

I would like to express my profound gratitude to **Prof. Mohammad Israil**, Department of Earth Sciences, Indian Institute of Technology Roorkee, for his substantial guidance, his valuable suggestions and constant encouragement throughout my dissertation work. His constructive criticism and arguments are of immense help to me.

I also offer my sincere thanks to **Prof. A. K. Saraf**, Head, Department of Earth Sciences, Indian Institute of Technology Roorkee, for providing me all the necessary facilities and administrative support required for the completion of this work.

I also offer my sincere thanks to **Mr. Suresh Kannaujiya for their help in the MT lab during my dissertation work.**

Most importantly, I wish to express my deep sense of respect and gratitude towards my **Family and friends** for their affection, care, support, encouragement and blessings which I continuously receive from them.

Well I must say at last that it was all God's grace that I gained so much of valuable knowledge and experience with this work.

MANOJ KUMAR ROUT

ABSTRACT

2 Dimensional inversion has been applied to the processed existing data of the Himalayan region to study the conductivity distribution of the subsurface. The profile I have used extends from Deoband to Gangotri of 200km length. I have used 33 sites which are earlier processed by MT group at IIT Roorkee in this profile. The 2D inversion over these sites provides valuable information regarding various geological features of the Himalayan region such as HFT, MBT, and MCT. This information can be used for the purpose of the study of the earthquake in this region. In this work 2D inversion method has been applied over the same data for three different frequency ranges in order to study the conductivity distribution in various depths. The three different frequency ranges are 0.001 to 10s, 0.001 -100s and 0.001 -10000s.

Here the inversion has been performed using the WinGlink software and the misfit between measured data and data synthesised from the model is performed by the Tikhnov's regularisation method. The starting model is a three layer homogeneous models of thicknesses 1km, 1-6km and below 6km having resistivity values 100ohm-m, 200ohm-m and 500ohm-m respectively .In first level the tipper data was inverted over the starting model. After this in second level TE mode phase (i.e. no weightage is given to resistivity) only is inverted over the tipper model as TE mode resistivity is more distorted by inductive distortions. Then in level third TM mode resistivity and phase is inverted over the TE mode. But the conductivity structures obtained from TE mode and TM mode were not same. In order to finalise the inversions joint inversion has been applied to the inverted TM mode to obtain the accurate conductivity distribution of the subsurface.

The main difference between TE and TM modes is that TM modes charges the structure and its anomalies are superimposed by galvanic effect, but the TE mode does not charge the structure and its anomalies are superimposed by inductive effect. But at near surface due to high frequency, inductive distortion is more as TE mode produces inductive distortions so we cannot apply TE mode to detect the near surface conductive structure. Hence TM model is suitable for near surface study. For deep study due to low frequency, galvanic distortion is high and inductive distortion is low. So in this case TE mode is suitable. As we find TE and TM mode are complementary to each other we prefer joint inversion to obtain good information of conductivity distribution of the subsurface.

The second part of my work includes the inversions of 36 sites data from the same profile but processed by MT group at GERMC. The purpose of this is to find the difference between the processing tools of IITR and GEMRC by comparing the results of the inversions.

The Third part of work includes the averaging of the adjacent sites using four different methods. The four averaging methods are (i) Weighted average of resistivity and phase values taking spacing with respect to reference site as weight (ii) Weighted average of resistivity and phase values taking corresponding error as weight (iii) Median (iv) Simple average. After obtaining four averaged values, four sets of EDI files are created and inversion has been applied over each set of EDI files. The idea behind the averaging is to smooth the resistivity and phase values so that maximum data we can use in the inversion rather than masking noisy data. Although smoothing the resistivity and phase values restricts to give the accurate picture of the subsurface. But in this case the profile length is of 200km and the result obtained from the inversions shows accuracy of the model has not been affected by averaging methods. It is clear that smoothing does not affect the accuracy of the subsurface image in case of long profile length.

As the geoelectric strike direction varies from site to site, an average value of strike direction of $N60^0W$ has been taken for the rotation purpose and the comparison between the non-rotated and rotated model has been studied in the final part of the work.

LIST OF FIGURES

FIGURE NO.	PAGE NO.
Fig.1.1 The division of thrust belt over the Himalaya	14
Fig.2.1 Interaction of solar particles with earth's magnetic field creates high-energy EM energy, which travel around the earth via thunderstorms	18 24
Fig.2.2 Two dimensional resistivity models with a lateral contact striking in the X direction	
Fig.3.1 The site of the parallel test MT survey	29
Fig.3.2 ADU06 data logger	30
Fig.3.3 A MFS06 magnetic induction coil in the parallel testing survey	32
Fig.3.4 A EFP06 (Metronix) electrode	34
Fig.3.5 A sketch of MT survey set up	37
Fig.3.6 Two buried vertical magnetic sensors in parallel test site	37
Fig.3.7 Two buried electrodes in parallel test site	38
Fig.4.1 Elevation Map of Deoband to Gangotri profile	40
Fig.4.2 The polar diagram maps of 33 sites at central frequency 10HZ	41
Fig.4.3 The induction arrows maps of 33 sites at central frequency 10HZ	41
Fig.4.4 The miniature curves of 33 sites at central frequency 10HZ	41
Fig.4.5 Apparent resistivity, Phase & polar diagrams of station rkg2	42
Fig.4.6 Apparent resistivity, Phase & induction arrows of station rkg2	43
Fig.4.7 Apparent resistivity, Phase & strike of station rkg2	43
Fig.4.8 Pseudo Section of TE Mode of station data	44
Fig.4.9 Pseudo Section of Tm Mode of station data	44
Fig.4.10 Pseudo Section of Tipper Mode of station data	44
Fig.5.1 Flowchart showing steps involved in Lesat structured inversion	47
Fig.5.2 The map showing all the sites those have been taken for the inversion purpose	49
Fig.5.3 Flowchart for the 2D inversion model	50

Fig.5.4 Initial model: Three layer model of 1KM, 6KM, and below having resistivity 100 ohm-m, 200 ohm-m and 600 ohm-m 50

Fig.5.5 Shows plot of RMS Error VS XDistance 53

Fig.5.6 Shows plot of Elevation VS XDistance 53

Fig.5.7 Shows Tipper models in three different frequency ranges 54

Fig.5.8Shows TE mode models in three different frequency ranges 55

Fig.5.9 Shows TM mode models in three different frequency ranges 56

Fig.5.10Shows TE+TM Mode models in three different frequency ranges 57

Fig.5.11 Reference Model 58

Fig.5.12 Flowchart for the 2D inversion model of 36 sites MT data 60

Fig.5.13 Shows plot of RMS Error VS X distance of all modes of 36 sites data in the frequency range 0.01 -2048s 63 63

Fig.5.14 Showing plot of Elevation VS X distance of 36 sites data in the frequency range 0.01 -2048s 64

Fig.5.15 All modes(TE, TM, TE+TM) of 36 sites MT data in the frequency range of 0.01 -2048s 71

Fig.5.16 Shows the comparison plots of the data processed by IITR Group and GERMC Group 72

Fig.5.17 Showing the 13 grouped sites that have been taken for the averaging purpose and their reference sites 79

Fig.5.18 Plotting of 4 Sets of Grouped Averaged Data 84

Fig.5.19 All Modes (TE, TM, TE+TM) of weighted spacing averaged data

Fig.5.20 Fitting of Apparent resistivity and Phase of weighted spacing averaged data 87

Fig.5.21 All modes (TE, TM, TE+TM) of weighted error averaged data 88

Fig.5.22 Fitting of Apparent resistivity and Phase of weighted error averaged data 91

Fig.5.23 All modes (TE, TM, TE+TM) of Simple average data 92

Fig.5.24 Fitting of Apparent resistivity and Phase of simple average data 95

Fig.5.25 All modes (TE, TM, TE+TM) of Median average data 96

Fig.5.26 Fitting of Apparent resistivity and Phase of weighted 99
error averaged data

Fig.5.27 Showing the 17 grouped sites that have been taken for the 100
averaging purpose and their reference sites

Fig.5. 28 Plotting of Median data with original data 104

Fig.5.29 All rotated modes (TE, TM, TE+TM) of Median average 105
data of 35 sites data processes by GERMC Group

LIST OF TABLES

TABLE NO.	PAGE NO.
Table 3.1Shows station coordinates and elevation	28
Table 3.2Shows data acquisitions timing at seven stations	28
Table3.3Features of the data logger ADU06 of Metronix 31	
Table 3.4Features of the magnetic sensors MFS06 of Metronix	32
Table 3.5Features of the electric field sensor EFP06 of Metronix	34
Table 5.1 Showing 33 sites coordinates and their X –distance in the profile	52
Table 5.2 Showing information of inversion parameters that have been used for the running of the 2D inversions of 33 sites in 3 different frequency ranges	52 61
Table 5.3 Showing 36 sites coordinates and their X –distance in the profile	61
Table 5.4 Shows information of inversion parameters that have been used for the running of the 2D inversions of 36 sites processed earlier by GEMRC	72
Table 5.5 Showing the calculation of spacing of different sites with respect to reference site in each grouped site	73
Table 5.6Showing information of inversion parameters for the 2D inversion of weighted spacing data	83
Table 5.7 Showing information of inversion parameters for the 2D inversion of weighted error data	87
Table 5.8 Showing information of inversion parameters for the 2D inversion of Simple average data	91
Table 5.9Showing information of inversion parameters for the 2D inversion of Median data	95
Table 5.10 Showing information of inversion parameters for the 2D inversion of Median data(Processed by GERMC Group)	104

CONTENTS

PAGE NO.

CANDIDATE'S DECLAIRATION 1

ACKNOWLEDGEMENT 2

ABSTRACT 3

LIST OF FIGURES 5

LIST OF TABLES 8

CHAPTER 1 INTRODUCTION 13

1.1 Objective of the study
1.2 Geology of the study area
1.3 Formation of Himalaya
1.4 Major Tectonic Division of Himalayas

CHAPTER 2 BASIC THEORY OF MT 16

2.1 Energy Source of MT

2.2 Assumption of the MT Method

2.3 Physics of the Electromagnetic Field Propagation into the Earth

2.4 Magneto telluric Response functions

2.5 Dimensionality of the data with sounding period

2.6 Concept of E and B Polarisation

2.7 Resolution of MT

2.8 Application of MT

CHAPTER 3 DATA ACQUISITION 27

3.1 General MT survey by using Metronix System

3.1.1 Site location

3.2 Field items used in MT survey

3.2.1 Data logger

3.2.1.1 Properties of data logger

3.2.2 Magnetic Sensors

3.2.2.1 Properties of MFS06 magnetic sensor

3.2.3 Electrodes

3.2.3.1 Properties of EFP06 Electrodes

3.3 Noise sources to MT survey

3.4 Installation of an MT station

CHAPTER 4 OVERVIEW OF WINGLINK SOFTWARE 40

4.1 Maps

4.2 Soundings

4.3 Pseudo Section

CHAPTER 5 INVERSIONS OF MT DATA 45

5.1 Overview

5.2 Least structure philosophy with 2D inversion

5.3 Inversion routines used by WinGlink

5.3.1A smooth model inversion routine

5.3.2 A sharp boundary model inversion routine

5.4Inversions of existing 33 sites data processed by IIT Roorkee Group

5.4.1 Models Descriptions

5.4.2Comparision of TIPPER models in three different frequency ranges

5.4.3Comparision of TE models in three different frequency ranges

5.4.4Comparision of TM models in three different frequency ranges

5.4.5Comparison of TE+TM modes in three different frequency ranges

5.4.6Results

5.5Inversions of existing data processed by GERMC

5.5.1 Comparison of all modes obtained from the inversions of existing processed data By GERMC group with the reference model

5.5.2Results

5.6Difference between the processed data of IITR group and GERM group

5.7Averaging of the 33 Sites data (Processed by IIT Roorkee group) using different Methods

5.7.1Procedures for weighted spacing average

5.7.2Procedures for weighted error average

5.7.3Procedures for median

5.7.4Procedures for simple average

5.7.5Plotting of 4 Sets of grouped Averaged Data

5.8Creation of EDI Files and Inversions of 4 Sets of Averaged Data

5.92D Inversion of weighted spacing average data

5.9.1Comparison of all modes of weighted spacing averaged data with reference model

5.9.2Fitting of apparent resistivity and phase

5.9.3Results

5.102D Inversion of weighted error data

5.10.1 Comparison of all modes of weighted error averaged data with reference model
5.10.2Fitting of apparent resistivity and phase

5.10.3 Results

5.112D Inversion of Simple Average data

5.11.1 Comparison of all modes of Simple averaged data with reference model

5.11.2 Fitting of apparent resistivity and phase

5.11.3 Results

5.122D Inversion of Median data

5.12.1 Comparison of all modes of Median data with reference model

5.12.2 Fitting of apparent resistivity and phase

5.12.3 Results

5.13Averaging of 35 sites data (Procssed by GERMC Group).

5.13.1 Plotting of Median data with original data

5.13.2 2D INVERSION OF 35 Sites Median Averaged Data

5.13.3 Comparison of all modes of median data with reference model

5.13.4Results

CHAPTER 6 CONCLUSION 107

REFERENCES 108

APPENDIX-A 110

A.1 Descriptions of inversion parameters in WinGlink software

A.1.1 Main inversion Parameters

A.1.2 Data Select

A.1.3 Smooth inversion parameters

A.1.4 Error floor

A.1.5 Static shift

A.1.6 Data errors

A.1.7 Fixed Parameters

CHAPTER 1.INTRODUCTION

Generally MT surveys are carried out along a single profile so two dimensional (2D) MT inversion plays an important role as a primary interpretation tool in real application. MT 2D modelling and inversion algorithms are very powerful and widely available. In this study WinGlink software has been used for 2D inversion. As there is a significant linking factor between electrical models and underlying structural tectonic patterns so it is necessary to study the electrical anisotropy in the earth's crust and upper mantle. In this work the study of electrical anisotropy of Himalayan region has been done by using 2D MT inversion. Here a smooth model two dimensional inversion routine has been used. This routine finds regularized solutions (Tikhonov Regularization) to the two dimensional inverse problem for magnetotelluric data using the method of nonlinear conjugate gradients. The forward model simulations are computed using finite difference equations generated by network analogs to Maxwell's equations. The program inverts for a user defined 2D mesh of resistivity blocks, extending laterally and downwards beyond the central detailed zone and incorporating topography.

1.1 Objective of the study

The sole aim of the present work is to obtain the information of the structural tectonic patterns of the Himalayan region up to crustal depth by analysing the lateral and vertical conductivity distribution from two dimensional models.

1.2 Geology of the study area

The electric anisotropy behaviour has been studied in this work along the Deoband – Gangotri profile of 200km length. The structural tectonics patterns and geology along the profile has been given below.

1.2.1 Formation of Himalaya

The formation of the Himalya and Tibetan platue had taken place due to the collision between the Indian subcontinent and Euresian continent. The Himalayas extends over 2400km between the Namche Barwa syntaxis in Tibet and the Nanga Parbat syntaxis in

CHAPTER 2. BASIC THEORY OF MAGNETOTELLURIC METHOD

Magnetotelluric is a passive electromagnetic geophysical method which measures naturally occurring electric and magnetic fields at the surface of the earth. From these measurements the resistivity of the subsurface can be estimated from few tens of meters to several hundreds of Km depth. It utilises a broad spectrum of naturally occurring geomagnetic variations as a power source for electromagnetic induction in earth. In the 1950, Tikhonov (1950) and Cagniard(1953) realised that if electric and magnetic field variations are measured simultaneously then compelx ratio (impedances) can be derived that describes the penetration of electromagnetic fields into the earth. The penetration depths of electromagnetic fields within the earth depend on the electromagnetic period and earth's conductivity structure. This principle is embodied in the electromagnetic skin depth relation, which describes the exponential decay of electromagnetic fields as they diffuse into a medium:

$$S(T) = (2/\omega\sigma\mu)^{1/2} \qquad 2.1$$

Where S (T) is the electromagnetic skin depth in metres at a given period, T, σ is the average conductivity of the medium penetrated, and μ is magnetic permeability. At a depth, S (T), electromagnetic fields are attenuated to 1/e of their amplitudes at the surface of the Earth. This exponential decay of electromagnetic fields with increasing depth renders them insensitive to conductivity structures lying deeper than S (T). Hence, in MT studies, one electromagnetic skin depth is generally equated with the penetration depth of electromagnetic fields into the Earth. In studies of the Earth, μ is usually assigned the free-space value ($\mu_0 = 4\pi 10^{-7}$W.A/m), and

Equation (2.1) can be approximated as

$$S(T) \approx 503\,(\rho_a T)^{1/2} \qquad 2.2$$

Where ρa is apparent resistivity, or the average resistivity of an uniform half-space. From Equations (2.1) and (2.2), we can deduce that for a given sounding period, the depth achieved by passive EM sounding will be dictated by the average conductivity of the overlying sample of earth that is penetrated. Electromagnetic fields that are naturally induced in the Earth and are exploitable for MT studies have wave periods ranging from 10^{-3} to 10^{5}s. Therefore, if we

Pakistan. The immense mountain range was formed by tectonic forces and sculpted by weathering and erosion.

1.4 Major tectonic division of Himalayas

One of the most striking aspects of the Himalayan orogeny is the lateral continuity of its major tectonic elements. The Himalaya is classically divided into four tectonic units that can be followed for more than 2400 km along the belt.

The Sub Himalaya forms the foothills of the Himalayan Range and is essentially composed of Miocene to Pleistocene molasses sediments derived from the erosion of the Himalaya. These molasses deposits, known as the Muree and Siwaliks Formations, are internally folded and imbricated. The Sub Himalaya is thrust along the Main Frontal Thrust (MFT) over the Quaternary alluvium deposited by the rivers coming from the Himalaya (Ganges, Indus, Brahmaputra and others), which demonstrates that the Himalaya is still a very active orogeny.

The Lesser Himalaya (LH) is mainly formed by Upper Proterozoic to lower Cambrian detrital sediments from the passive Indian margin intercalated with some granites and acid volcanic (1840 ±70 Ma. These sediments are thrust over the Sub Himalaya along the Main Boundary Thrust (MBT). The Lesser Himalaya often appears in tectonic windows (Kishtwar or Larji-Kulu-Rampur windows) within the High Himalaya Crystalline Sequence.

The Central Himalayan Domain, (CHD) or High Himalaya, forms the backbone of the Himalayan orogeny and encompasses the areas with the highest topographic relief. The Main Central Thrust (MCT) lies in this domain.

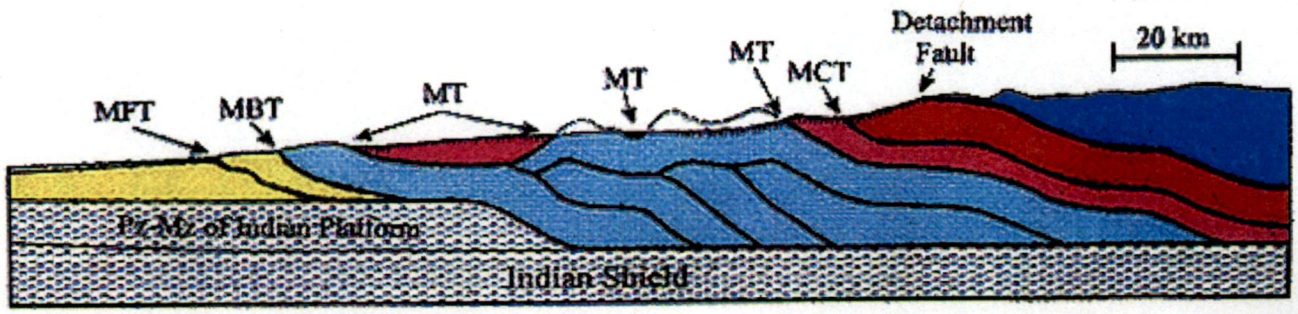

Fig.1.1 Showing the division of thrust belt over the Himalaya
Source: (http://oak.ucc.nau.edu/wittke/Tibet/Himalaya.html)

From north to south, these rock packages and fault zones are the Tibetan Sedimentary Sequence (blue), South Tibetan Detachment Zone (Detachment Fault), Greater Himalayan

Sequence (red and pink), Main Central Thrust (MCT) and Maha Bharat Thrust (MT), Lesser Himalayan Sequence (light blue), Main Boundary Thrust (MBT) and Main Frontal Thrust (MFT), and Gangetic Basin of the Indian subcontinent (yellow).

assume an average resistivity of the Earth's crust and upper mantle of 100m, we can see how penetration depths in the range of 160 m to >500 km might be possible. The broad span of depths that can be imaged using the MT technique is one advantage of the method compared with active EM methods for which the maximum depth that can be probed is always limited by the size of the available source, and realisable source–receiver configurations.

2.1 Energy source of MT

The Earth's time varying magnetic field is generated by two different sources, which strongly differ in amplitude and their time dependent behaviour. The primary source is the magneto hydrodynamic processes in the Earth's outer core. But the MT sounding seeks to exploit the superimposed, more transient and lower amplitude fluctuations of external origin as they induce eddy currents and secondary magnetic fields in the earth due to their transient behaviour. The external source of MT signal is caused by two things.

(i) The interaction of the solar wind (Parker, 1958)with the Earth's magnetic field produces signals of lower frequencies (generally less than 1 Hertz or 1 cycle per second). As solar storms emit streams of ions, this energy disturbs the earth's magnetic field and causes low-frequency energy to penetrate the earth's surface. Briefly, the solar wind is a continual stream of plasma, radiating mainly proton and electrons from the Sun. When these plasma encounter the terrestrial magnetic field (at the magnetopause), these protons and electrons get deflected in opposite directions and establish an electric field. Variations in density, velocity and magnetic field intensity of the solar wind produce rapidly varying distortions of the Earth's magnetosphere. For example increases in solar wind cause rapid compression of the magnetosphere, and therefore compaction of magnetic field lines, affecting an increase in the horizontal geomagnetic field. Oscillations of the magnetosphere generate small, almost sinusoidal variations of the geomagnetic field, called geomagnetic pulsations. Inductive and magneto hydrodynamic interactions between the magnetosphere and ions complexly modify these fluctuating fields before they reach the Earth's surface (Bahr and Simpson,2005)

(ii) The meteorological activity such as worldwide Lightening discharges generates higher frequency signals usually near the equator. The energy created by these electrical storms travels around the earth (in a wave guide between the earth's surface and the ionosphere), with some of the energy penetrating into the earth.

The signals discharged by lightening are known as 'sferics' and encompass a broad range of electromagnetic frequencies. Local lightening discharges may saturate amplifiers, and it is not these, but rather the sferics from the highly disturbed equatorial regions, which propagate around the world within the waveguide bounded by the ionosphere and Earth's surface that are of most significance. Sferics propagate within the waveguide as transverse electric (TE), and transverse magnetic (TM) or transverse electric and magnetic (TEM) waves, and are enhanced or attenuated depending on frequency(Dobbs, 1985). During the day, the waveguide is 60 km wide, increasing to 90 km at night time. Sferics peaks in the early afternoon. However, statistically a part of the world may witness thunderstorm activity at any given universal time.

Between 0.5 -5 Hz lies the dead band at which the natural EM fluctuations have a low intensity. MT measurement in this frequency range usually suffers from the poor data quality.

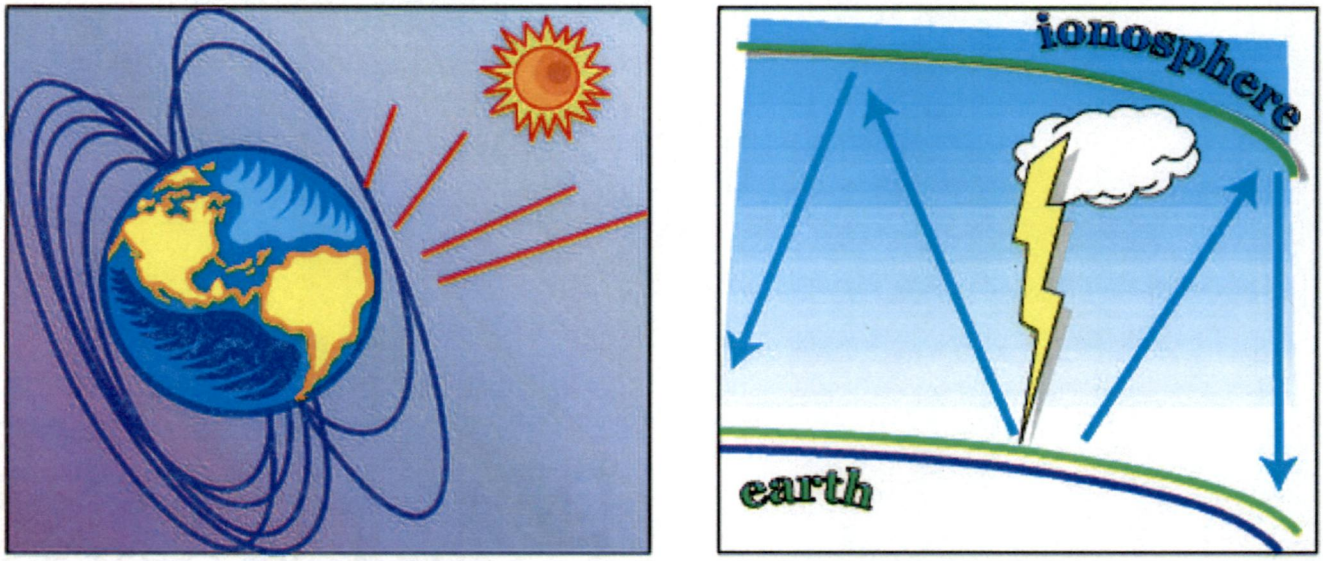

Fig.2.1 Interaction of solar particles with earth's magnetic field creates high-energy EM energy, which travel around the earth via thunderstorms.

Source:(http://www.searchanddiscovery.com/documents/geophysical/christopherson/images/fig01.htm)

2.2 Assumption of the MT method

A number of assumptions are considered for the purpose of electromagnetic induction into the Earth (Cagniard, 1953; Keller and Frischknecht, 1966).

(i) Maxwell's electromagnetic equations are obeyed.

(ii) The source of electromagnetic energy is of external origin. The Earth does not produce electromagnetic energy but only dissipates or absorbs it.

(iii) All fields are assumed conservative in nature.

(iv) It is assumed that the telluric currents systems are relatively far away from the Earth's surface may be treated as uniform, plane polarised electromagnetic waves impinging on the Earth at near vertical incidence. This assumption may be violated in polar and equatorial regions.

(v) As in MT surveys Earth is considered as two dimensional so it is assumed as no accumulation of free charges occur within a layered Earth. But in practical Earth is a multi-dimensional Earth, charges can accumulate at discontinuities which produce a galvanic phenomenon known as static shift.

(vi) Charge is conserved so the Ohm's equation is applied.

$$J = \sigma E \tag{2.3}$$

Where J is the current density, σ is the conductivity and E is the electric field

(vii) Time varying displacement currents are negligible compared to time varying conduction currents which indicates the electromagnetic induction in Earth is purely diffusion process.

(viii) Electrical permittivity and magnetic permeability of the rocks varies in a negligible manner as compared to variation in bulk rock conductivities.

2.3 Physics of the electromagnetic field propagation into the earth

The physics of electromagnetic field propagation into the Earth can be explained by a set of four relations known as Maxwell's equations, which for a polarisable and magnetisable medium containing no electric and magnetic sources can be expressed as:

$$\nabla . B = 0 \tag{2.4}$$

$$\nabla . D = \rho \tag{2.5}$$

$$\nabla \times E = -\partial B/\partial t \tag{2.6}$$

$$\nabla \times H = J + \partial D/\partial t \tag{2.7}$$

The equation (2.4) describes the gauss law of magnetism which states that the magnetic field is always source free (i.e. no magnetic monopole exists). The equation (2.5) represents gauss law of electricity which states that the electric displacement field is solely due to electric charge density. The equation (2.6) explains Faraday's law of electromagnetic induction which states that time varying magnetic field induces electric field in a closed loop. The equation (2.7) is a mathematical representation of Ampere's law which states that the current flowing in a closed loop produces magnetic field perpendicular to the plane of the loop and the magnitude of magnetic field is proportional to the current flow in the loop(Bahr and Simpson,2005).

According to assumption of MT method time varying displacement currents are negligible compared to the time varying conduction current so the equation (2.6) is reduced to

$$\nabla \times B = J \tag{2.8}$$

For a linear and isotropic medium the material equations can be introduced:

$$B = \mu H \tag{2.9}$$

$$D = \varepsilon E \tag{2.10}$$

According to MT assumption the variations in electric permittivity and magnetic permeability are very less compared to variations in rock bulk conductivities so free space values ($\mu_0 = 1.2566 \times 10^{-6} H/m$and $\varepsilon_0 = 8.85 \times 10^{-12} F/m$) are considered in MT studies.
Applying equation (2.3), (2.9) and (2.10) to the Maxwell's equations, we can have

$$\nabla . H = 0 \tag{2.11}$$

$$\nabla.E= \rho/\varepsilon \tag{2.12}$$

$$\nabla \times E = -\mu \partial H/\partial t \tag{2.13}$$

$$\nabla \times B = \mu \sigma E \tag{2.14}$$

Assuming that no current sources exist within the Earth, we have

$$\nabla . j = \nabla . \sigma E = 0 \tag{2.15}$$

For the case of homogeneous half space (i.e. $\nabla \sigma = 0$)

$$\nabla . \sigma E = \sigma \nabla . E + E . \nabla \sigma = \sigma \nabla . E \tag{2.16}$$

The steps from $\nabla . j = 0$ to $\nabla . E = 0$ are correct for layered earth giving rise only to horizontal electric field.

Let us consider a conductivity distribution that varies in the vertical direction and one in horizontal direction, in this case the divergence of electric field parallel to the conductivity boundary is zero.

Here $d\sigma/dx = 0$ and $d\sigma/dy \neq 0$ and $E = (E_x\ 0\ 0)$

When the electric field is perpendicular to the direction of boundary, we have

$\nabla . E \neq 0$ and $E = (0\ E_y\ 0)$

Using equations (2.6) and (2.7), we can derive a diffusion equation in terms of the time varying electric field from which information about the conductivity structure of the Earth can be obtained.

Let us applying curl operation on the both sides of equation (2.6), we have

$$\nabla \times (\nabla \times E) = \nabla(\nabla . E) - (\nabla . \nabla)E = -\nabla \times \partial B/\partial t \qquad 2.17$$

The above equation can be simplified by assuming $\nabla . E = 0$ for no current source medium as:

$$-\nabla^2 E = -\partial/\partial t(\nabla \times B) = -\mu_0 \sigma\ \partial E/\partial t \qquad 2.18$$

The above equation can be simplified as

$$\nabla^2 E = \mu_0 \sigma\, \partial E/\partial t \qquad 2.19$$

The above equation is in the form of diffusion equation. Let us consider a plane wave with a surface amplitude E_0 and varies harmonically with time in the form of $e^{-i\omega t}$. So the equation (2.19) can be written to

$$\nabla^2 E = i\omega\mu_0\sigma E \qquad 2.20$$

Similarly applying curl operator on equation (2.7), we can obtain diffusion equation as:

$$\nabla^2 B = \mu_0 \sigma\, \partial B/\partial t \qquad 2.21$$

Or

$$\nabla^2 B = i\omega\mu_0\sigma B \qquad 2.22$$

As air is of highly resistive so the electromagnetic field does not attenuate by the air layer between the ionosphere and Earth's surface.

From equation (2.19) and (2.21) it is clear that MT depends on a source of energy which undergoes diffusion though the Earth and dissipates exponentially.

2.4 Magneto telluric response functions

The basic response functions in magneto telluric are impedance tensors, tipper vectors and magnetic tensors.

Impedance tensor is defined from the relationships between the horizontal components of electric and magnetic fields at an observation site (Berdichevsky and Dmitriev, 2008):

$$[Z] = \begin{bmatrix} Zxx & Zxy \\ Zyx & Zyy \end{bmatrix} \quad 2.23$$

$$E_X = Z_{XX}H_X + Z_{XY}H_Y \quad 2.24$$

$$E_Y = Z_{YX}H_X + Z_{YY}H_Y \quad 2.25$$

The apparent resistivity can be calculated using impedance tensors Z_{XY} and Z_{YX} are

$$\rho_{XY} = |Z_{XY}|^2/\omega\mu_0 \quad 2.26$$

And

$$\rho_{yx} = |Z_{yx}|^2/\omega\mu_0 \quad 2.27$$

Tipper vectors are defined from the relations between the vertical component of the magnetic field and its horizontal components at an observation site.

$$W = W_{ZX}H_X + W_{ZY}H_Y \quad 2.28$$

The magnetic tensors are defined from relations between the horizontal components of magnetic fields at an observation site (o) and at a base (reference) site (B) (Berdichevsky and Zhdanov, 1984):

$$[M] = \begin{bmatrix} Mxx & Mxy \\ Myx & Myy \end{bmatrix} \quad 2.29$$

$$H_X(0) = M_{XX}H_X(B) + M_{XY}H_Y(B) \quad 2.30$$

$$H_Y(0) = M_{YX}H_X(B) + M_{YY}H_Y(B) \quad 2.31$$

As Z is a tensor it provides information about dimensionality and directions. For one dimensional Earth, conductivity varies in one direction. In this case the diagonal elements of

the impedance tensor, Z_{XX} and Z_{YY} are zero whereas the off-diagonal elements Z_{XY} and Z_{YX} are equal in magnitude and opposite in sign.

$$Z_{XX} = Z_{YY} = 0 \quad 2.32$$

$$Z_{XY} = -Z_{YX} \quad 2.33$$

For 2D Earth, conductivity varies along one horizontal direction as well as with depth. In this case Z_{XX} and Z_{YY} are equal in magnitude but have opposite sign whereas Z_{XY} and Z_{YX} differ.

$$Z_{XX} = -Z_{YY} \quad 2.34$$

$$Z_{XY} \neq Z_{YX} \quad 2.35$$

But for a 2D Earth with the X and Y directions are along electromagnetic strike for which Z_{XX} and $Z_{YY}$are again zero. Mathematically it is clear that 2D Earth is equivalent to 1D anisotropic Earth. But practically measured data shows$Z_{XX} \neq Z_{YY} \neq 0$, it is due to distortion effect.

2.5 Dimensionality of the data with sounding period

Let us consider a homogeneous three dimensional conductivity body lies inside the observation site. For high frequency sounding, transfer functions should appear 1D because skin depth is very small compared to the smallest dimensions of the conductivity anomaly. When sounding period increases skin depth increases and one of the edges of the anomaly can be resolved and we get transfer functions of 2D. Further increasing sounding period, we can resolve many of the edges of the conductivity anomaly and transfer functions appear in the form of 3D. In case of very long sounding period, skin depth will be very large compared to dimension of the conductivity anomaly and galvanic distortions become predominant over inductive distortions so it will be difficult to resolve the anomalous body. In order to resolve the body we need to strip away the galvanic distortions by various decomposition methods.

2.6 Concept of E and B polarisation

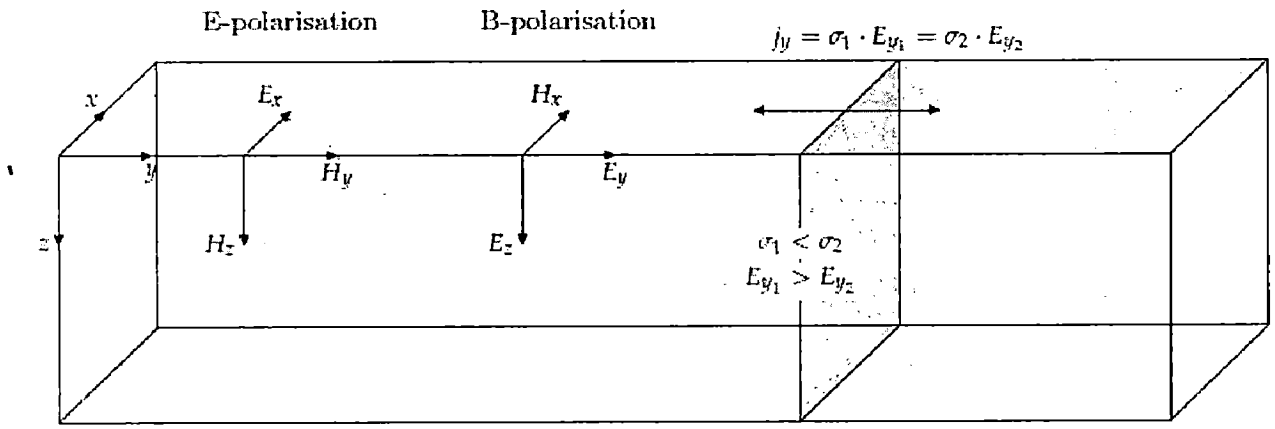

Fig.2.2 Two dimensional resistivity model with a lateral contact striking in the X direction

Source:(http://digital.library.adelaide.edu.au/dspace/bitstream/2440/48492/6/02chapters1-3.pdf)

The resistivity boundary separates two regions of different conductivities σ_1 and σ_2 . The E field is discontinuous across the vertical contact because of current preservation. The E polarisation and the B polarisation modes arise out of the two-dimensionality

The physical concept at the discontinuity is the conservation of current which follows the Ohmic equation:

$$j = \sigma E$$

The vertical contact separates the region into two parts of conductivities σ_1 and σ_2 .
From the law of conservation of current at the discontinuity, we have

$$\sigma_1 E_1 = \sigma_2 E_2 \qquad 2.36$$

The above equation indicates that electric field is not continuous across the boundary. But all other components of electromagnetic fields are continuous. The 2D assumption requires that the strike length is significantly longer than skin depth and the variations of all fields along the strike is zero.

As electric and magnetic fields are mutually orthogonal to each other, it creates two situations. In first case if electric field along the strike direction, it induces magnetic fields which are perpendicular to strike and in a vertical plane. This case is known as E polarisation. Hence E polarisation describes current flowing parallel to strike in terms of electromagnetic

field components E_X, $B_Y$and B_Z. The E polarisation can be described through following equations:

$$\partial E_X/\partial y = \partial B_Z/\partial t = i\omega B_Z \quad 2.37$$

$$\partial E_X/\partial z = \partial B_y/\partial t = -i\omega B_Y \quad 2.38$$

$$\partial B_Z/\partial y - \partial B_Y/\partial z = \mu\sigma E_X \quad 2.39$$

In second case if magnetic field is along strike direction, it induces electric fields which are perpendicular to strike and in a vertical plane. This case is known as B polarisation. Hence B polarisation describes current flowing perpendicular to strike in terms of electromagnetic field components B_X, $E_Y$and E_Z. The B polarisation can be described through following equations:

$$\partial B_X/\partial y = \mu\sigma E_Z \quad 2.40$$

$$\partial B_X/\partial z = \partial - \mu\sigma E_Y \quad 2.41$$

$$\partial E_Z/\partial y - \partial E_Y/\partial z = i\omega B_X \quad 2.42$$

It is clear that B polarisation produces discontinuity in electric field at the vertical contact. Discontinuity in electric field indicates the discontinuity in impedance tensor Z_{YX}. The magnitude of the discontinuity in $Z_{YX}$is σ_2/σ_1. As apparent resistivity varies proportional to the square of the impedance so the magnitude in discontinuity in apparent resistivity is of $\left(\sigma_2/\sigma_1\right)^2$(Bahr and Simpson,2005). Hence B polarisation can be used to study lateral resistivity gradient.

As we know E polarisation has an associated vertical magnetic field. But vertical magnetic fields are generated by lateral conductivity gradients so the spatial ratio H_Z/H_Y can be used for the study of lateral resistivity contrast in E polarisation. But B polarisation is a better tool to resolve lateral resistivity gradient than E polarisation.

Generally in magneto telluric data acquisition, the coordinates of the measurement of the electromagnetic fields rarely match with the strike of the 2D structure. So the impedance tensor obtained contains nonzero diagonal elements. So we need to rotate the coordinate axis at an angle so that the coordinate frames become parallel and perpendicular to the strike of the resistivity boundary.

$$Z' = \begin{bmatrix} Z'_{XX} & Z'_{XY} \\ Z'_{YX} & Z'_{YY} \end{bmatrix} = R \begin{bmatrix} 0 & Z_{XY} \\ Z_{YX} & 0 \end{bmatrix} R^T$$

With

$$R = \begin{bmatrix} cos\alpha & sin\alpha \\ -sin\alpha & cos\alpha \end{bmatrix}$$

R is known as rotational matrix.

2.7 Resolution of MT

Horizontal resolution of MT depends on the distance between sounding locations. The closer the sounding locations better the horizontal resolution.

Vertical resolution depends on the frequency being measured. As lower frequencies have greater depth of penetration, vertical resolution decreases with increase in depth of investigation.

2.8 Application of MT

MT method is used in hydrocarbon exploration as a complement to the primary technique of reflection seismology exploration. While seismic imaging is able to image the subsurface structure, it cannot detect the changes in resistivity associated with hydrocarbons and hydrocarbon bearing formations. MT detects resistivity variations in subsurface structures, which can differentiate between structures bearing hydrocarbons and those that do not.

In mining exploration, MT is used for various base metals mapping. MT technique is also used for groundwater exploration and mapping, hydrocarbon reservoir monitoring, deep investigations of the electrical properties of the bed rock for high voltage direct current transmission systems, carbon dioxide sequestration and nuclear waste disposal site monitoring (Sourcehttp://en.wikipedia.org/wiki/Magnetotellurics).

CHAPTER 3.DATA ACQUISITION

Magneto telluric data acquisition was carried out in seven sites along Deoband to Gangotri profile from October 10^{th} to 24^{th} of 2011 by using Phoneix systems and in one site by using Metronix system under the supervision of Prof. MohhamadIsrail.

Field set up and geometry for both the system is same but the softwares used for processing of data files in two systems are different.Metronix system uses ADU06 data logger . data stored on the 512 MB flash disk, is transferred through the network to the hard disk of the connected control computer. The ADU (Analog Digital Unit) is controlled either by the control software GMS06 (used for offline recording mode) or by the MAPROS software (used for online recording mode and data processing). The Steps used in Metronixbefore the data recording have been given below.

Check LED indication, that everything is OK is not.

Then connect PC to the ADU06 through network cable and make setting in LAN so PC connects to ADU06.

Open GMS06 and edit survey information.

Go to configuration menu, and set channel type, sensor, sensor serial no., channel position and angle for each sensor (Ex, Ey, Hx, Hy and Hz).

After setting the configuration, next edit the recording for HF, LF1, FREE, LF2/LF3.

Then set the starting time and end time of acquisition, date etc.

After completion of setting start data recording.

The seven sites (Phoneix) details has been summarized in the following tables.

S. No.	Station Name and corresponding TBL file	Site Code	Latitude	Longitude	Elevation (m)
1	points-2 (1853A14A)	P2	30:10.423 N	78:05.390 E	448
2	base-3 (1852A17A)	B3	30:11.323 N	77:50.176 E	389
3	base-3 (1852A18B)	B3	30:11.324 N	77:50.179 E	390
4	points-3 (1855A18A)	P3	30:13.424 N	78:12.253 E	664
5	points-4 (1853A19A)	P4	30:19.791 N	78:21.483 E	1072
6	point-5 (1909A21A)	P5	30:26.946 N	78: 25.594 E	819
7	Point-1r (1855A22A)	Pr1	29:49.011 N	77:49.837 E	240

Table 3.1 Shows station coordinates and elevation

S. No.	Site Code	Starting		Ending	
		Date (dd/mm/yyyy)	Time (hh/mn/ss)	Date (dd/mm/yyyy)	Time (hh/mn/ss)
1	P2	14/10/2011	13:01:02	18/10/2011	08:09:25
2	B3	17/10/2011	05/54/02	18/10/2011	04:59:55
3	B3	18/10/2011	06:07:02	24/10/2011	09:00:28
4	P3	18/10/2011	12:36:02	22/10/2011	02:47:52
5	P4	19/10/2011	13:08:02	23/10/2011	08:08:45
6	P5	21/10/2011	03:54:02	24/10/2011	08:47:31
7	Pr1	22/10/2011	11:28:02	23/10/2011	15: 19:23

Table 3.2 Shows data acquisitions timing at seven stations

3.1 General MT survey by using Metronix system

Here I am describing general MT survey by using Metronix instruments.

3.1.1 Site location

Latitude: 29.51.7.63N

Longitude: 77.47.52.3E

Fig.3.1 The site of the parallel test MT survey

3.2 Field items used in MT survey

1. data logger
2. 3 magnetic sensors
3. 4 electrodes
4. 4 telluric cables
5. 3 magnetic sensor cables
6. One metal stake to earth
7. Two global positioning system
8. 2 batteries
9. Computer
10. Compass
11. Spirit level
12. Digging tools
13. Measuring tapes

14. Digital millimetre

3.2.1 Data logger

A magnetotelluric equipment measures horizontal electric field and all magnetic field components. The sensors are realized by electrodes and induction coils. The heart of measuring equipment is data logger for signal recording. The data logger used in the parallel testing was ADU06 (Metronix). It provides a long time stability concerning time accuracy and outdoor influences like variable temperature, moisture etc. it also provides an exact synchronous recording of five input channels for all field components.

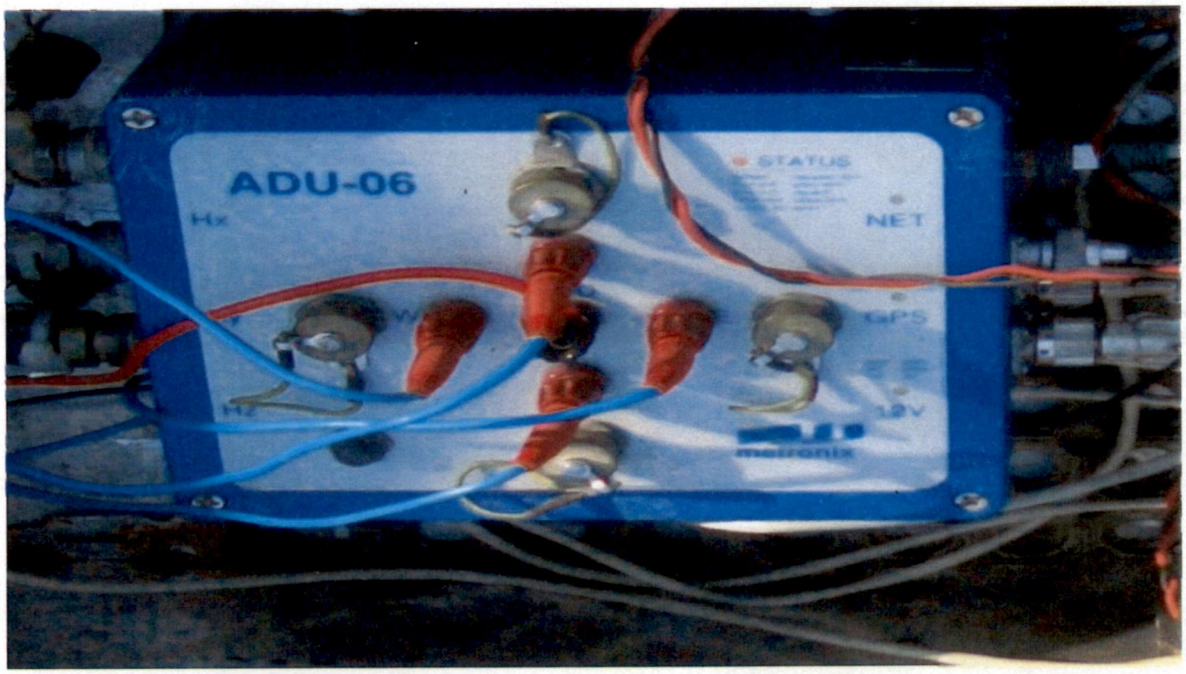

Fig.3.2ADU06 data logger

3.2.1.1 Properties of data logger

It contains five A/D boards for recording the signals of two pairs of electrodes and three magnetometers in a frequency range from DC up to 1 kHz. A 24 Bit sampling resolution allows a wide dynamic signal range. This is necessary in areas with high artificial noise, where records are over modulated easily.

A GPS board realizes an exact time base. This is especially important for measurements in a remote reference setup, when synchronous data is processed. The configuration board is based on a 386 CPU for low power Consumption of only 7W to 12W depending on the

measuring configuration. A network board realizes controlling and downloading of data via laptop. The features are summed up in Table 3.3 as an excerpt of the datasheet

Frequency range	DC to 20 kHz
A/D conversion	24 Bit
System computer	386 based
Storage media	Flash disk 100MB
Network	Standard coaxial
synchronization	GPS clock ±130 ns to satellite reference
Power consumption	7W -12W
Operating temperature range	-40^0C to $+70^0$C

Table 3.3Features of the data logger ADU06 of Metronix

Source: (http://88.198.212.158/mtxweb/uploads/media/flyerADU-06_v1.pdf)

3.2.2 Magnetic sensors

Two principal types of magnetic sensors are used in MT studies: induction coils and fluxgate magnetometers. Induction coils usually consist of a coil of copper wire wound onto a high-permeability core, sealed within a shock-resistant casing. A set of three induction coils plus a spirit level and a compass for aligning their axes are required in order to measure all three components of the time varying magnetic field. The output voltage of an induction coil is directly proportional to the number of loops in the coil and their cross-sectional area(Tipler,1991). Therefore, the design of coils suitable for MT fieldwork is essentially a compromise between transportability (i.e., weight and length), and sensitivity. Because the response of an induction coil is governed by the rate of change of magnetic flux within the coil, which is directly proportional to dB/dt, the sensitivity of induction coils is highest for the case of rapidly varying (i.e., short-period) fields. Fluxgate magnetometers generally consist of three ring-core sensors (elements composed of two cores of easily saturable, high-permeability material, oppositely wound with coaxial excitation coils) mounted onto a plate such that their axes are mutually orthogonal, and enclosed in a waterproof capsule that can be buried in the Earth. The construction usually includes a spirit level for ensuring that the plate is planted horizontally in the ground and a screw mechanism that allows fine tuning of the orientation. Fluxgate magnetometers rely on the principle of hysteresis, (which occurs when the core of the sensor is driven to saturation by an alternating current in the surrounding coil). Hysteresis cycles generate an output that is sensitive to the intensity of the time-varying exciting magnetic field. Therefore fluxgate magnetometers are suitable for measuring long-period magnetic field variations, which have high amplitudes for periods shorter than a threshold period; the amplitude of the natural signal becomes weaker than the noise of the

sensor. The choice of equipment used in a particular survey should depend on the depth range under consideration: in crustal studies, induction coil magnetometers are used frequently, the sampling is quick and the 'processing' is usually performed in the field. Fluxgate magnetometers provide a response at longer periods than induction coils, and are used if larger penetration depths are under consideration. In many cases, data from very short to very long periods are desirable, and two different sensors are combined at each site(Bahr and Simpson,2005). In this MT survey three MFS06 type magnetic sensors has been used to measure both horizontal and vertical components of magnetic fields.

3.2.2.1 Properties of MFS06 magnetic sensor

It covers a wide frequency range from 0.0001 Hz up to 10 kHz. In spite of its wide bandwidth, the MFS-06 shows outstanding low-noise characteristics, extremely low temperature drift of input offset voltage and offset current and a very stable transfer function over temperature and time.

Fig.3.3 A MFS06 magnetic induction coil in the parallel testing survey

Frequency range	0.00025 Hz ..... 10 kHz
Frequency bands	0.00025 Hz ..... 500 Hz (chopper on) 10 Hz ....10 kHz (chopper off)
Sensor noise	1.1*10-2 nT/□Hz @0.01 Hz 1.1*10-4 nT/□Hz @1 Hz 1*10-6 nT/□Hz @ 1000 Hz (chopper off)
Output sensitivity	0.2 V/(nT*Hz) f << 4 Hz 0.8 V/nT f >> 4 Hz
Output voltage range	+/- 10V
Function	Induction coil with magnetic field feed back

Connector	8 pole PT02SE12-10S
Calibration input sensitivity	4 nT / V
Feedback cut-off frequency	4 Hz
Supply voltage	+/- 12V to +/- 15V stabilized and filtered
Supply current	+/- 25mA
Case	ruggedized, waterproof glass fibre reinforced case
Weight	approx. 8.5 kg
External dimensions	length 1250 mm, diameter 75mm
Operating temperature range	-25°C to + 70°C

Table 3.4Features of the magnetic sensors MFS06 of Metronix

Source: (http://178.63.62.205/mtxgeo/index.php/sensors/mfs-06e)

3.2.3 Electrodes

Electric field fluctuations are determined by measuring the potential difference, U, between pairs of electrodes, which are connected via a shielded cable to form a dipole and buried in the ground at known distances, d, 10–100m apart:

Two dipoles are required in order to ascertain the two horizontal components of the electric field (Bahr and Simpson, 2005). These dipoles are typically configured orthogonal to each other, with one dipole oriented in the magnetic north–south (N–S) direction, and the other in the magnetic east–west (E–W) direction. Steel nails can suffice as electrodes for high-frequency audiomagnetotellurics (AMT) measurements, but longer-period measurements require non-polarisable electrodes in which electrochemical effects (which modify the potential difference that is registered) are avoided as far as possible. Non-polarisable electrodes usually consist of a porous pot containing a metal (e.g., silver [Ag]) in contact with a salt of the same metal (e.g., silver chloride [AgCl]). Junge (1990) adapted the Ag–AgCl ocean-bottom MT electrode of Filloux (1973, 1987) for long-period land measurements. In this design, the oceanic environment is simulated by a saturated KCl solution, and the electrical contact between theKCl solution and the ground is provided by a ceramic diaphragm .This design allows for MT measurements in the period range of the daily variation(Simpson, 2001b). In this MT survey four EFP06 type electrodes has been used to measure horizontal components of electric fields at both ends of the cable spreading.

3.2.3.1 Properties of EFP06 electrodes

The EFP-06 electrode is a sealed PbPbCl2 type and is not required to be refilled with liquid. It is delivered in a reusable plastic transportation container which also keeps it wet.

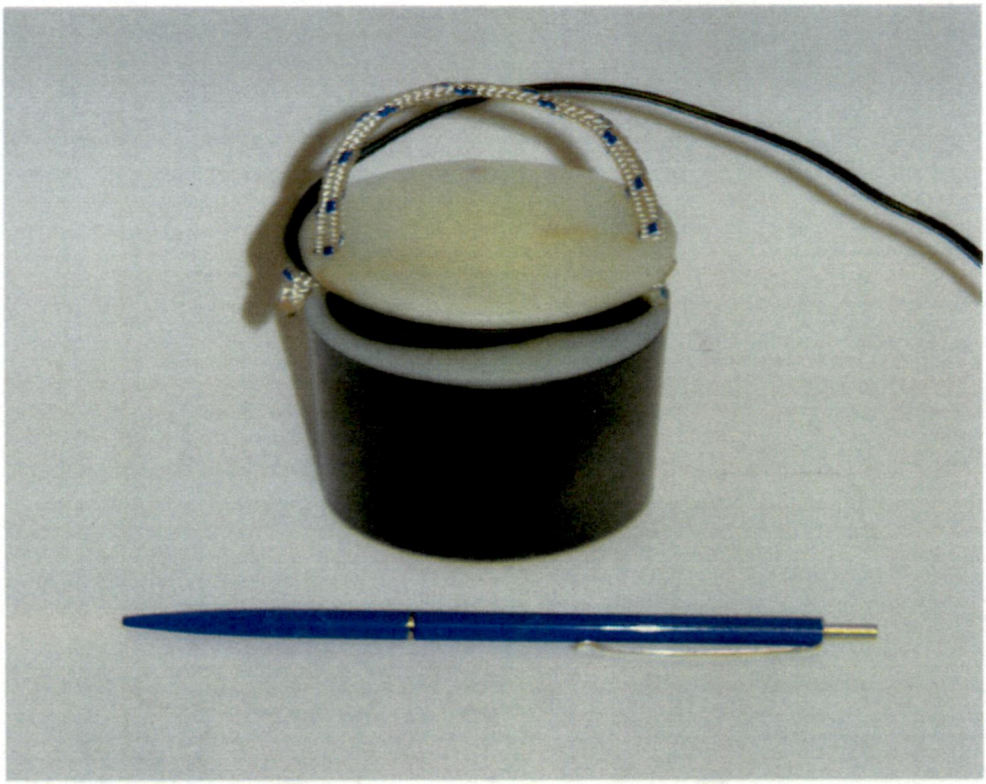

Fig.3.4 A EFP06 (Metronix) electrode

Source: (http://178.63.62.205/mtxgeo/images/brochures/FlyerEFP-06_v33.pdf)

Frequency range	DC to 100 kHz
Contact resistance	50 – 500 Ω (for normal soils)
Effective surface	27 cm^2
DC potential	a few mV
Temperature Range	+5 to +50 °C
Temperature Drift	0.66 µV/°C the temperature drift of two electrodes in the current circle is much lower than 0.66 µV/°C because of the same electrical behaviour; electrodes can be used at a wider outside temperature range if buried deep enough.
Weight	approx. 0.7 kg
External dimensions	length 117 mm, diameter 64 mm

Table 3.5 Features of the electric field sensor EFP06 of Metronix

Source: (http://178.63.62.205/mtxgeo/images/brochures/FlyerEFP-06_v33.pdf)

3.3 Noise sources to MT survey

There are three sources of noise associated with Magneto telluric survey

Cultural Noise

Meteorological Noise

Sensor Noise

In populated areas, electricity power lines produce dominant 50Hz and 150Hz electromagnetic fields. Whilst noise at such frequencies is relatively easily eliminated by notch filtering, it can limit the dynamic range of magnetic induction coils and cause instrumental saturation. Power-line noise is highly polarised. Therefore, the effects of power-line noise are usually more prevalent in one orthogonal measurement direction than in the other. Electricity generators can also produce significant levels of noise in the 50 Hz range. Generator noise is harder to eliminate than power-line noise using notch filters owing to its more variable bandwidth. Electric field measurements are also susceptible to contamination from ground leakage currents arising from electric railways and electric fences, the noise spectra from which span broad frequency ranges making filtering difficult. Automobiles represent a dual source of noise, creating both magnetic and seismic disturbances. Generally, magnetic disturbances can be negated by ensuring that sensors are placed more than 20 m away from any road. Seismic noise, although considerably reduced when the road is founded on firm bedrock, generally exhibits a longer range than magnetic noise. Seismic vibration generates noise on the telluric components by modulating the potential between the electrodes and the ground, and rotational movement, of the magnetic sensors in the Earth's magnetic field transforms seismic noise into a perturbation of the magnetic field.

A ubiquitous source of meteorological noise is wind. The vibration of telluric lines in the wind can generate voltages comparable to short-period telluric signals. As a result of wind blowing on trees and bushes their roots may move within the Earth, generating seismic noise, which may, in turn, cause movement of the sensors and corresponding perturbations of the measured fields. High frequency vertical magnetic field measurements are generally worst effected by wind vibration and ground roll. Another source of meteorological noise is generated by local lightning discharges, which superimpose noise on the source field owing

to their inhomogeneous and impulsive nature. Lightning may also cause saturation of telluric amplifiers.

Sensor noise and noise arising from electronic circuitry is usually independent of signal power and random in nature, making it difficult to distinguish and harder to evaluate. However, sensor noise is generally low for modern instrumentation. Care should be exercised to ensure that the effects of temperature variations on the sensors and electronic components are minimised. This can be achieved by burying sensors as deeply as possible, and choosing a shady place for the datalogger. At periods exceeding 1000 s, the signal-to-noise ratio is independent of signal power(Egbert and Booker, 1986)but at shorter periods, for which the power of the natural source field is more variable and contamination by cultural noise is more prevalent, signal-to-noise ratios can vary significantly. The presence of noise causes bias effects, including false depression or enhancement of calculated impedance tensors.

3.4 Installation of an MT station

A sketch of a magneto telluric station is shown in Fig.3 5. The magnetic fields were measured in the AMT range by induction coil magnetometers. The induction coil magnetometers were properly levelled with the help of spirit levels Electric fields were measured using non-polarisable electrodes. The direction of Ex was taken along the North-South direction and Ey along East-West. With the help of measuring tapes the dipole length for Ex and Ey were fixed to 70 and 75m respectively. Electrodes were buried at a depth of a few tens of centimetres to reduce temperature variations and to ensure wet environment and low contact resistance of electrodes. A solution of clay, water and salt was used to reduce the contact resistance of electrodes. For the measurement of vertical magnetic field components the sensor was buried in the vertical direction at the depth of 2m.A GPS receiver was used for the purpose of accurate time measurement which is needed for the synchronization of the data recorded by data logger as well as for the determination of the exact site location. The magnetic sensors were buried from 5m away from the data logger. The telluric cables were covered by the soils to keep it safe from cattle. After that data was recorded in three steps as run1, run2 and run3.

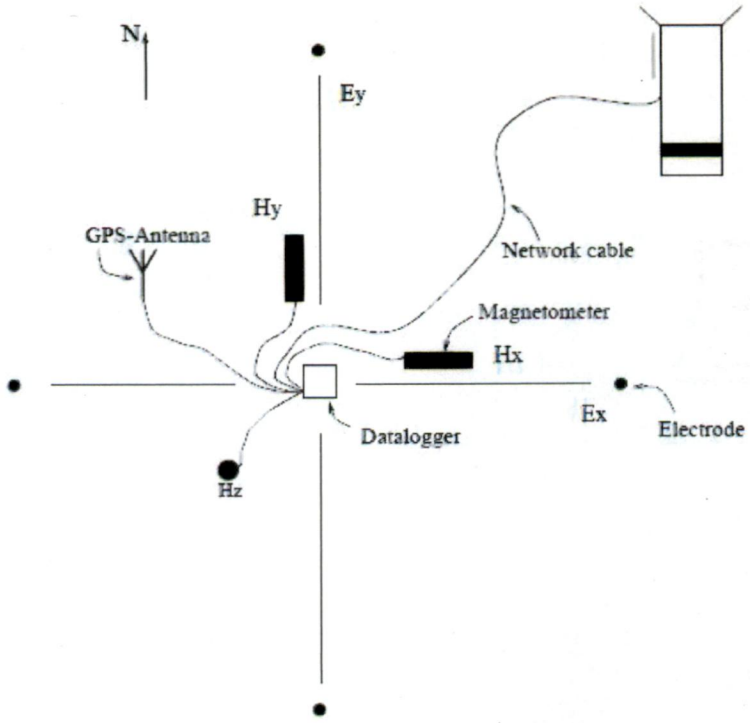

Fig.3.5 A sketch of MT survey set up

Source:(Simpson and Bhar, 2005)

Fig.3.6 Two buried vertical magnetic sensors in parallel test site

Fig.3.7 Two buried electrodes in parallel test site.

Two metronix system ADU 061 and ADU 058 were used in this parallel testing. ADU 061 is considered as for site 55(a) and ADU 058 is considered as for site 55(b). The dipole lengths for Ex ,Ey are 70 and 75 for both sites.

Adu 058(site 55(a))	Adu 061 (site 55(b))
$Ex^+ = 34.00m$	$Ex^+ = 32.00m$
$Ex^- = 36.00m$	$Ex^- = 38.00m$
$Ey^+ = 39.00m$	$Ey^+ = 39.00m$
$Ey^- = 36.00m$	$Ey^- = 36.00m$

Serial no. of the sensors used in site 55(a) are 130, 131 and 132, and in site 56 are 122, 123 and 125.

Time set in Run 1 for various bands are HF: 3.30PM, LF_1: 3.32 -3.45PM, Free: 3.47 – 4.00PM

Time set in Run 2 for various bands are HF: 5.03PM, LF_1: 5.05 -5.10PM, Free: 5.12 – 5.20PM

Time set in Run 3 for various bands are HF : 5.47PM, LF_1: 5.49 -6.15PM, Free: 6.17 - 6.47PM, LF_2: 6.49PM – 6.49AM(11.10.2011- 12.10.2011), LF_3: 6.51AM – 3.00PM(12.10.2011 – 14.10.2011)

CHAPTER 4.OVERVIEW OF WINGLINK SOFTWARE

WinGlink software can be used to obtain ID, 2D and 3D model of the subsurface. In this work 2D model has been obtained by using 2D inversion. This software provides 2D inversion module both for smooth and sharped boundary inversions of MT data. It performs inversions using exact finite difference routines developed by Dr. Randy Mackie which provides a comfortable interface for creating and editing 2D meshes and allows the user detailed control over the inversion parameters.

For the interpretation of modelled data, the module includes maps, pseudo sections and comparing observed and computed responses.

4.1 Maps

The Maps is used for the purpose of creating and displaying contoured and colour filled maps which represents the value types associated with a broad range of MT survey data. It allows the display of stations from different surveys and the constructions of integrated maps. Figure 4.1 shows map of 33 sites elevation values of Deoband to Gangotri profile.

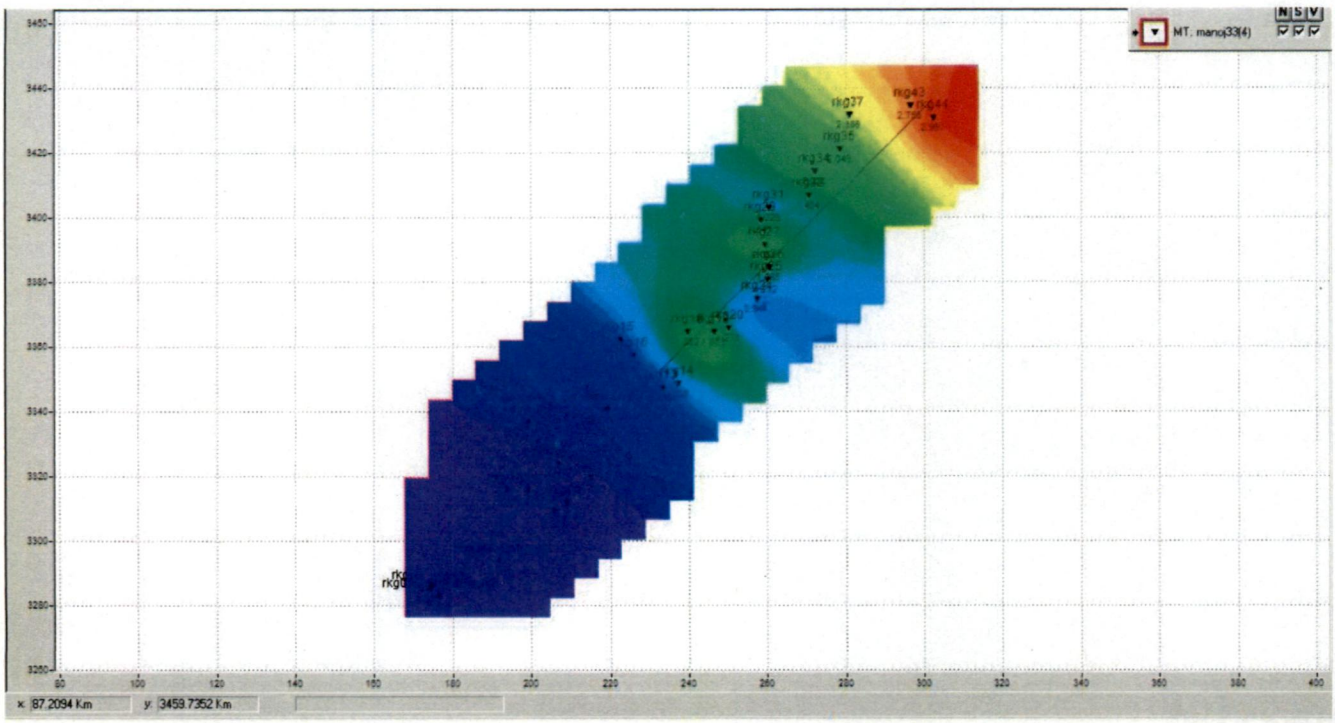

Fig.4.1 Elevation Map of Deoband to Gangotri profile.

Besides of the elevation map it also shows polar diagrams map, induction arrows map and miniature curves. Figure 4.2, 4.3 and 4.4 shows the polar diagrams map, induction arrows map and miniature curves.

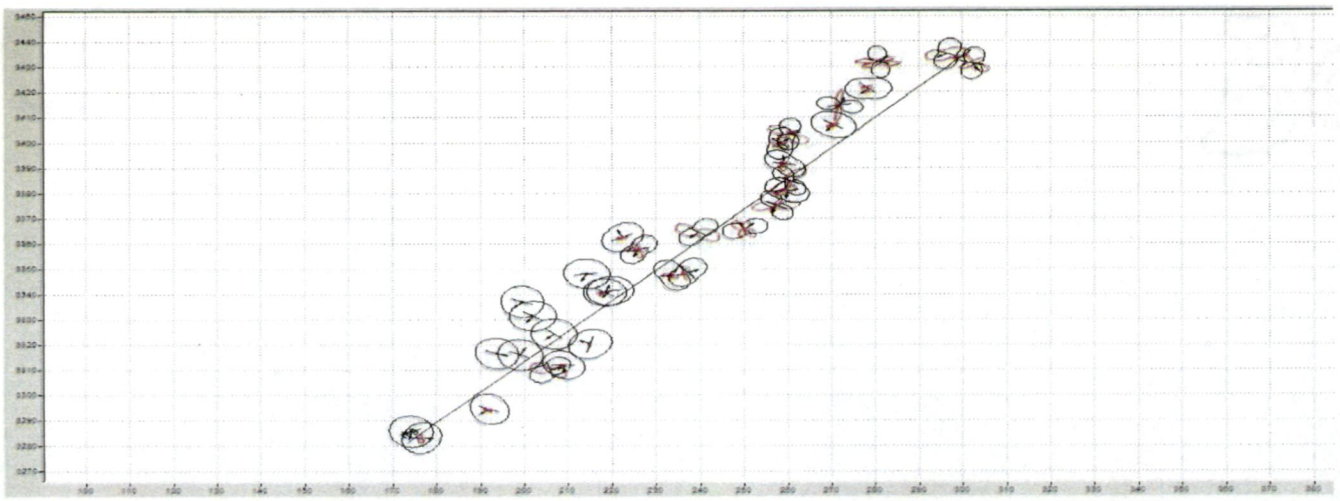

Fig.4.2 The polar diagram maps of 33 sites at central frequency 10HZ

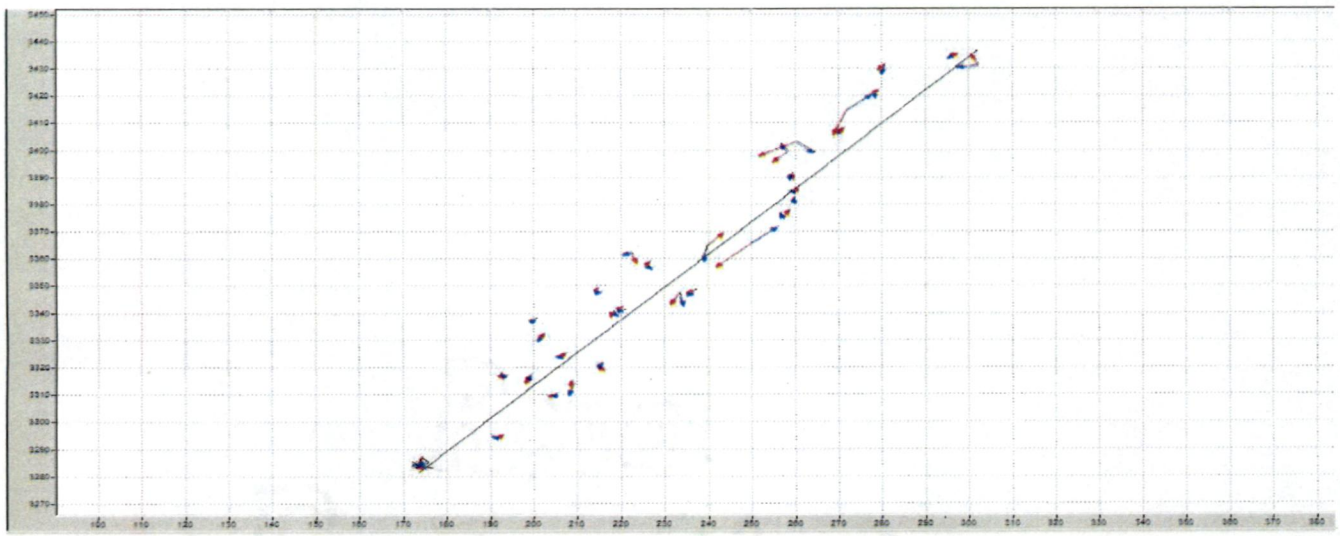

Fig.4.3 The induction arrows maps of 33 sites at central frequency 10HZ

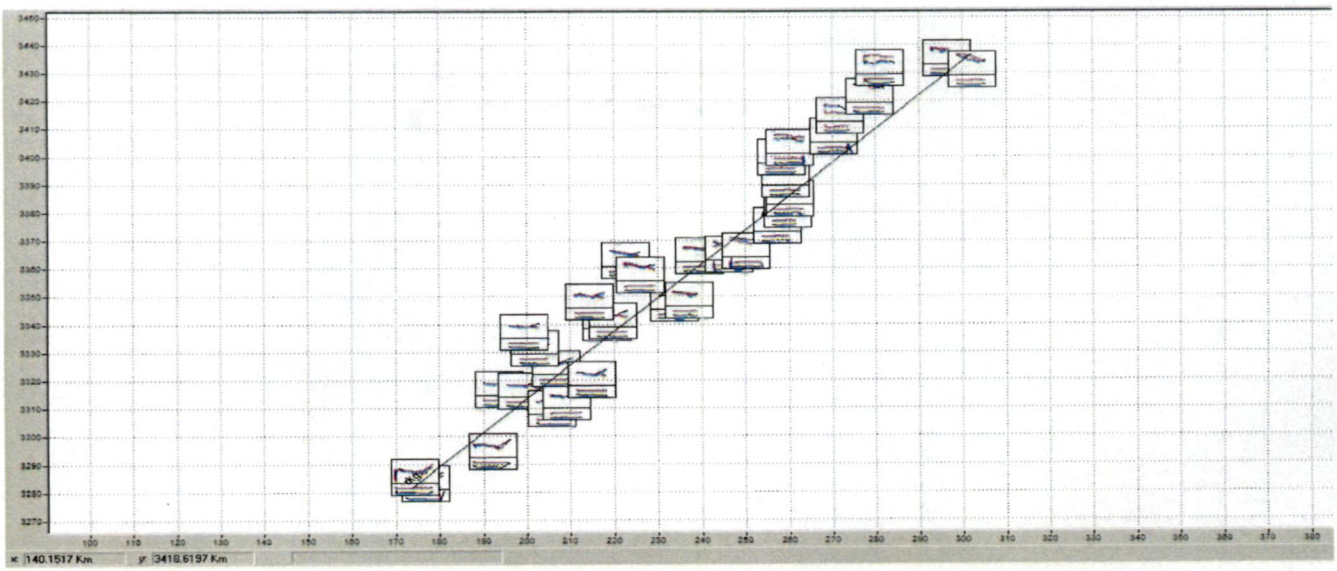

Fig.4. 4 The miniature curves of 33 sites at central frequency 10HZ

4.2 Soundings

The Soundings module is used to display, edit and model individual MT stations. It displays MT parameters such as resistivity, phase, polar diagrams, induction arrows and strike.We can edit individual modes at each frequency, swap modes and perform static shifting and stripping, calculate smooth curves. It also provides option for rotating stations using standard methods. The edited data saved by the Soundings program are used by other WinGLink programs: Edited resistivity curves are used to calculate resistivity Pseudo Sections. For MT soundings, phase and tipper are also used to calculate corresponding pseudo sections.

Figure 4.5 shows the apparent resistivity, phase and impedance polar diagram of station no. rkg2 are given. Circular and elliptical induction polar diagram (IPD) indicates the presence of 1D and 2D structures respectively, while the structure become complex in lower frequency range. Figure 4.6 and 4.7showing the apparent resistivity phase and induction arrows of station no. rkg2 and apparent resistivity, phase and strike respectively.

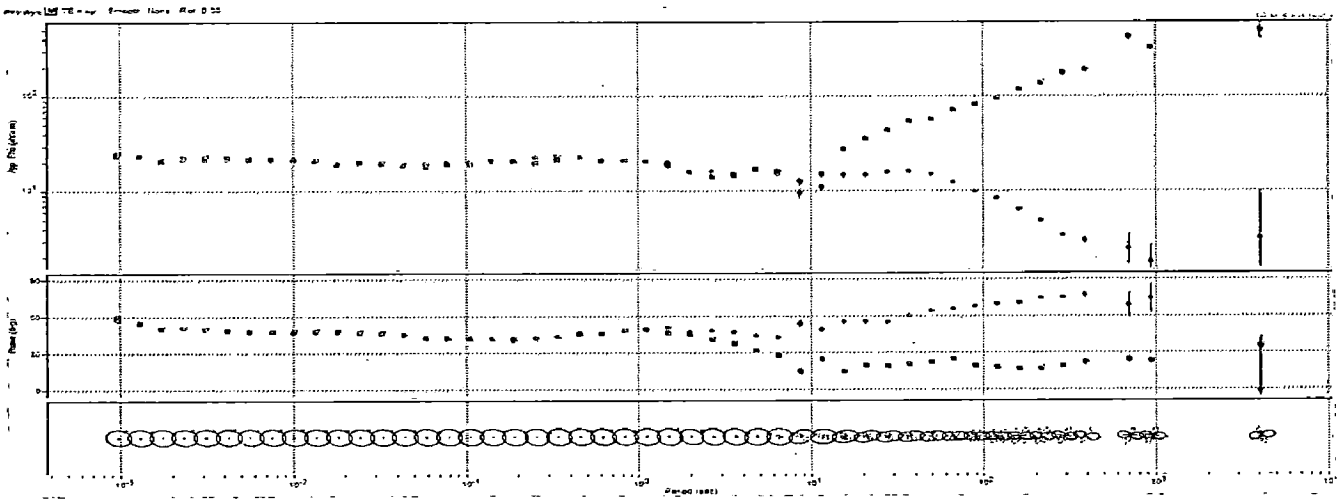

Fig.4.5 Apparent resistivity, Phase &impedance polar diagrams of station rkg2

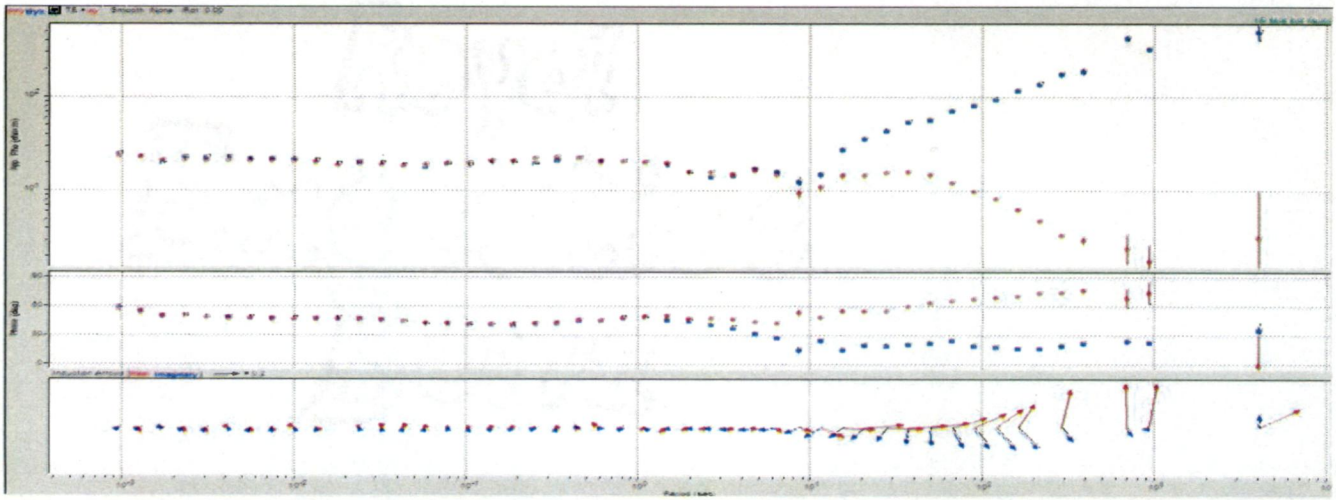

Fig.4.6 Apparent resistivity, Phase & induction arrows of station rkg2

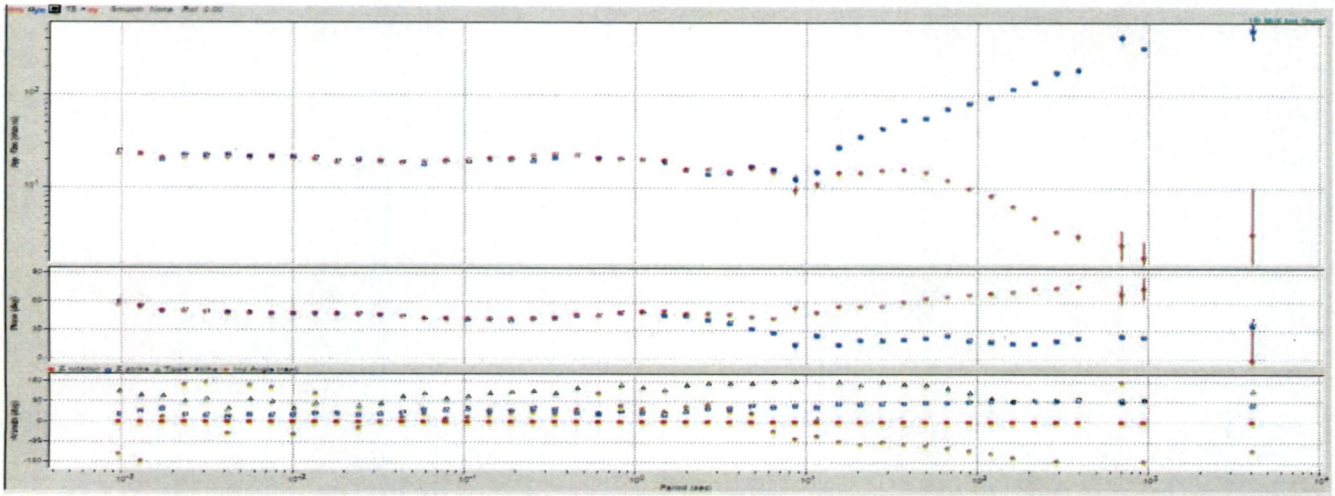

Fig.4.7 Apparent resistivity, Phase & strike of station rkg2

4.3 Pseudo section

The MT Pseudo sections module displays pseudo-sections for apparent resistivity and phase, tipper, and skew angle for both observed and synthetic data. Moreover, the module offers functions for creating difference pseudo-sections between any two sections of the same type, e.g. TM observed – TM calculated.

Each pseudo-section is defined by a profile trace and its associated stations, which supply the datasets with the apparent resistivity values vs. the measured parameter (i.e.: AB/2, time, or frequency, depending on the data type of the project). Figure 4.8, 4.9 and 4.10 showing the pseudo sections of TE, TM and Tipper mode respectively.

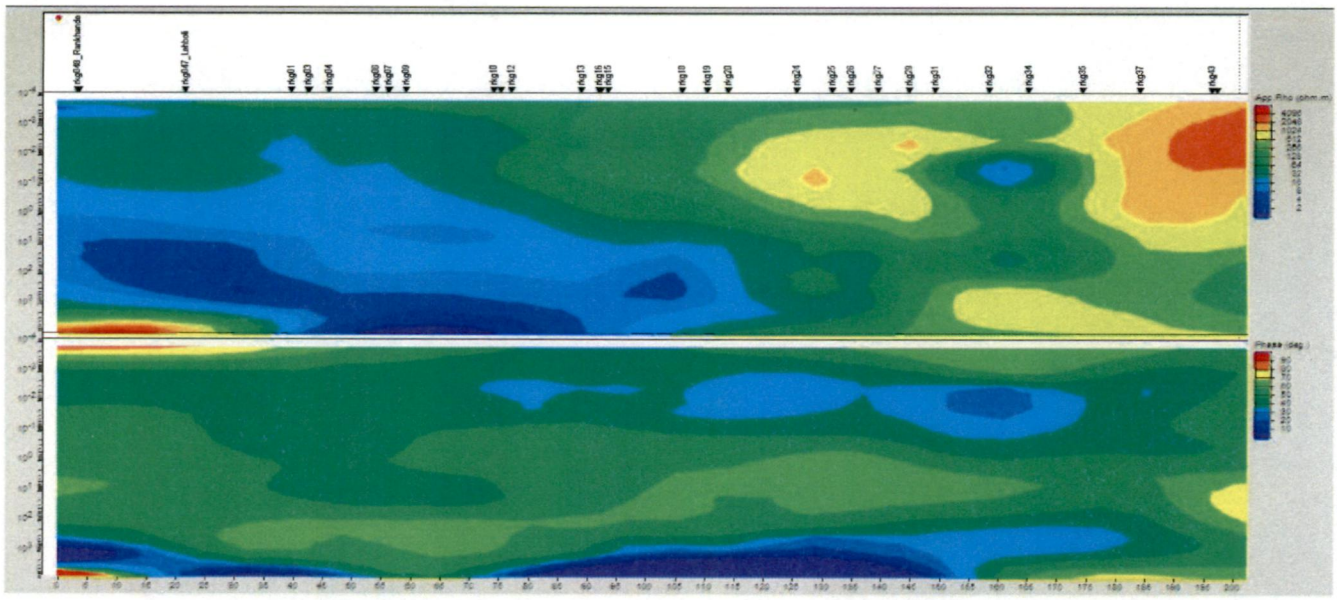

Fig.4.8 Pseudo Section of TE Mode of station data

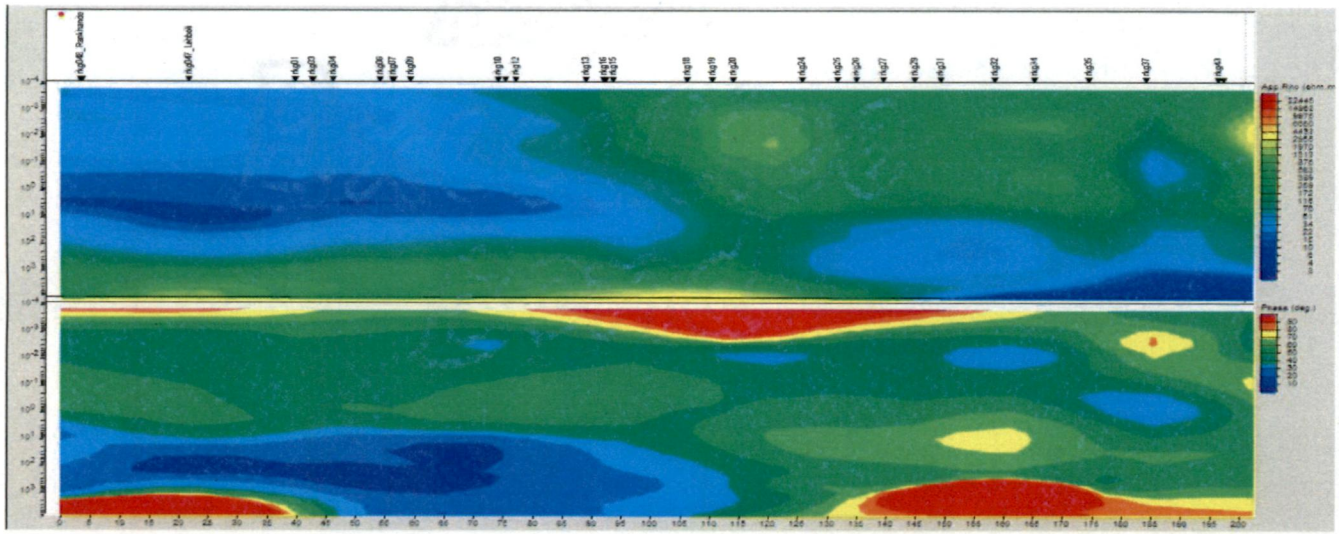

Fig.4.9 Pseudo Section of Tm Mode of station data

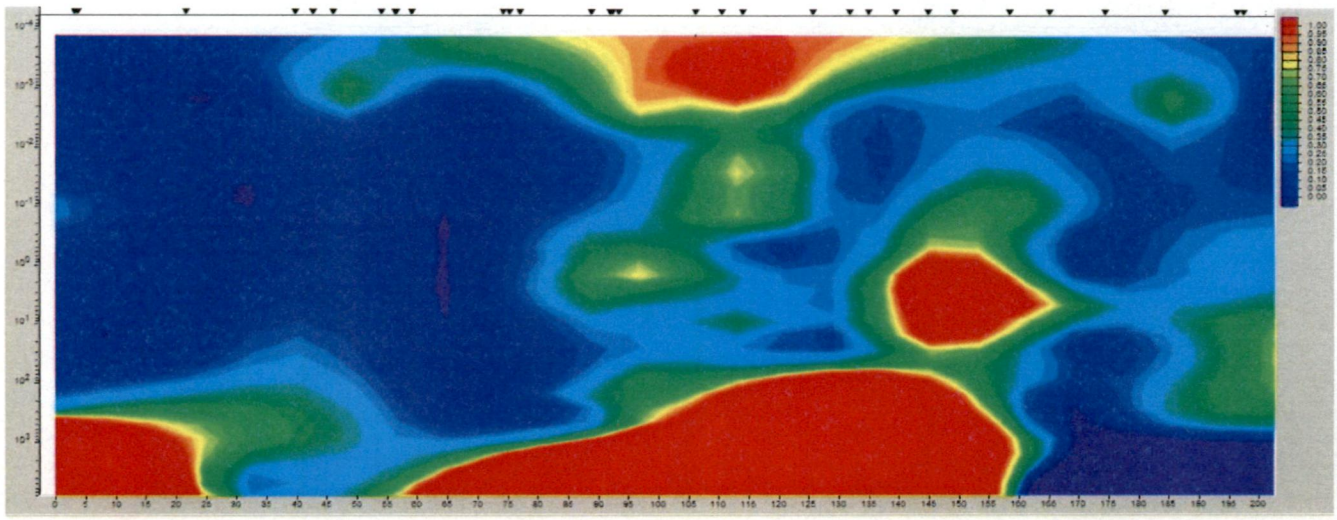

Fig.4.10 Pseudo Section of Tipper Mode of station data

CHAPTER 5.INVERSION OF MT DATA

5.1 Overview

Inversion scheme implies going from data to model. But practically there exists a nonlinear relationship between data and the model which indicates small change in data domain produces significant change in model where as a small model changes are assumed to have a linear relationship to small data changes. So the data is forced to be quasi linear by use of transformation into a substitute model and data. Once the required linear system of equations has been derived, the problem is reduced to one of inverting a matrix and it becomes easy to apply various modelling algorithm to it. Due to diffusivity nature of electromagnetic energy, MT sounding only resolves conductivity gradients rather than sharp boundaries and thin layers, so MT sounding produces blurred rather than a focused image of the subsurface. There are many inversion schemes are available to minimise model complexity rather than fitting the experimental data as well as possible. The smoothest model over- interprets the data where as smooth or least structure model reduce the temptation to over- interpret data. As non-uniqueness is inherently associated with the modelling, forward modelling is a good way of exploring allowable perturbation to a model output from an inversion. As one dimensional inversion scheme only provides the burial depth and three dimensional scheme is unavailable, so two dimensional inversion scheme is more preferred over 1 –D and 3 –D inversion schemes. Forward modelling is an iterative procedure involving progressive trial-and-error fitting of data by (i) computing the responses of an input model, (ii) comparing these with measured data, (iii) modifying the model where the data are poorly fitted and then (iv) re-computing the responses, until a satisfactory fit to the measured data is achieved.

As with forward modelling, inversion is an iterative process, the aim of which is to progressively reduce the misfit between measured data and data synthesised from a model. All inversion problems require the ability to solve the forward problem as a pre-requisite.

The inverse problem that transforms a set of MT responses to a conductivity model is non-linear. The non-linear relationship between the model and the data can often be adequately approximated as quasi-linear by expanding the MT response(Bahr and Simpson,2005), R, for a conductivity model, $\sigma(z)$, at period, T, about an arbitrary starting model, $\sigma_0(z)$, according to the following equation

$$R(\sigma,T) = R(\sigma_0 + \delta\sigma, T) = R(\sigma_0, T) + \int_0^\infty G(\sigma_0, T, Z)\delta\sigma(z)dz + R_\sigma) \quad 5.1$$

Where R represents the remainder term for the first-order expansion in conductivity and G is the Frechet kernel (assuming that R is Frechet differentiable). Assuming that the remainder term is second order in $\delta\sigma$, and can therefore be neglected, Equation (5.1) can be expanded as an approximate linear equation that relates changes in the modelled responses to a linear functional of the conductivity model (Dosso and Oldenburg, 1991):

$$\delta R(\sigma, \sigma_0, T) + \int_0^\infty G(\sigma_0, T, Z)\sigma_0(z)dz = \int_0^\infty G(\sigma_0, T, Z)\sigma(z)dz \quad 5.2$$

Where $\delta R(\sigma, \sigma_0, T) = R(\sigma, T) - R(\sigma_0, T)$

and$\delta\sigma(z) = \sigma(z) - \sigma_0(z)$

After quasi linearization, mathematical algorithms schemes can be easily applied to minimise the misfit between observed data and modelled data. Because higher-order terms in the expansion are neglected, the procedure must be applied iteratively until an acceptable model is realised. Out of many algorithm schemes least structure Philosophy with 2D inversion schemes (Constable et al., 1987) is preferred more because it produces smooth model.

5.2 Least structure philosophy with 2D inversion

Occam's razor (Simpson and Bhar, 2005) proposed finding the smoothest possible model (known as the least-structure model) consistent with an acceptable (user-definable) fit to the data. Given the diffusive nature of electromagnetic fields, passive EM techniques resolve conductivity gradients rather than sharp boundaries at depth, giving least-structure models a certain appeal. By explicitly minimising structural discontinuities, unjustifiably complex interpretations of data are avoided, and any structure present within the model should lie within the resolving power of the data. Therefore, the temptation of over-interpreting data is reduced. Therefore, layered models and least-structure (smooth) models represent two extremes between which the resistivity–depth distribution of the real Earth is likely to lie. 2-D models are constructed on a rectangular grid of rows and columns intersecting at nodes in the y–z co-ordinate plane to form blocks or cells, each of which is attributed a uniform conductivity. Once defined, the mesh remains fixed from one iteration to the next. Most 2-D inversion algorithms (Occam Inversion (De Groot-Hedlin and Constable, 1990); Rapid Relaxation Inversion (RRI) (Smith and Booker, 1991)) are founded on the least-structure

philosophy, and involve joint minimisation of data misfit (e.g., expressed as an rms statistic and model roughness.

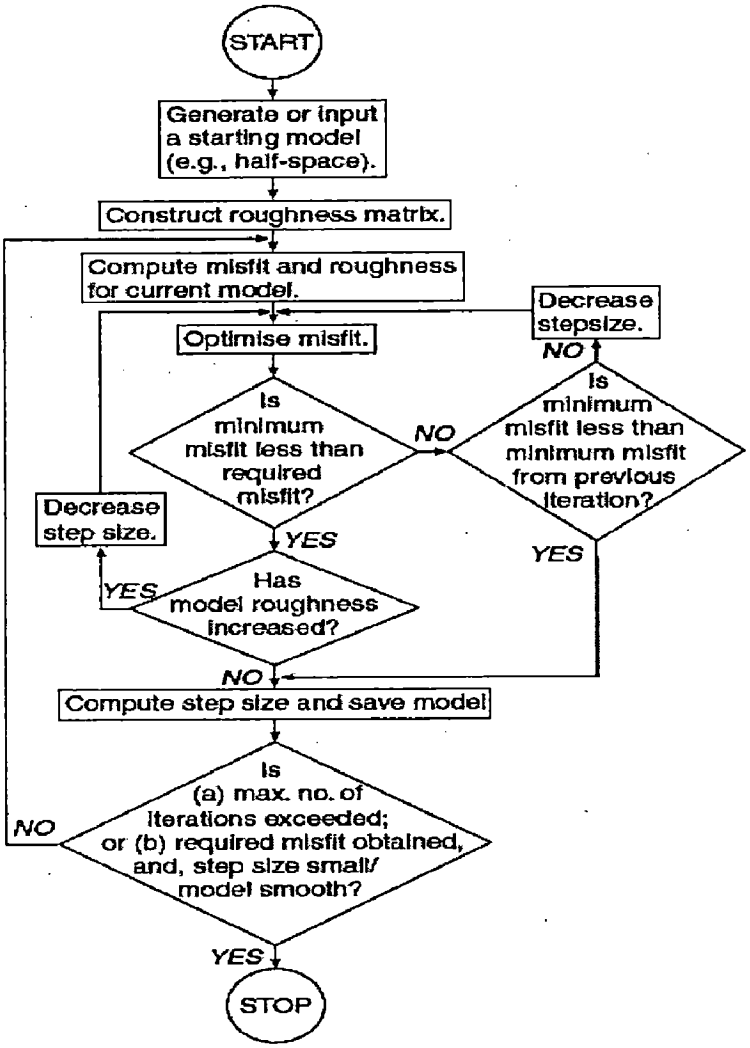

Fig.5.1 Flowchart showing steps involved in Lesat structured inversion

Source:(Simpson and Bhar, 2005)

5.3 Inversion routines used by WinGlink

Two dimensional inversion in this work has been performed by using WinGlink software. This software contains two different routines for running inversions:

5.3.1 A smooth model inversion routine

This routine was developed by Randy Mackie in 2001 and made further improvements to it in 2002. This routine finds regularized solutions (Tikhonov Regularization) to the two dimensional inverse problem for the magneto telluric data using the method of nonlinear conjugate gradients. The forward model simulations are computed using finite difference equations generated by network analogy to Maxwell's equations. The program inverts for a

user defined 2D mesh of resistivity blocks, extending laterally and downwards beyond the central detailed zone, and incorporating topography.

5.3.2 A sharp boundary model inversion routine

This routine was developed in 1998 by Randy Mackie, this routine is based on the inversions of 2D MT data for discrete interfaces and the resistivities of the layers between those interfaces. The interfaces are described by a series of nodes, whose horizontal positions are fixed, but whose vertical positions can vary in the inversion. The interfaces are assumed to transect the entire model, i.e; there are no closed bodies. The interface varies linearly between each interface nodes at fixed horizontal positions within each layer. The resistivity is assumed to vary linearly between nodes. The interface and resistivity information is projected onto a finite –difference mesh for computation, and the inversion calculates the best fitting interface node locations and resistivity nodal values in order to fit the observed data. In this work a smooth model inversion routine has been followed over the magneto telluric data.

In this work, 2D inversion algorithm based on Tikhonov's regularisation has been applied on the MT data along Deoband – Gangotri profile. The first part of my work includes 2D inversions of 33 sites MT data which were earlier processed in IIT Roorkee, the second part of my work includes inversions of 36 sites along the same profile MT data processed by Geoelctric and magnetic research centre, Germany Group. The purpose of using 2 sets of processed data was to find which processing method yields good results. The third part of my work includes averaging of the MT data taking adjacent stations and converting the data files obtained from averaging to EDI file format for the purpose of performing 2D inversions by WinGlink software. 33 sites of the processed data have been grouped into 13 parts for averaging. The purpose of averaging was to reduce the spreading of the data and finding which method of averaging provides smoothed data. The final part of the work includes grouping of 36 sites data into 17 groups on the basis of X distance and averaging (Median) of resistivity and phase values of MT stations data in each group. Before averaging data has been rotated $N60^0W$ to match the coordinates of the measurement along the strike directions and the comparison has been made between the rotated and non-rotated model.

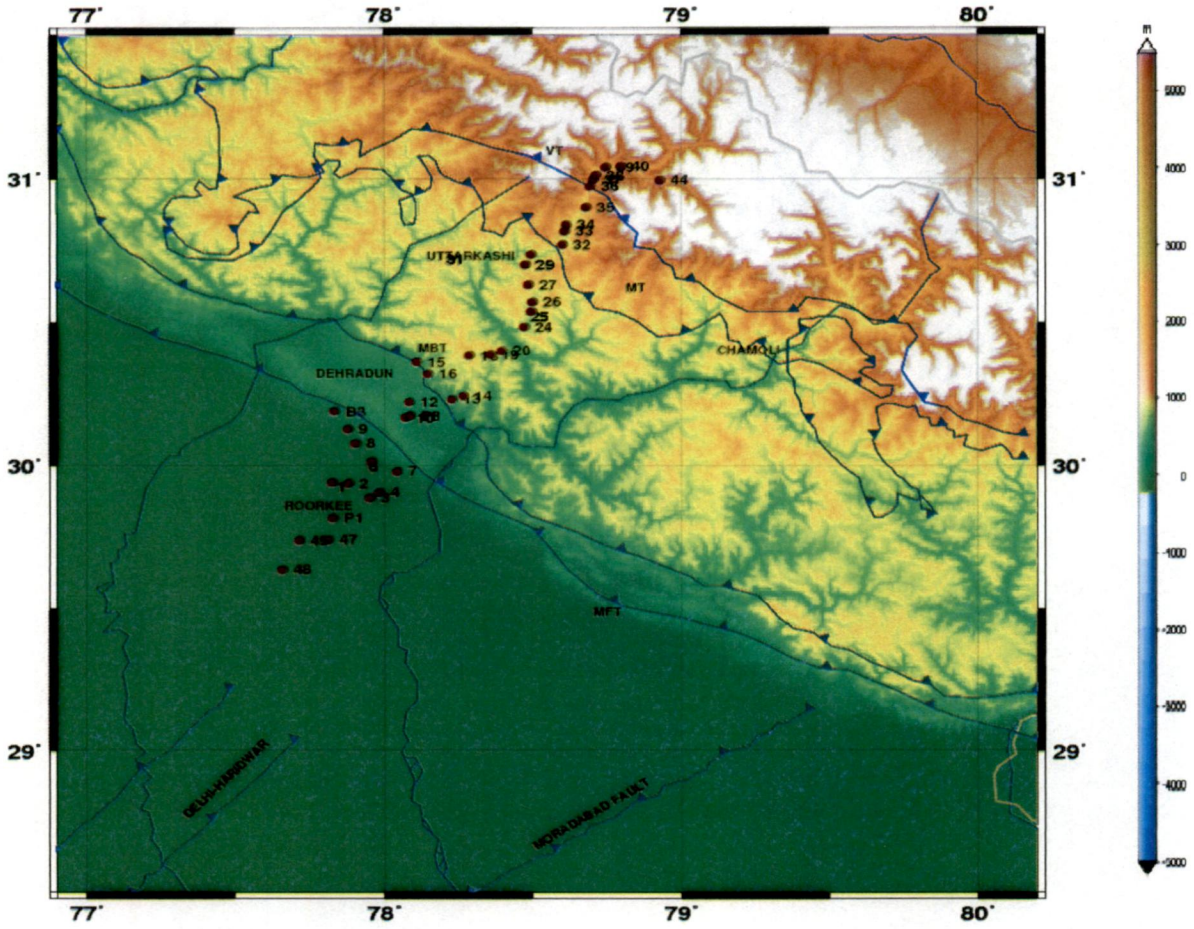

Fig.5.2 The map showing all the sites those have been taken for the inversion purpose

5.4 Inversions of existing 33 sites data processed by IIT Roorkee Group

The profile that has been considered from southwest to northeast using the 33 sites in the order of 48, 50, 47, 1, 3, 2, 4, 6, 7, 8, 9, 10, 11, 12, 13, 16, 14, 15, 18, 19, 20, 24, 25, 26, 27, 29,31,32,34,35,37,43 and 44 for the purpose of preparation of 2D INVERSION models using the WINGLINK software.

2D inversion models have been prepared in three different frequency ranges which are given below

1. 0.001 – 10s
2. 0.001 – 100s
3. 0.001 -1000s

The following flow chart has been followed for the preparation of 2D INV models for each frequency range.

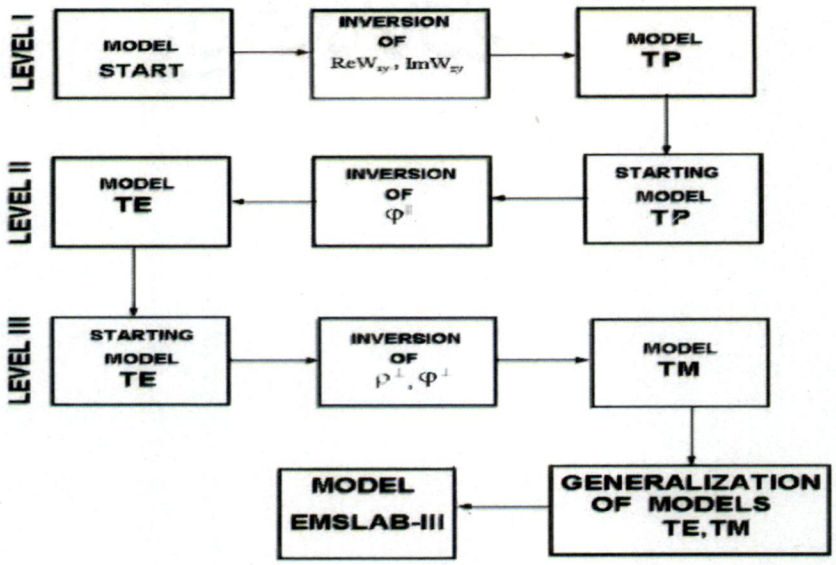

Fig.5.3 Flowchart for the 2D inversion model

5.4.1 Models descriptions

The initial model is a 3 layered model from top to downward 1Km, 6Km and below with resistivity 100 , 200 and 600 Ohm-m respectively.

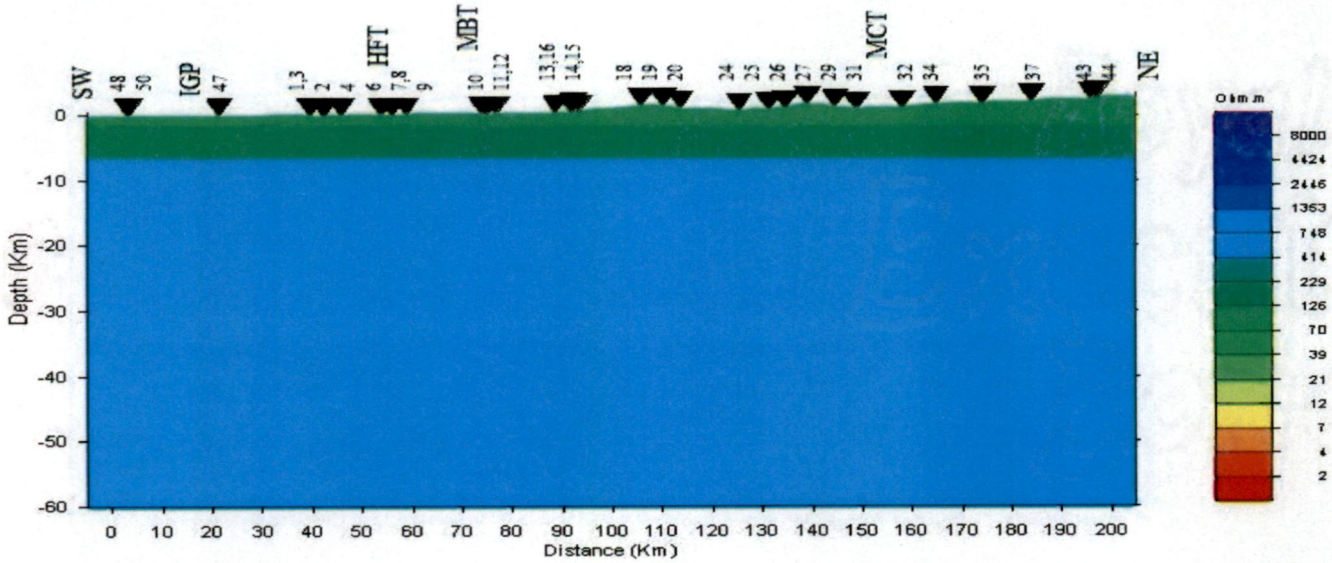

Fig.5.4 INITIAL MODEL: Three layer model of 1KM, 6KM, and below, having resistivity 100 ohm-m, 200 ohm-m and 600 ohm-m

Tipper data was inverted over initial model then TE phase was inverted over tipper model. After that TM apparent resistivity and phase was inverted over TE model. Finally joint TE – TM was inverted over TM model.

S.No.	Site No.	Location		X (KM)	WINGLINK X-location(km)	Avg. Site no	Reference Site	X-location (Winglink)
		Lat. (Degree)	Long. (Degree)					
0	Starting Point	29.5999	77.6295	0	3.59			
1	RKG48	29.6361	77.6607	5	2.96	1	RKG48	2.96
2	RKG50	29.7409	29.7409	6	3.37			
3	RKG47	29.7409	29.7409	24	21.36	2	RKG47	21.36
4	RKG01	29.7409	77.8283	42	39.58			
5	RKG02	29.9372	77.8828	45	42.53	3	RKG02	42.53
6	RKG03	29.8867	77.9547	45	42.43			
7	RKG04	29.905	77.9853	48	45.85			
8	RKG06	30.0139	77.9611	56	53.9	4	RKG06	53.9
9	RKG07	29.9789	78.0472	58	56.0			
10	RKG08	30.0769	77.9072	59	56.19			
11	RKG09	30.1261	77.8811	63	58.92			
12	RKG10	30.1658	78.0753	76	73.96			
13	RKG11	30.17	78.0878	77	75.05	5	RKG11	75.05
14	RKG12	30.23	78.0308	80	76.9			
15	RKG13	30.2294	78.2306	91	88.75			
16	RKG16	29.7409	78.1509	94	91.86	6	RKG16	91.86
16	RKG14	30.2414	78.27	94	92.18			
17	RKG15	30.3622	78.1125	97	93.29			
18	RKG18	30.3856	78.2906	108	105.93	7	RKG18	105.93
19	RKG19	30.3878	78.3606	112	110.29			
20	RKG20	30.4006	78.3994	116	113.73			
21	RKG24	30.4842	78.4739	127	125.44			
22	RKG25	30.5378	78.4983	134	131.55	8	RKG25	131.55
23	RKG26	30.5719	78.5019	137	134.72			
24		30.6325	78.4889	141	139.21	9	RKG27	139.21

	RKG27							
25	RKG29	30.7028	78.4778	147	144.66			
26	RKG31	30.7383	78.4981	152	148.97			
27	RKG32	30.7728	78.6025	160	158.15			
29	RKG34	30.8417	78.6158	167	164.95	10	RKG34	164.95
30	RKG35	30.9028	78.6819	177	174.2	11	RKG35	174.2
31	RKG37	30.9992	78.7060	187	183.98	12	RKG37	183.98
32	RKG43	31.0278	78.8678	198	196.12			
33	RKG44	30.9964	78.9297	199	197.06	13	RKG44	197.06
34	LAST POINT	29.7409	78.9797	202	207.67			

Table 5.1 Showing 33 sites coordinates and their X –distance in the profile

33 Sites (0.001 – 10s)	Modes	Error Floor		Initial RMS	Final RMS	No. of iterations	Weight Factors α=3, β =1 Minimum Block dimensions 500H, 550V Tau for smoothing operator =10, Data Errors RHO -10, Phase -5
		Resistivity	Phase				
	Tipper	*	*	0.929	0.7562	900	
	TE	100	10	9.705	1.9534	489	
	TM	25	10	6.7792	2.4903	412	
	TE+TM	TE-25 TM -25	TE-10 TM -10	4.5631	2.4917	435	
33 Sites (0.001 – 100s)	Tipper	*	*	0.807	0.7207	426	
	TE	100	10	6.361	2.4291	420	
	TM	25	10	7.463	2.0291	361	
	TE+TM	TE-25 TM -25	TE-10 TM -10	3.112	2.2438	480	
33 Sites (0.001 – 1000s)	Tipper	*	*	0.7566	0.6777	600	
	TE	100	10	8.365	2.2115	395	
	TM	25	10	8.545	2.1337	375	
	TE+TM	TE-25 TM -25	TE-10 TM -10	3.5273	2.4148	420	

Table 5.2 Showing information of inversion parameters that have been used for the running of the 2D inversions of 33 sites in 3 different frequency ranges

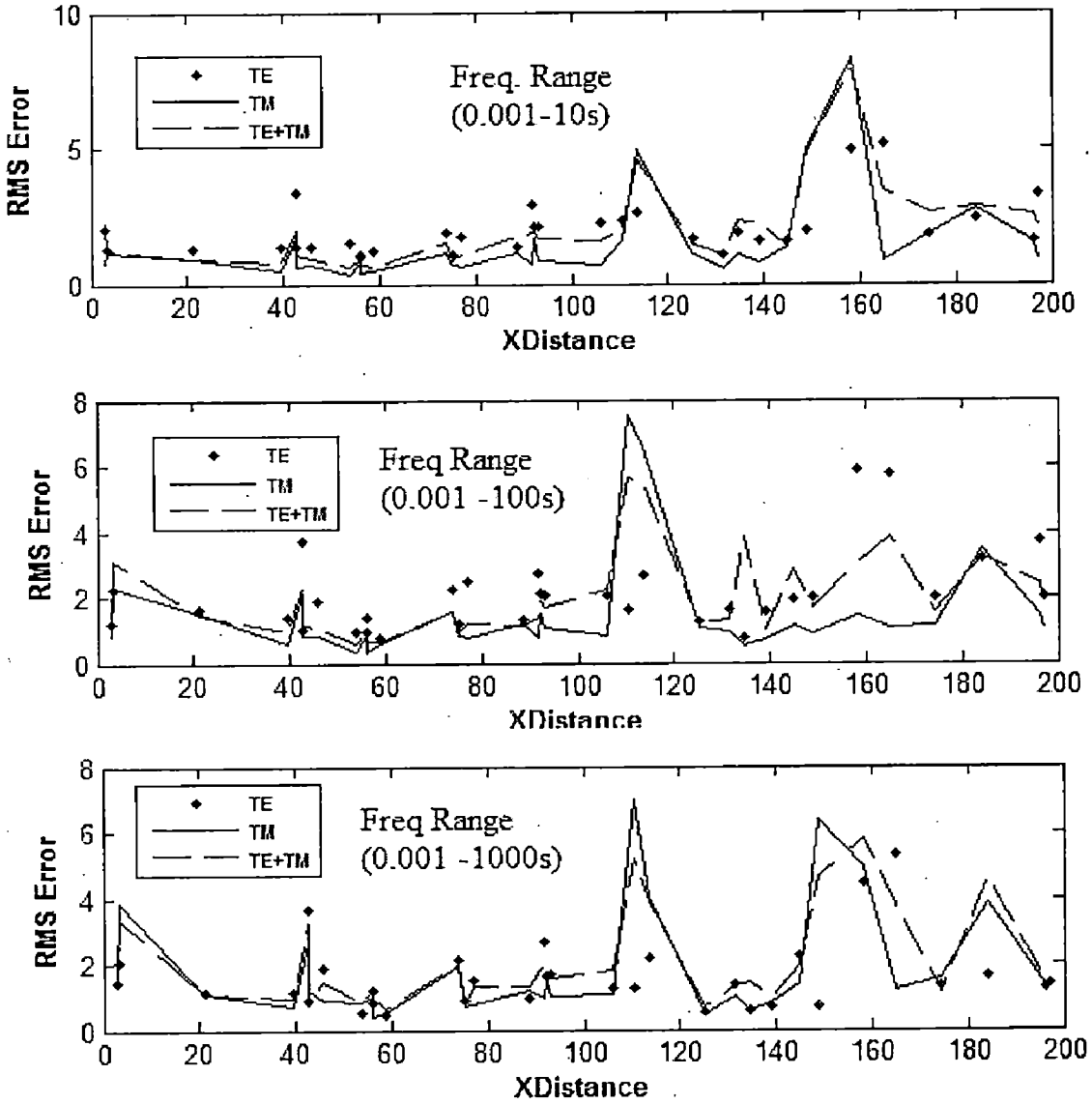

RMS Error vs X Distance plot in three different frequency

Fig.5.5 Shows plot of RMS Error VS XDistance

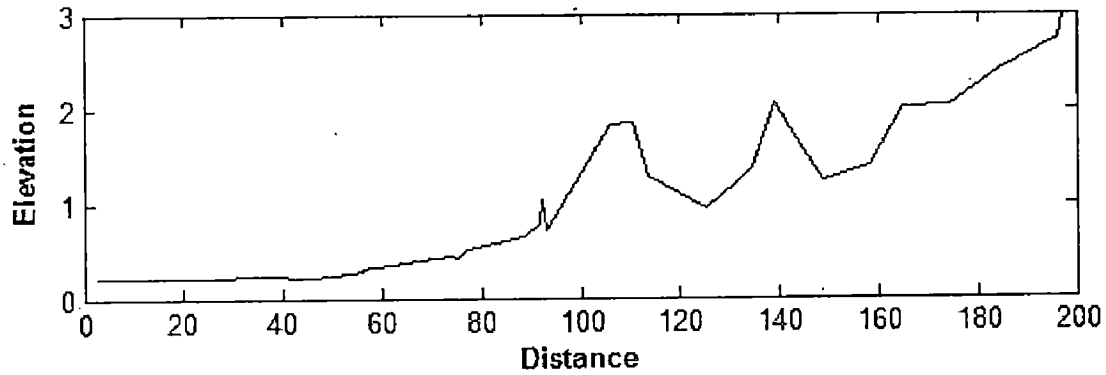

XDistance VS Elevation plot of 33 sites MT data

Fig.5.6 Shows plot of ElevationVS XDistance

5.4.2 Comparision of TIPPER models in three different frequency ranges

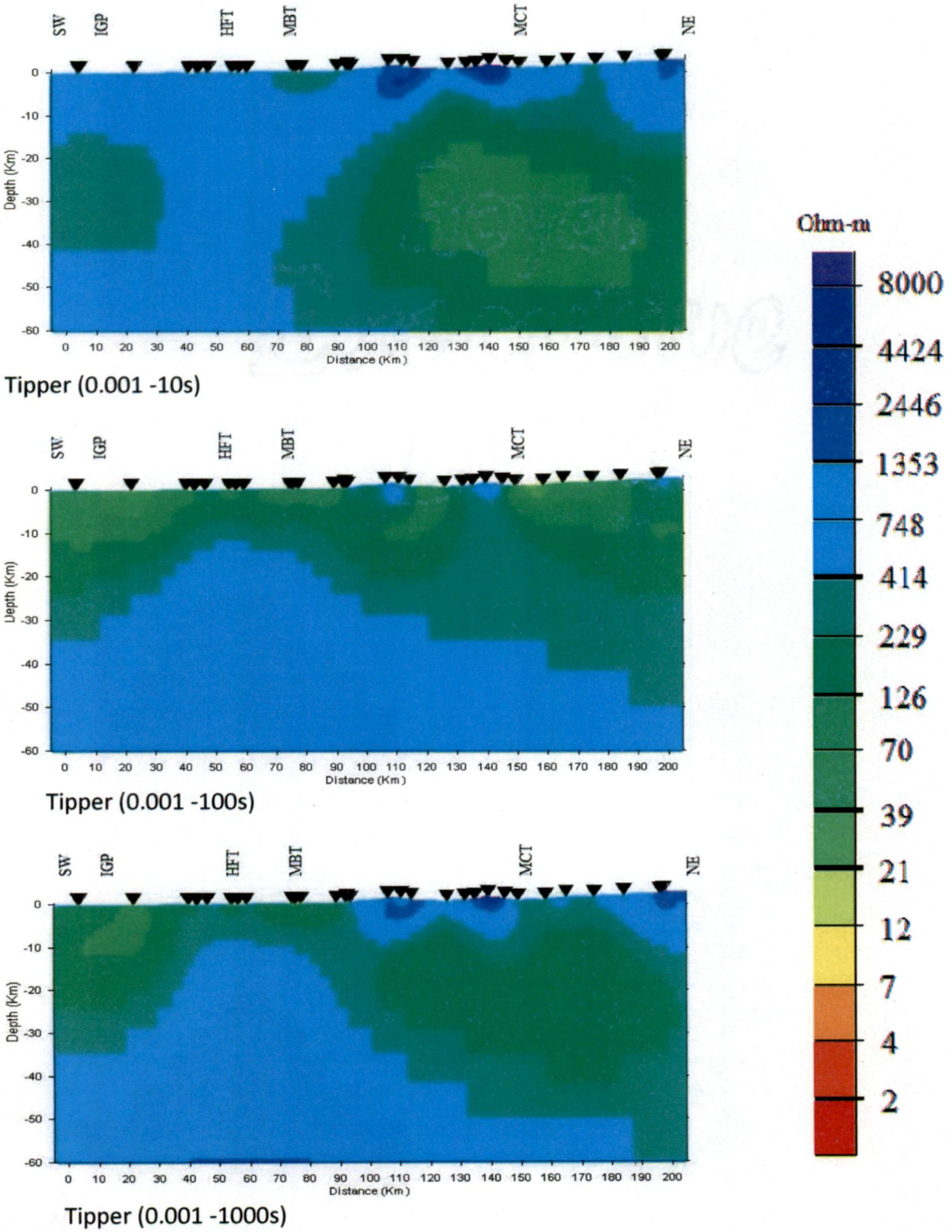

Fig.5.7 Shows Tipper models in three different frequency ranges

5.4.3 Comparision of TE models in three different frequency ranges

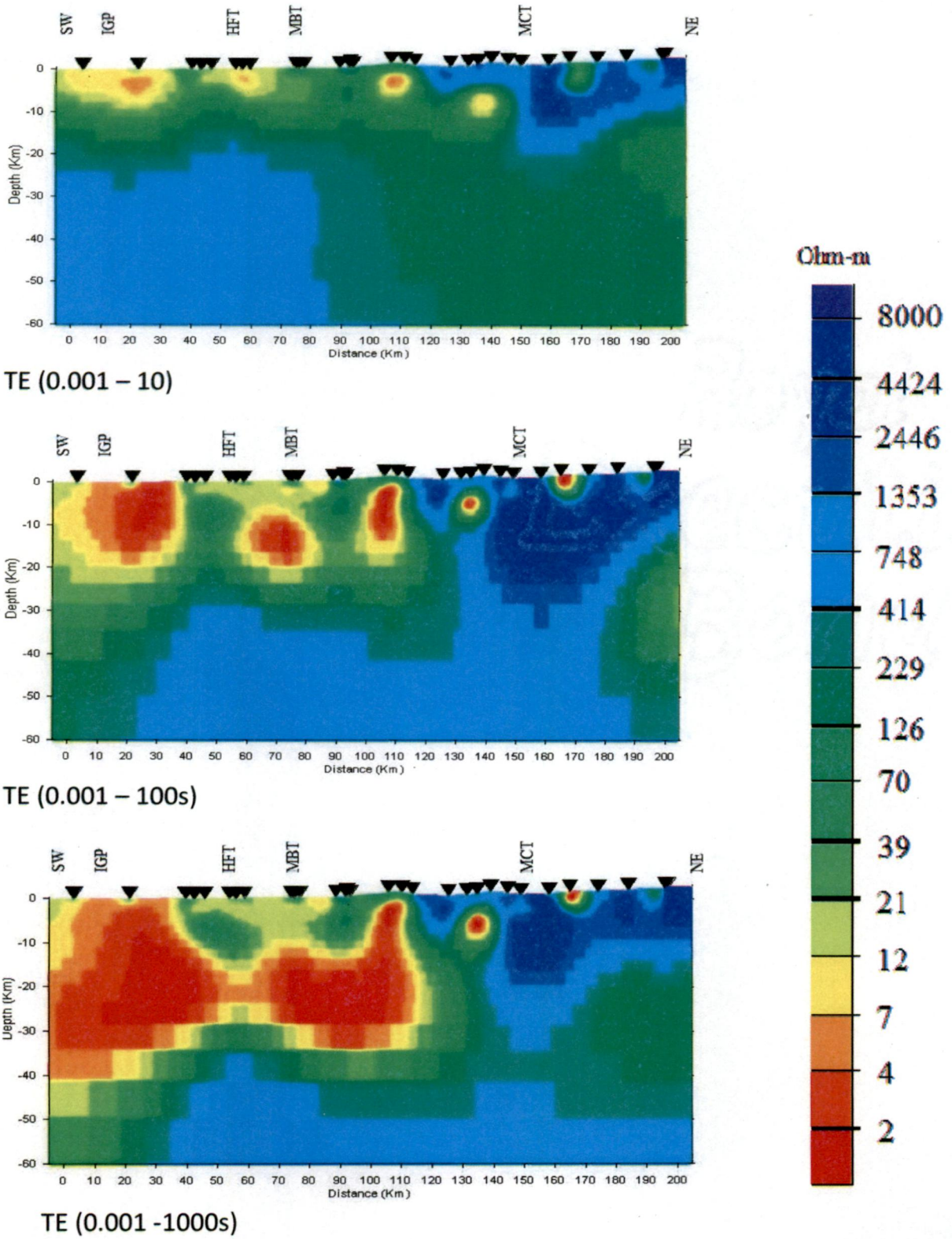

Fig.5.8 Shows TE mode models in three different frequency ranges

5.4.4 Comparision of TM models in three different frequency ranges

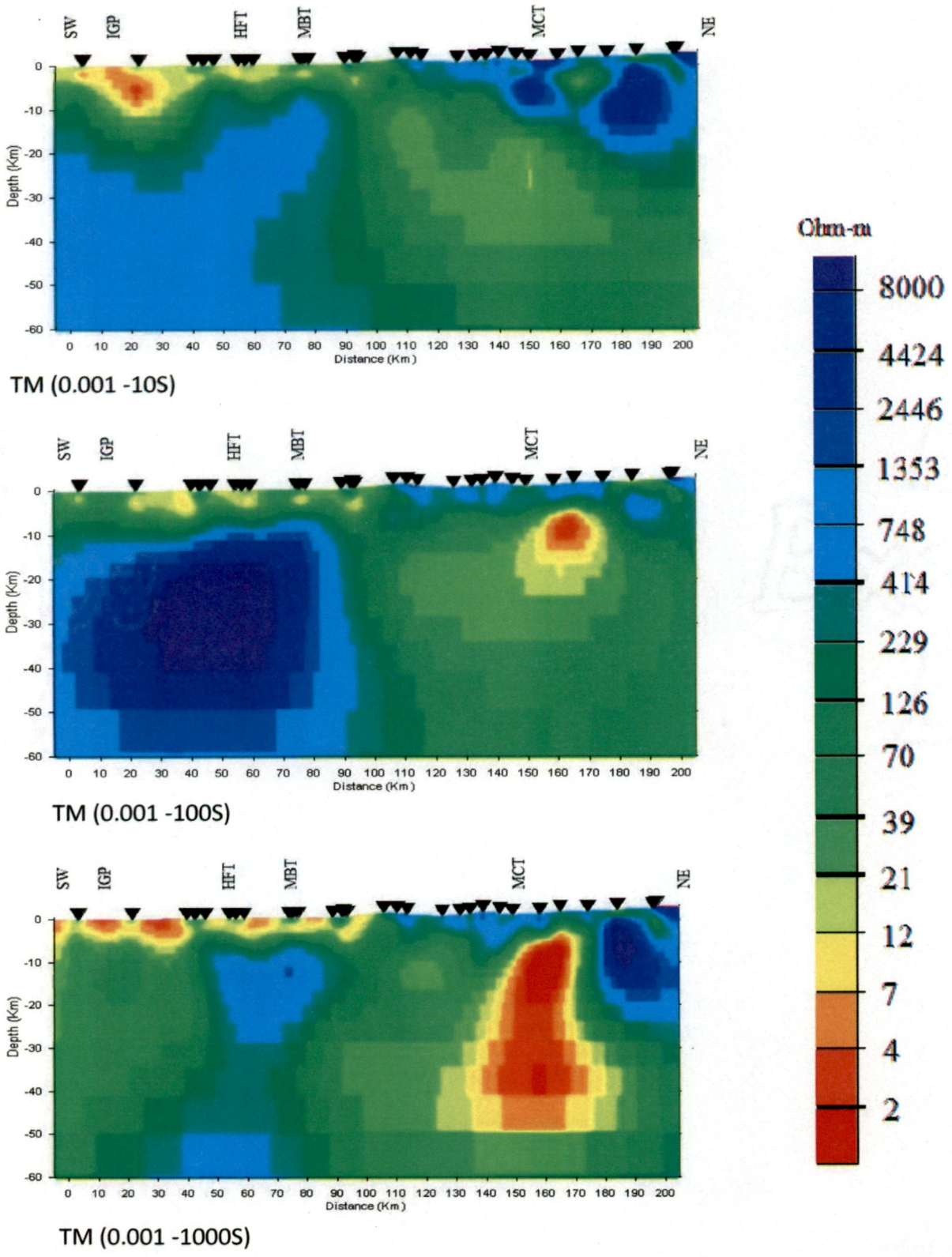

Fig.5.9 Shows TM mode models in three different frequency ranges

5.4.5 Comparison of TE+TM modes in three different frequency ranges

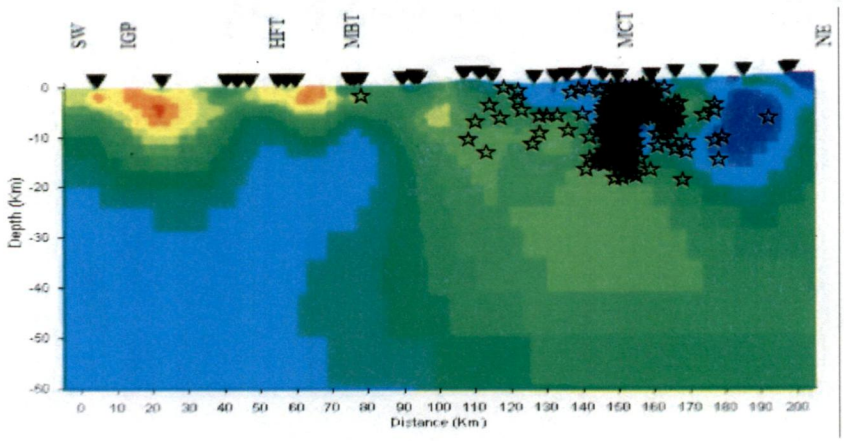

TE+TM (0.001 -10S)

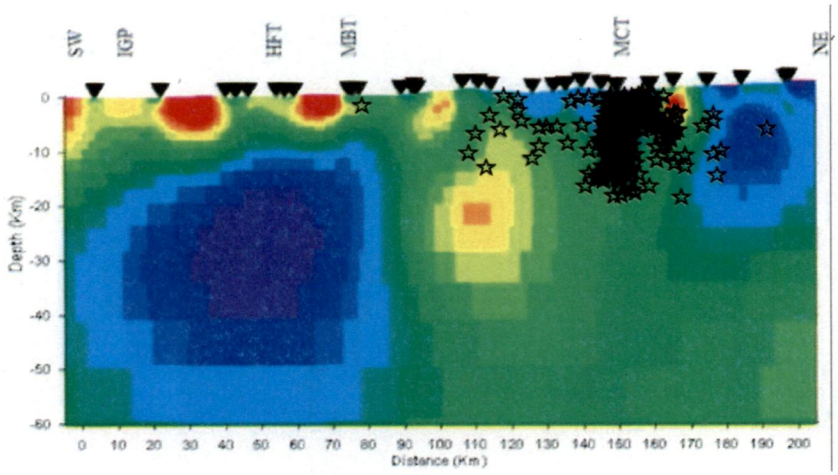

TE+TM (0.001 -100S)

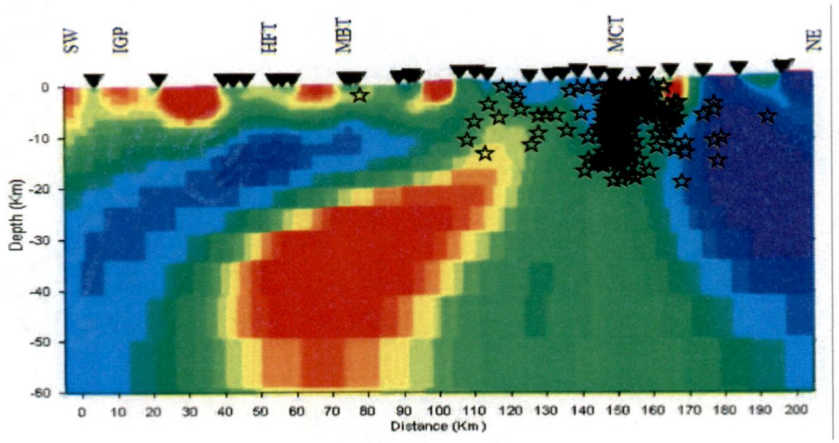

TE+TM (0.001 -1000S)

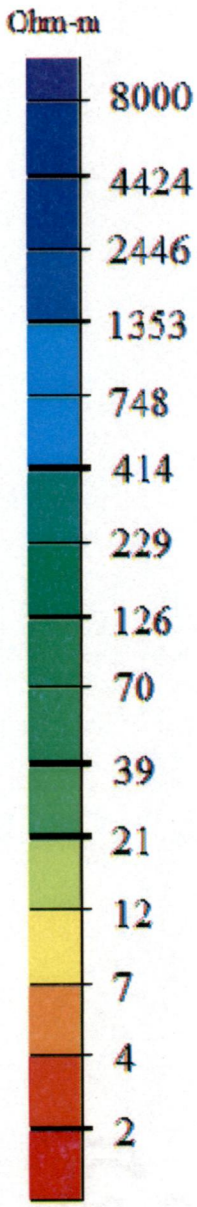

Fig.5.10 Shows TE+ TM mode models in three different frequency ranges

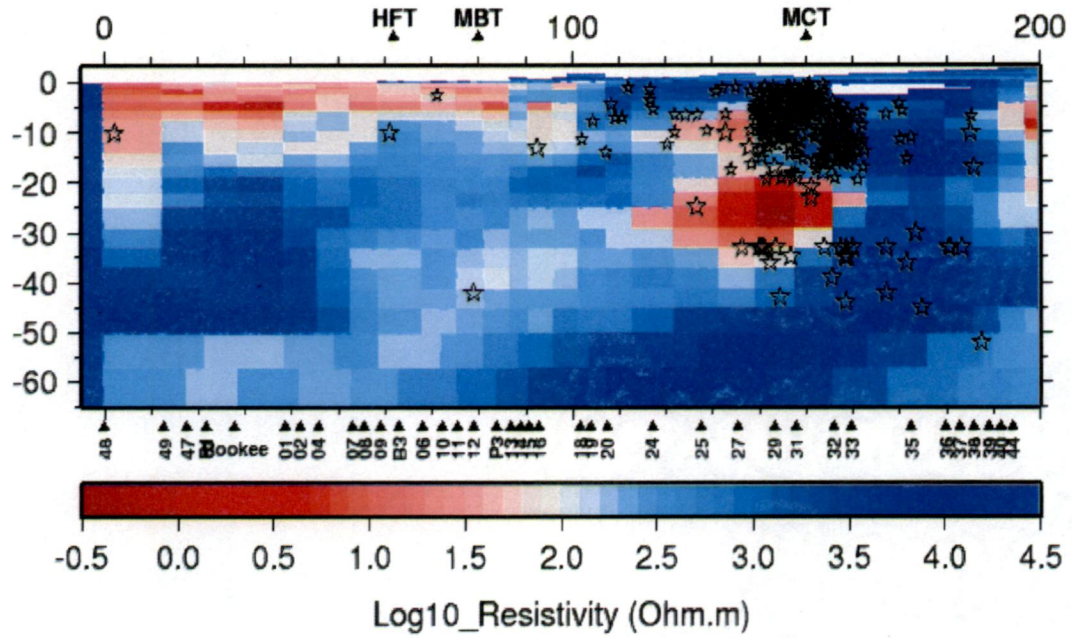

Fig.5.11 Reference Model

5.4.6 Results

The study area extends from lesser Himalaya to Higher Himalaya region up to near surface to crustal study. 2D inversion has been performed for tipper, TE mode, TM mode as well as joint mode in three different frequency ranges. The comparison of all models in different frequency ranges shows with increase in frequency range; we are getting deep structure information. The resolution of models obtained in Frequency range 0.001 -10Hz is very poor because the most part of it is covered by dead band frequency range 0.5 -5Hz.

The tipper mode models don't detect any conductive structures. The resolutions of tipper models increase with lowering the frequency. The tipper models at 0.001 -100s and 0.001 -1000s delineates high resistive structures at the depth of 25 to 60Km extending from 0 to 110Km along the profile. The comparison of tipper model with the reference model shows only the resistivity part in the lower crust of Indo-Gangatic plain (IGP) and clearly delineating the various thrusts like HFT, MBT and MCT in the Himalayan region

The reference model delineates the small scale conductive features at near surface regions of the IGP. This model also provides the increase in resistivity with depth up to lithospheric regions and embedment of conductive body in a resistive region which is extending from 24 sites to 33 sites at the depth of 10 to 40 Km. The comparison of all TE models with the reference model shows the conductive features of the IGP area are detected at only high

frequency range. It shows with increasing the range of frequency i.e lowering the frequency more there is a shift of conductive features at the IGP region. As we know TE mode produces inductive distortion and it becomes higher at near depth regions because of high frequency so model is pretty much affected by inductive distortion so it is unable to detect the current gathering produced by the conductive body at the Higher Himalayan region at the depth of 25 to 40 Km. But it is delineating the resistivity part of the reference model properly. So, it is clear from the above study that TE mode is suitable for detecting the near surface resistivity structures and

The comparison of all TM models with the reference model shows these are well matching with the reference model. The resolutions of the models increase with lowering the frequency. Although TM mode produces galvanic distortions but it becomes less at near depth regions because of high frequency so model is not much affected by galvanic distortion. Hence it is clear that the TM mode is suitable for delineating the near surface conductive features and the presence of the conductive sub vertical channels (Fluid saturated faults) crossing the resistive lithosphere.

As TE and TM modes are complementary to each other (i.e. one model producing one type of distortions and another model lessen that distortion), joint model is preferred in many situation but in these above models we are finding that with increase in frequency range the conductive structure is shifting towards left. This may be because of galvanic distortion. In this case TM models providing good results than joint model. The RMS error vsXDistance plots for three different frequency ranges shows the variation of RMS Error of TM mode lies beyond the TE and joint mode. The variation of RMS Error is more in TE mode. TM mode provides smooth model which is well matching with the reference model as well as gives good fitting of the data with lower RMS Error, so clearly it can be inferred TM mode is suitable mode to study the conductivity structures of the subsurface of the earth at near depth crustal regions. As the study region extends up to the resistive lithosphere and not including the conductive asthenosphere so TM model is giving better results than TE model.

5.5 Inversions of existing data processed by GERMC group

2D inversion has been applied on 36 MT sites data along the same profile in the order of 48,49,47,1,2,4,6,7,8,9,B3,10,11,P312,13,14,16,15,18,19,20,24,25,27,29,31,32,33,35,36,37,38 ,39,40 and 44. The purpose of using the same data is to compare the processing methods used by IITR and GERMC groups.

The Initial model used in this case is same as previous case. But the difference is that it inverts both TE resistivity and phase while in the previous case only TE phase has been inverted. In this case tipper data has not been inverted.

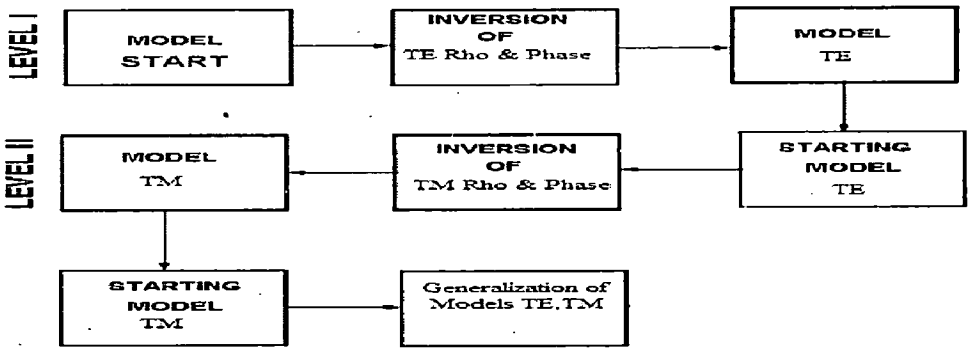

Fig.5.12 Flowchart for the 2D inversion model of 36 sites MT data

S.No.	Site No.	Location		X (KM)	WINGLINK X-location(km)	Avg. Site no	Reference Site	X-location (Winglink)
		Lat. (Degree)	Long. (Degree)					
1	RKG48	29.6361	77.6607	5	4.89	1	RKG48	4.89
2	RKG49	29.7393	77.7176	18	17.39	2	RKG49	17.39
3	RKG47	27.7409	77.8153	24	23.16			
4	RKG01	29.9406	77.8283	42	41.68			
5	RKG02	29.9372	77.8828	45	44.55	3	RKG02	44.55
6	RKG04	29.905	77.9853	48	47.6			
7	RKG06	30.0139	77.9611	56	55.87			
8	RKG07	29.9789	78.0472	58	57.75	4	RKG07	57.75
9	RKG08	30.0769	77.9072	59	57.87			

10	RKG09	30.1261	77.8811	63	58.35			
11	B3	30.1886	77.8361	68	61.24	5	B3	61.24
12	RKG10	30.1658	78.0753	76	64.17			
13	RKG11	30.17	78.0878	77	75.96			
14	P3	30.1736	78.0897	78	77.06	6	P3	77.06
15	RKG12	30.23	78.0308	80	79.1			
16	RKG13	30.2294	78.2306	91	90.58			
17	RKG14	30.2414	78.27	94	93.97	7	RKG14	93.97
18	RKG16	30.3198	78.1509	97	93.99			
19	RKG15	30.3622	78.1125	94	95.56			
20	RKG18	30.3856	78.2906	108	107.9			
21	RKG19	30.3878	78.3606	112	112.14	8	RKG19	112.14
22	RKG20	30.4006	78.3994	116	115.53			
23	RKG24	30.4842	78.4739	127	127.25	9	RKG24	127.25
24	RKG25	30.5378	78.4983	134	133.39			
25	RKG27	30.6325	78.4889	141	141.25			
26	RKG29	30.7028	78.4778	147	146.81	10	RKG29	146.81
27	RKG31	30.7383	78.4981	152	151.14			
28	RKG32	30.7728	78.6025	160	160.2			
29	RKG33	30.8193	78.6103	165	164.8	11	RKG33	164.76
30	RKG35	30.9028	78.6819	177	176.3	12	RKG35	176.3
31	RKG36	30.9766	78.6958	184	177.58	13	RKG36	177.58
32	RKG37	30.9992	78.7060	187	186.16	14	RKG37	186.16
33	RKG38	31.0148	78.7146	189	188.06	15	RKG38	188.06
34	RKG39	31.0427	78.7481	193	192.46			
35	RKG40	31.0451	78.7990	196	195.61	16	RKG40	195.61
36	RKG44	30.9964	78.9297	199	198.89	17	RKG44	198.89

Table 5.3 Showing 36 sites coordinates and their X –distance in the profile

Inversion Parameters for 36sites

36 Sites (0.001 – 2048s)	Modes	Error Floor		Initial RMS	Final RMS	No. of iterations	Weight Factors α=3, β=1 Minimum Block dimensions 250H, 50V Tau for smoothing operator =10, Data Errors RHO -10, Phase -5
		Resistivity	Phase				
	TE	100	10	7.894	2.0156	200	
	TM	25	10	6.873	2.2314	180	
	TE+TM	TE-25 TM -25	TE-10 TM -10	4.305	2.2618	145	

Table 5.4 Shows information of inversion parameters of the 2D inversions of 36 sites processed earlier by GEMRC Group.

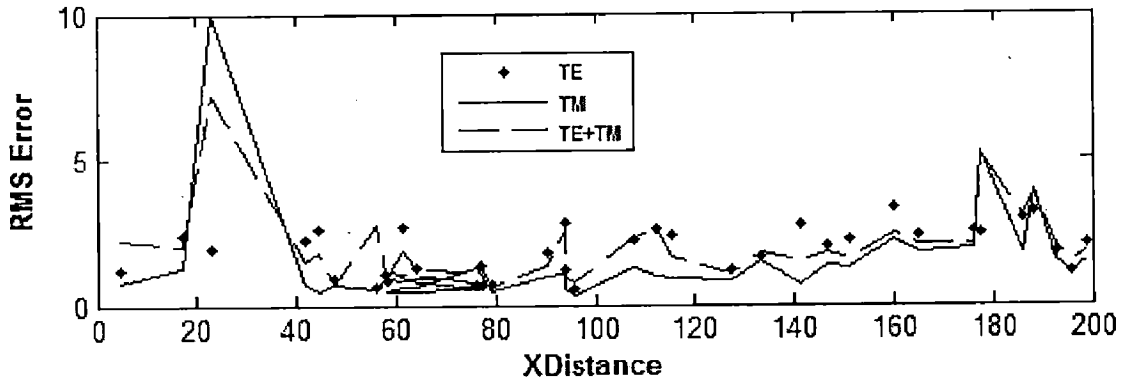

RMS Error VS XDistance Plot of all modes of 36 sites data in the frequency range 0.01 -2048s

Fig.5.13Showsplot of RMS Error VS X distance of all modes of 36 sites data in the frequency range 0.01 -2048S

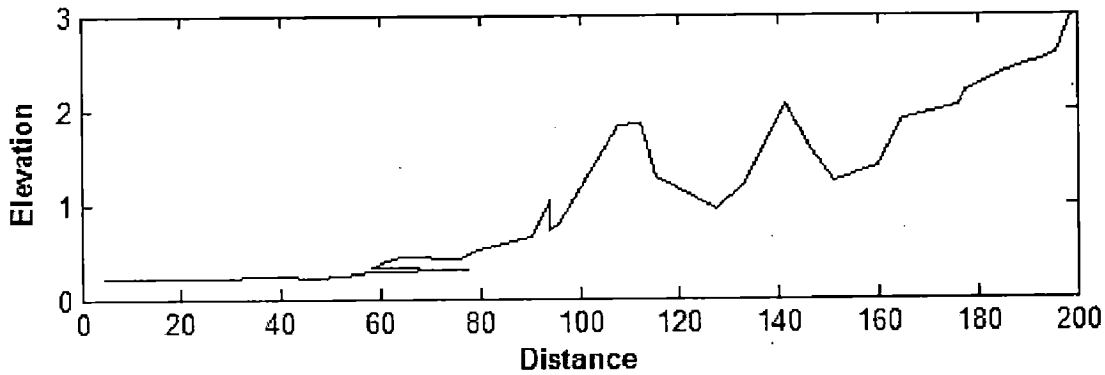

XDistance vs Elevation plot of 36 sites MT data

Fig.5.14Showing plot of Elevation VS X distance of 36 sites data in the frequency range 0.01 -2048s

5.5.1 Comparison of all modes obtained from the inversions of existing processed data by GERMC group with the reference model

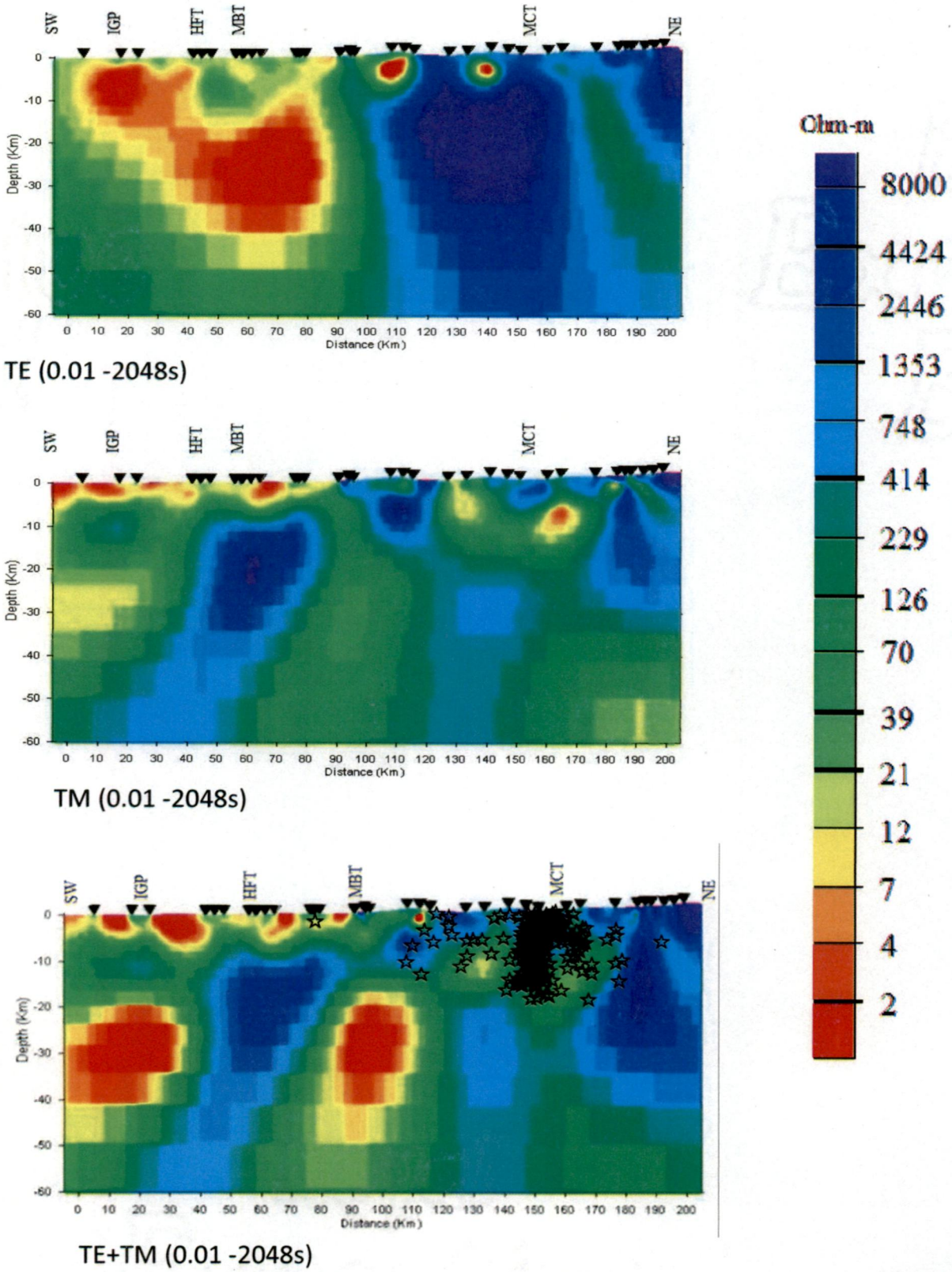

Fig.5.15All modes(TE, TM, TE+TM) of 36 sites MT data in the frequency range of 0.01 -2048s

5.5.2 Results

The TE model is not delineating the near surface conductivity features in the IGP region as well as the conductive channels in the resistive lithosphere region of the Higher Himalaya. The conductive features get distorted by galvanic distortion because of low frequency and shifted towards downwards. It is clear that TE mode is not suitable to delineate near surface conductive features as well as conductive channels in a high resistive area. But it is delineating the near surface resistive part of the Higher Himalayan. The comparison of TE model with reference model shows no matching. But in TM model the conductive structure up to 10 Km depth matching with the reference model but the conductive structure which lies 20Km to 40Km is not detected by the TM model. This is because of the screening effect of deep conductive structures which is due to long period data (0.01 – 2048s). It clearly infers that to study the vertical channels in a higher resistive lithosphere. The proper frequency range should be chosen otherwise there will be missing of this information. In TE+TM model the conductive body has been shifted to left this may be because of galvanic distortion (static shift) effect. As we are not studying the deeper part (i.e conductive part of the asthenosphere), it is better to take into account the TM model for the interpretational purpose of the study area.

5.6 Difference between the processed data of IITR Group and GERM Group

The following pot shows the comparison between the apparent resistivity and phase plot of IITR and GEMRC

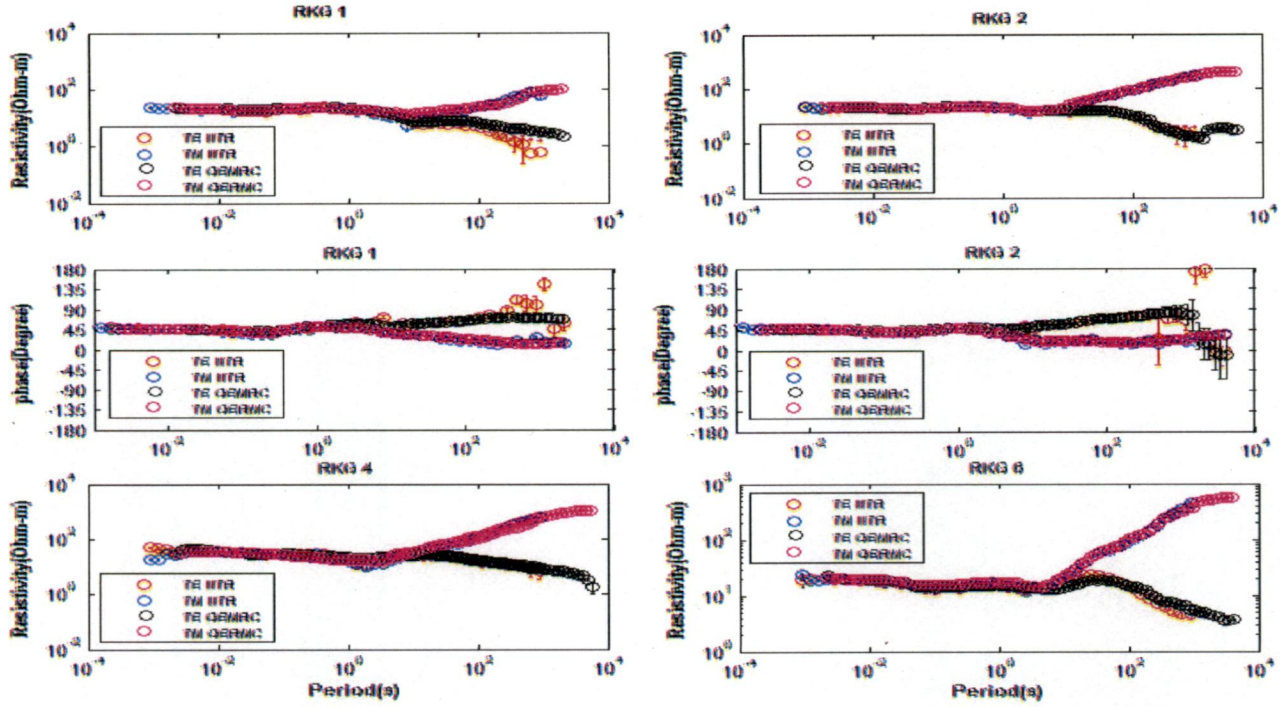
RKG 1
Resistivity(Ohm-m)
TE MTR
TM MTR
TE GEMRC
TM GERMC
RKG 2
RKG 1
phase(Degree)
RKG 2
RKG 4
RKG 6
Period(s)

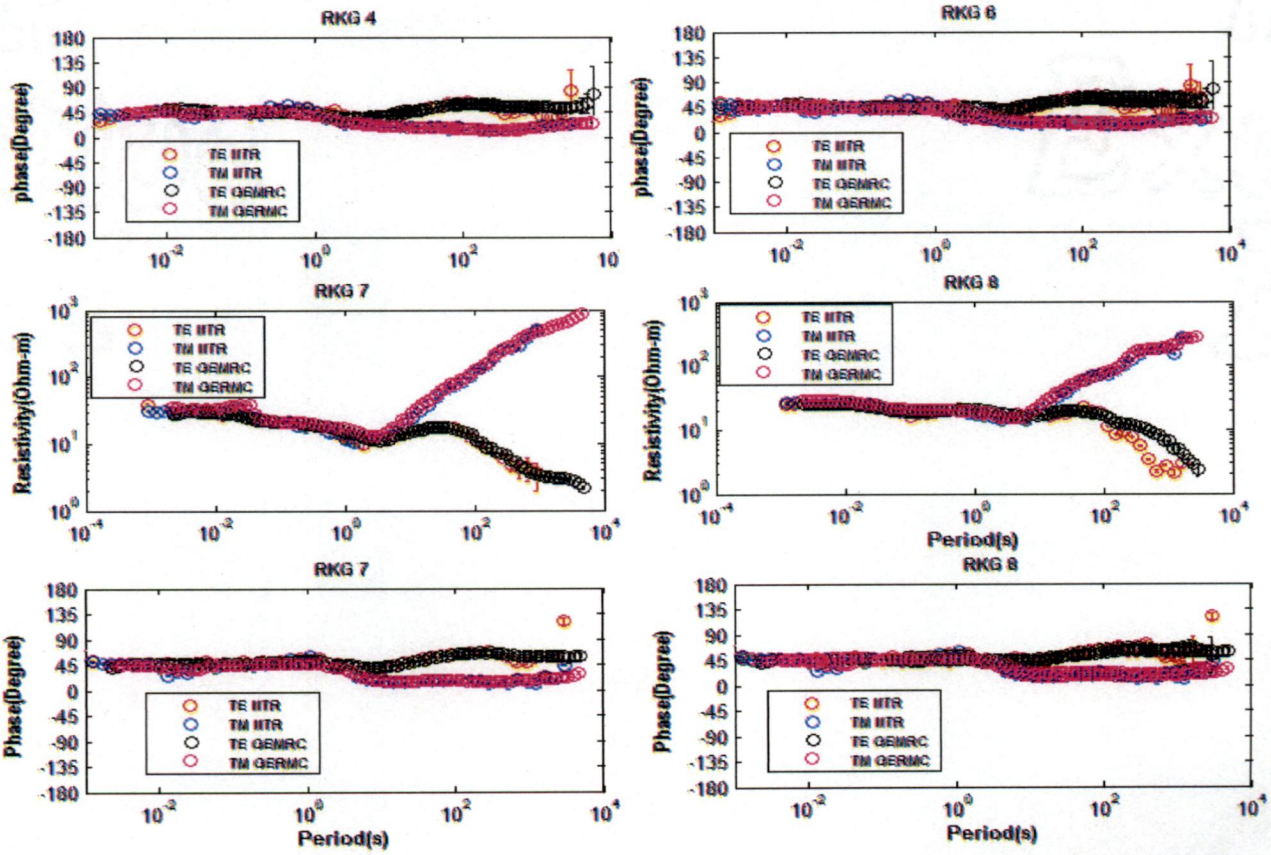
RKG 4
phase(Degree)
RKG 6
RKG 7
Resistivity(Ohm-m)
RKG 8
Period(s)
RKG 7
Phase(Degree)
RKG 8

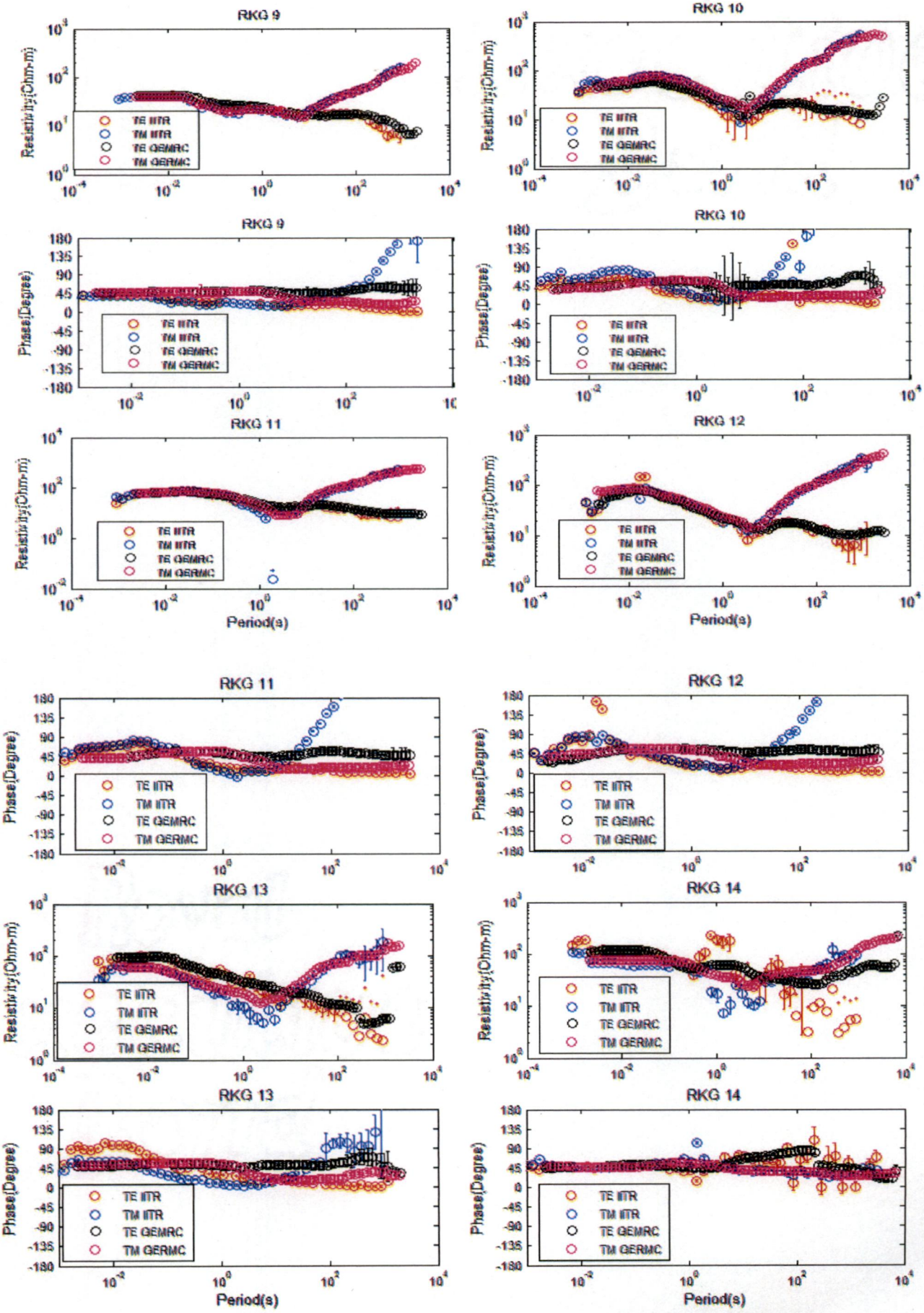
RKG 9
RKG 10
RKG 11
RKG 12
RKG 13
RKG 14
Resistivity(Ohm-m)
Phase(Degree)
Period(s)
TE IITR
TM IITR
TE GEMRC
TM GERMC

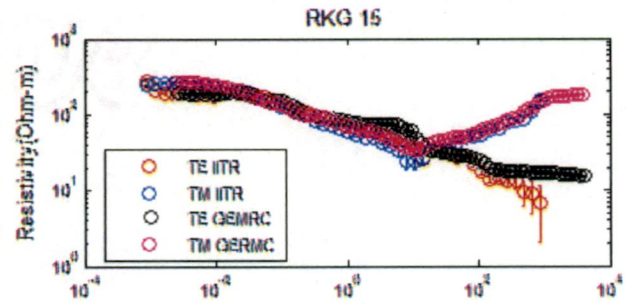
RKG 15
Resistivity(Ohm-m)
TE IITR
TM IITR
TE GEMRC
TM GERMC

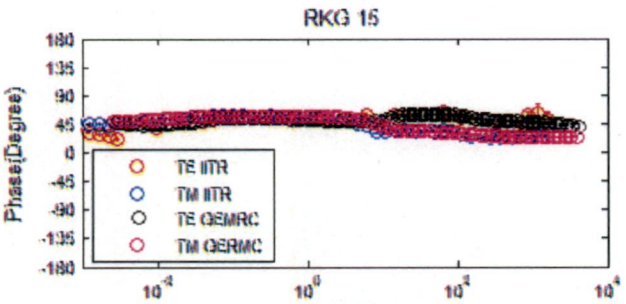
RKG 15
Phase(Degree)
TE IITR
TM IITR
TE GEMRC
TM GERMC

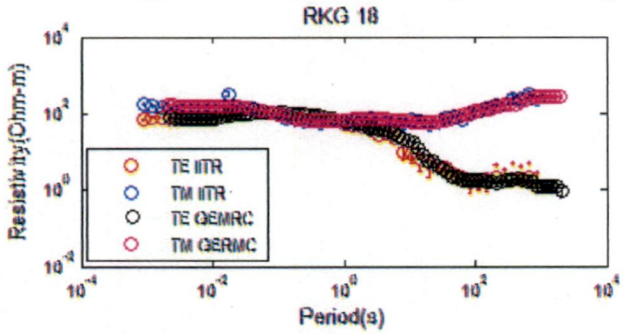
RKG 18
Resistivity(Ohm-m)
TE IITR
TM IITR
TE GEMRC
TM GERMC
Period(s)

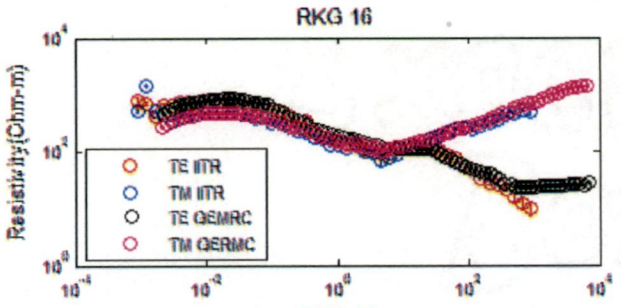
RKG 16
Resistivity(Ohm-m)
TE IITR
TM IITR
TE GEMRC
TM GERMC

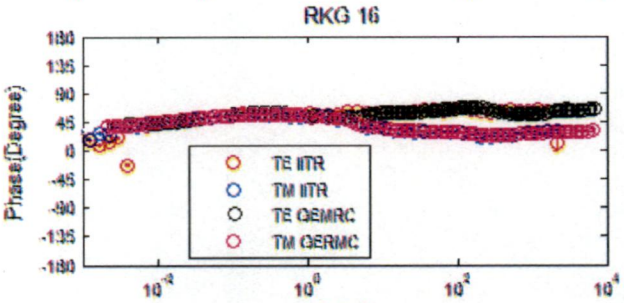
RKG 16
Phase(Degree)
TE IITR
TM IITR
TE GEMRC
TM GERMC

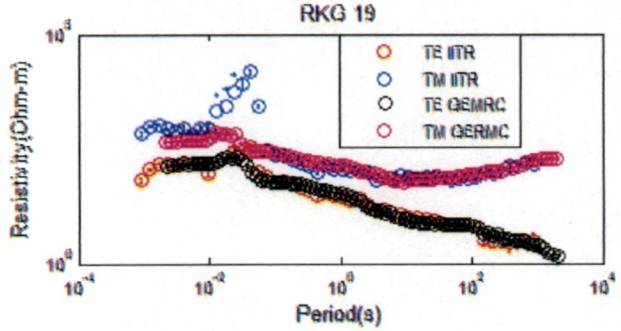
RKG 19
Resistivity(Ohm-m)
TE IITR
TM IITR
TE GEMRC
TM GERMC
Period(s)

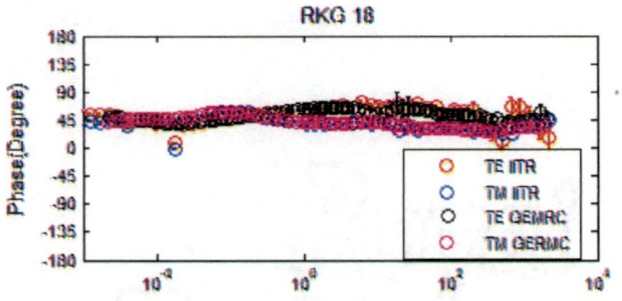
RKG 18
Phase(Degree)
TE IITR
TM IITR
TE GEMRC
TM GERMC

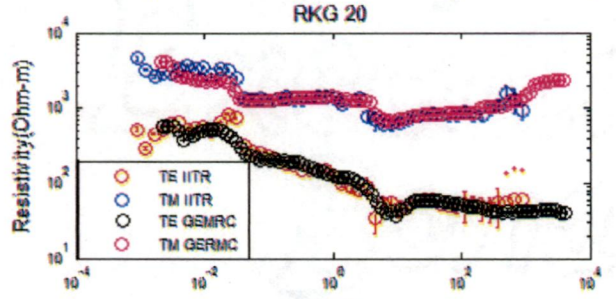
RKG 20
Resistivity(Ohm-m)
TE IITR
TM IITR
TE GEMRC
TM GERMC

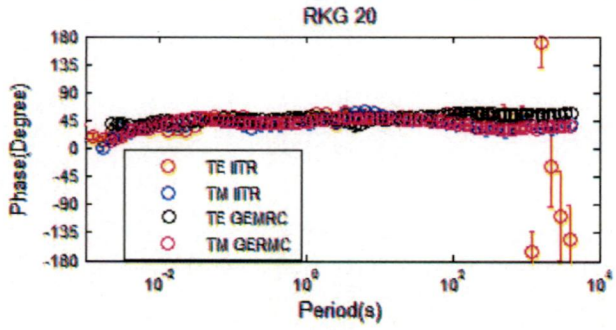
RKG 20
Phase(Degree)
TE IITR
TM IITR
TE GEMRC
TM GERMC
Period(s)

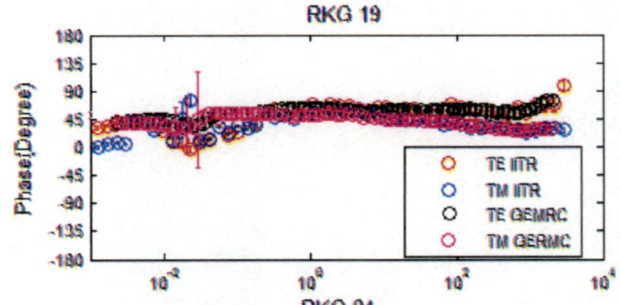
RKG 19
Phase(Degree)
TE IITR
TM IITR
TE GEMRC
TM GERMC

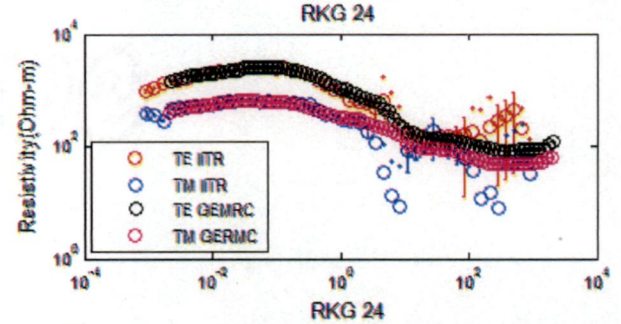
RKG 24
Resistivity(Ohm-m)
TE IITR
TM IITR
TE GEMRC
TM GERMC

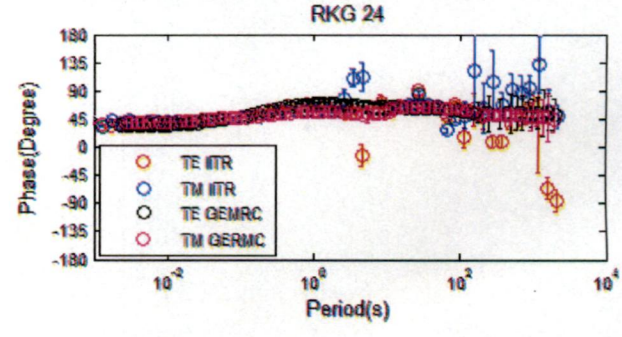
RKG 24
Phase(Degree)
TE IITR
TM IITR
TE GEMRC
TM GERMC
Period(s)

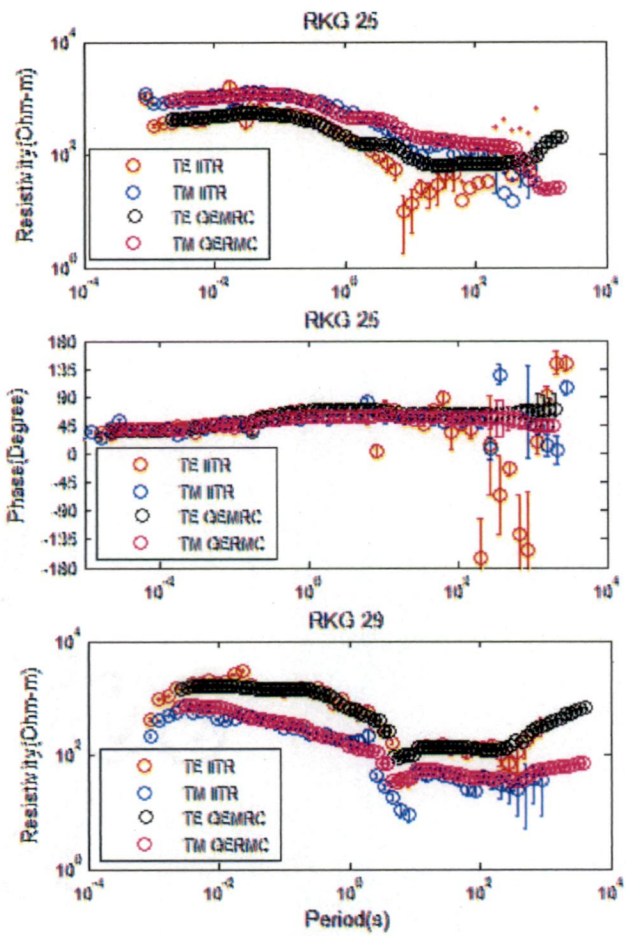
RKG 25
Resistivity(Ohm-m)
TE IITR
TM IITR
TE GEMRC
TM GERMC
RKG 25
Phase(Degree)
TE IITR
TM IITR
TE GEMRC
TM GERMC
RKG 29
Resistivity(Ohm-m)
TE IITR
TM IITR
TE GEMRC
TM GERMC
Period(s)

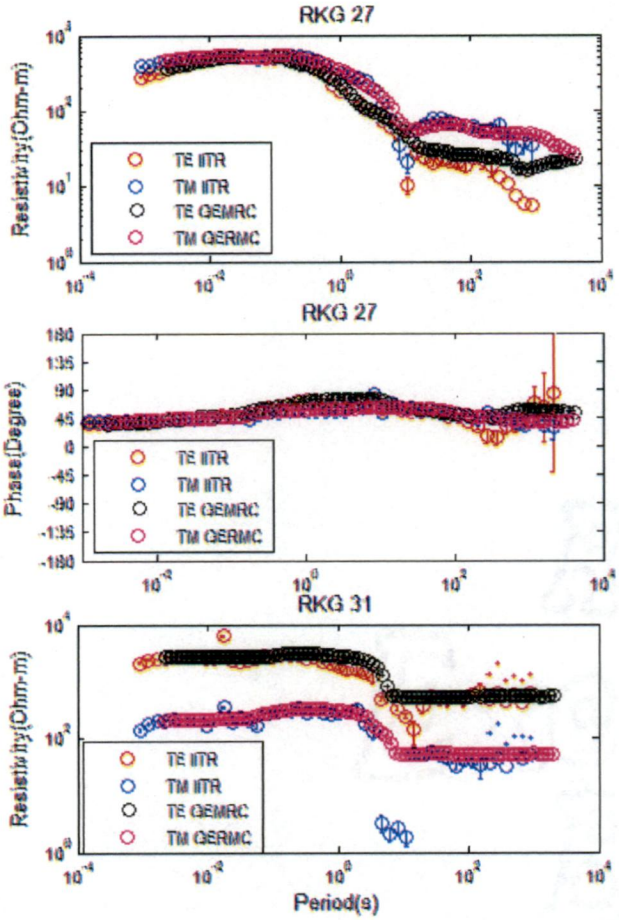
RKG 27
Resistivity(Ohm-m)
TE IITR
TM IITR
TE GEMRC
TM GERMC
RKG 27
Phase(Degree)
TE IITR
TM IITR
TE GEMRC
TM GERMC
RKG 31
Resistivity(Ohm-m)
TE IITR
TM IITR
TE GEMRC
TM GERMC
Period(s)

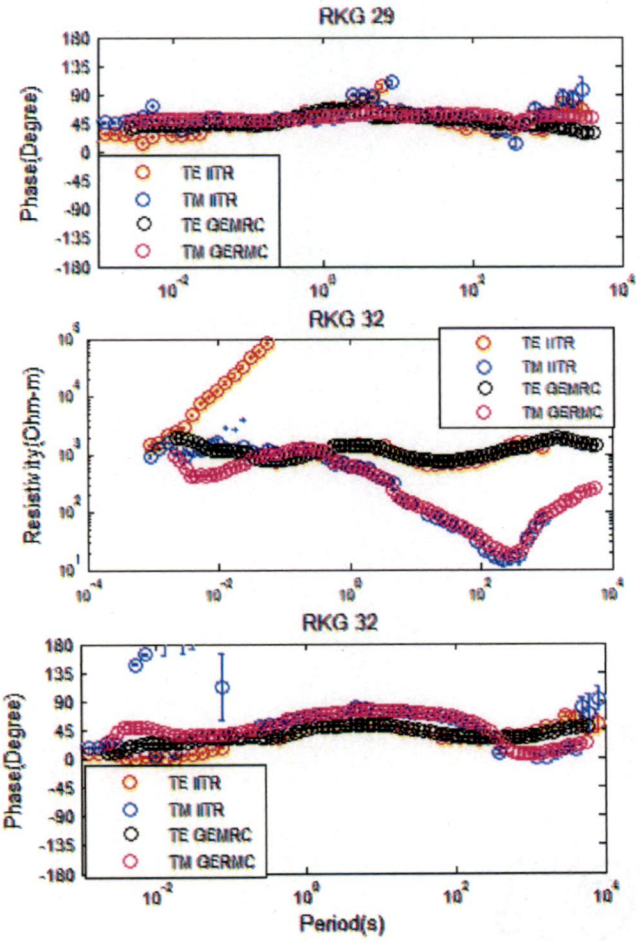
RKG 29
Phase(Degree)
TE IITR
TM IITR
TE GEMRC
TM GERMC
RKG 32
Resistivity(Ohm-m)
TE IITR
TM IITR
TE GEMRC
TM GERMC
RKG 32
Phase(Degree)
TE IITR
TM IITR
TE GEMRC
TM GERMC
Period(s)

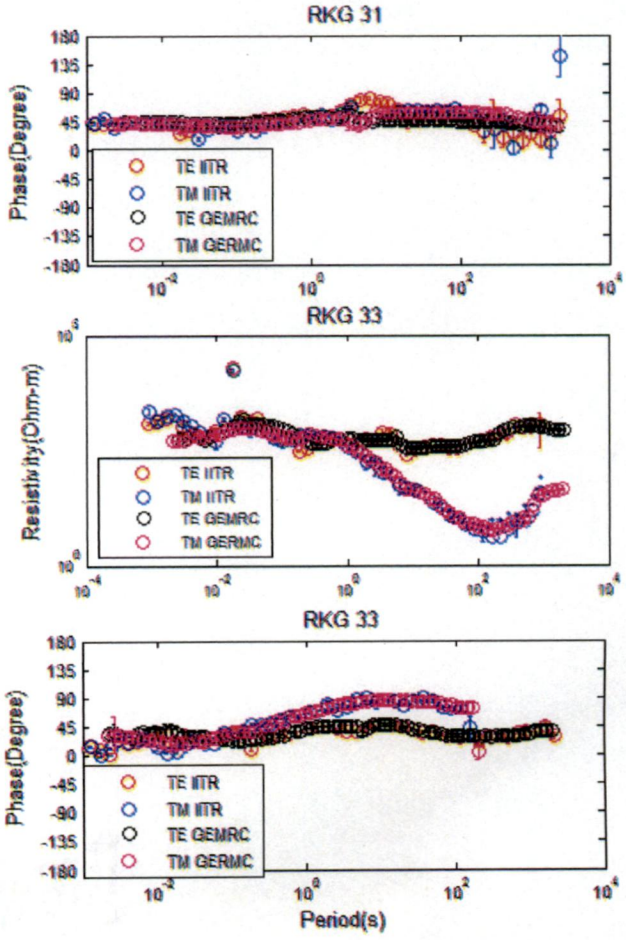
RKG 31
Phase(Degree)
TE IITR
TM IITR
TE GEMRC
TM GERMC
RKG 33
Resistivity(Ohm-m)
TE IITR
TM IITR
TE GEMRC
TM GERMC
RKG 33
Phase(Degree)
TE IITR
TM IITR
TE GEMRC
TM GERMC
Period(s)

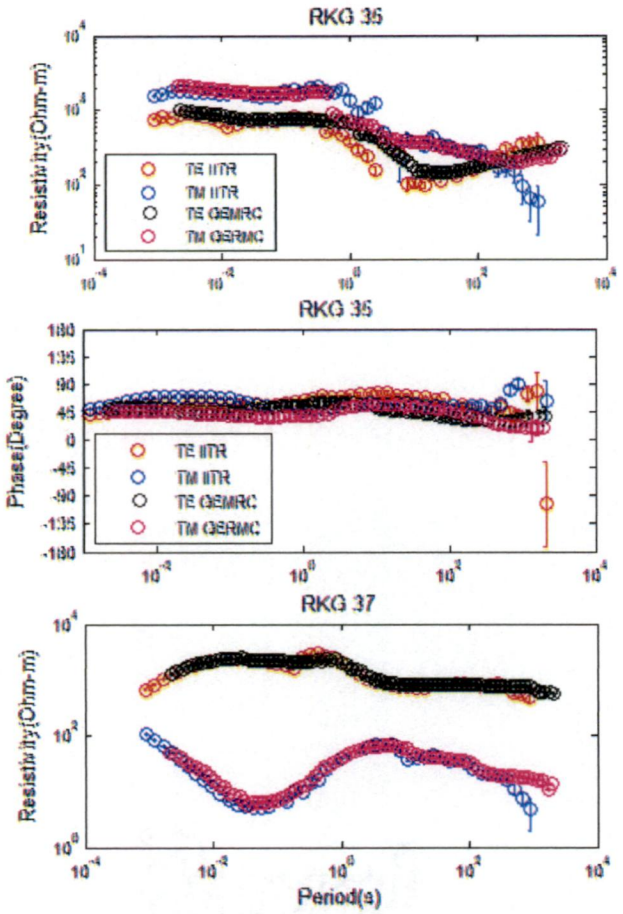
RKG 35
Resistivity(Ohm-m)
TE IITR
TM IITR
TE GEMRC
TM GERMC
RKG 35
Phase(Degree)
TE IITR
TM IITR
TE GEMRC
TM GERMC
RKG 37
Resistivity(Ohm-m)
Period(s)

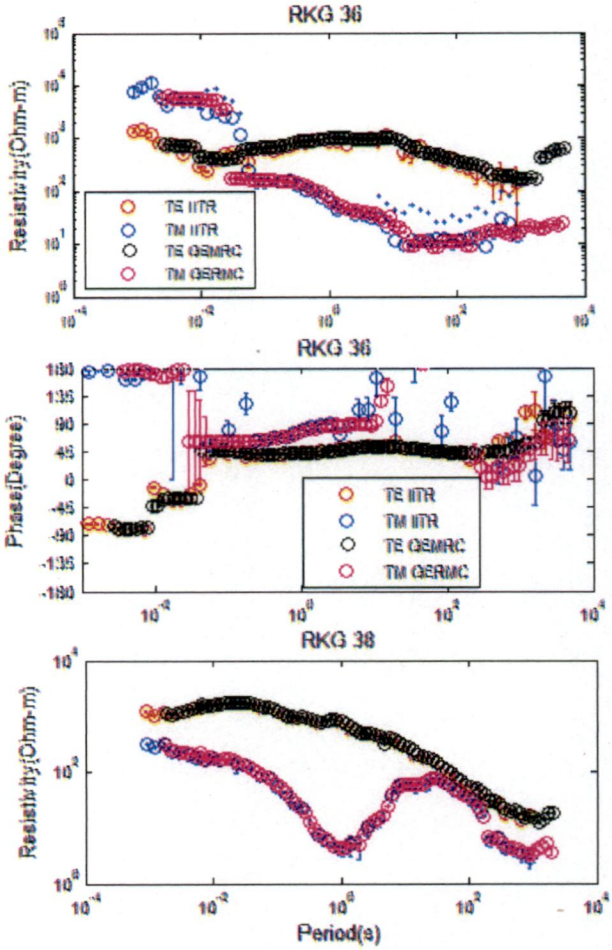
RKG 36
Resistivity(Ohm-m)
TE IITR
TM IITR
TE GEMRC
TM GERMC
RKG 36
Phase(Degree)
TE IITR
TM IITR
TE GEMRC
TM GERMC
RKG 38
Resistivity(Ohm-m)
Period(s)

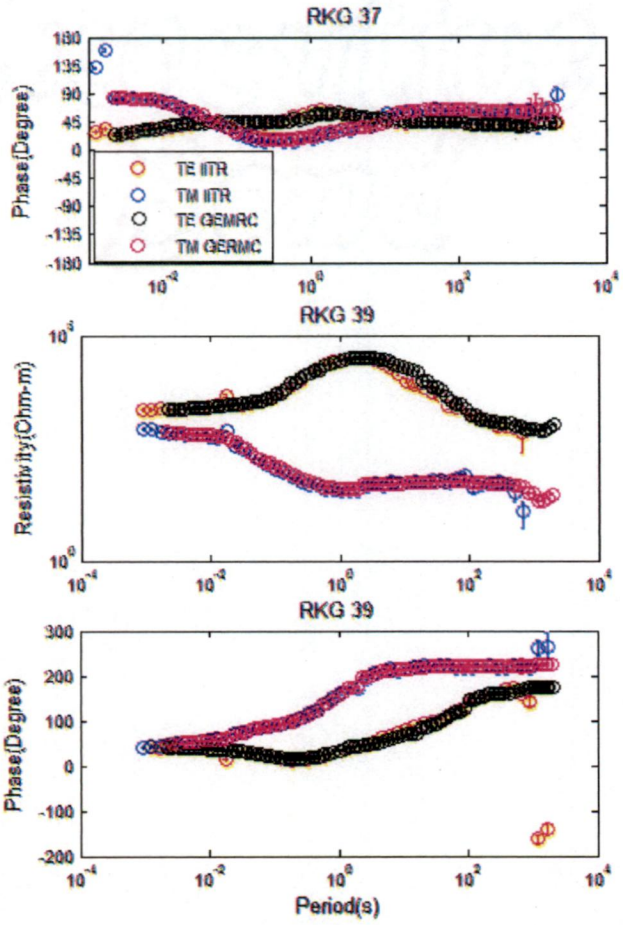
RKG 37
Phase(Degree)
TE IITR
TM IITR
TE GEMRC
TM GERMC
RKG 39
Resistivity(Ohm-m)
RKG 39
Phase(Degree)
Period(s)

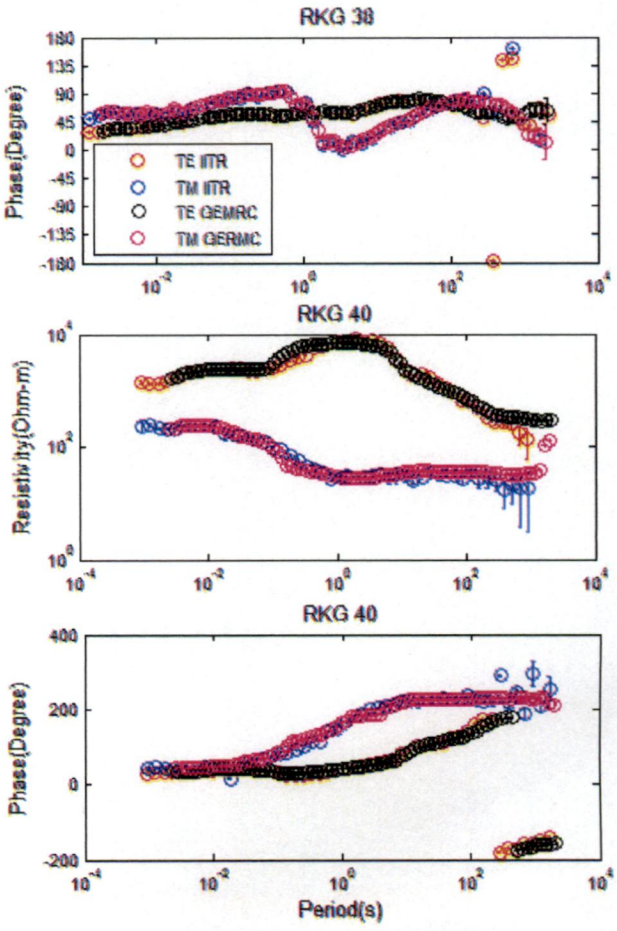
RKG 38
Phase(Degree)
TE IITR
TM IITR
TE GEMRC
TM GERMC
RKG 40
Resistivity(Ohm-m)
RKG 40
Phase(Degree)
Period(s)

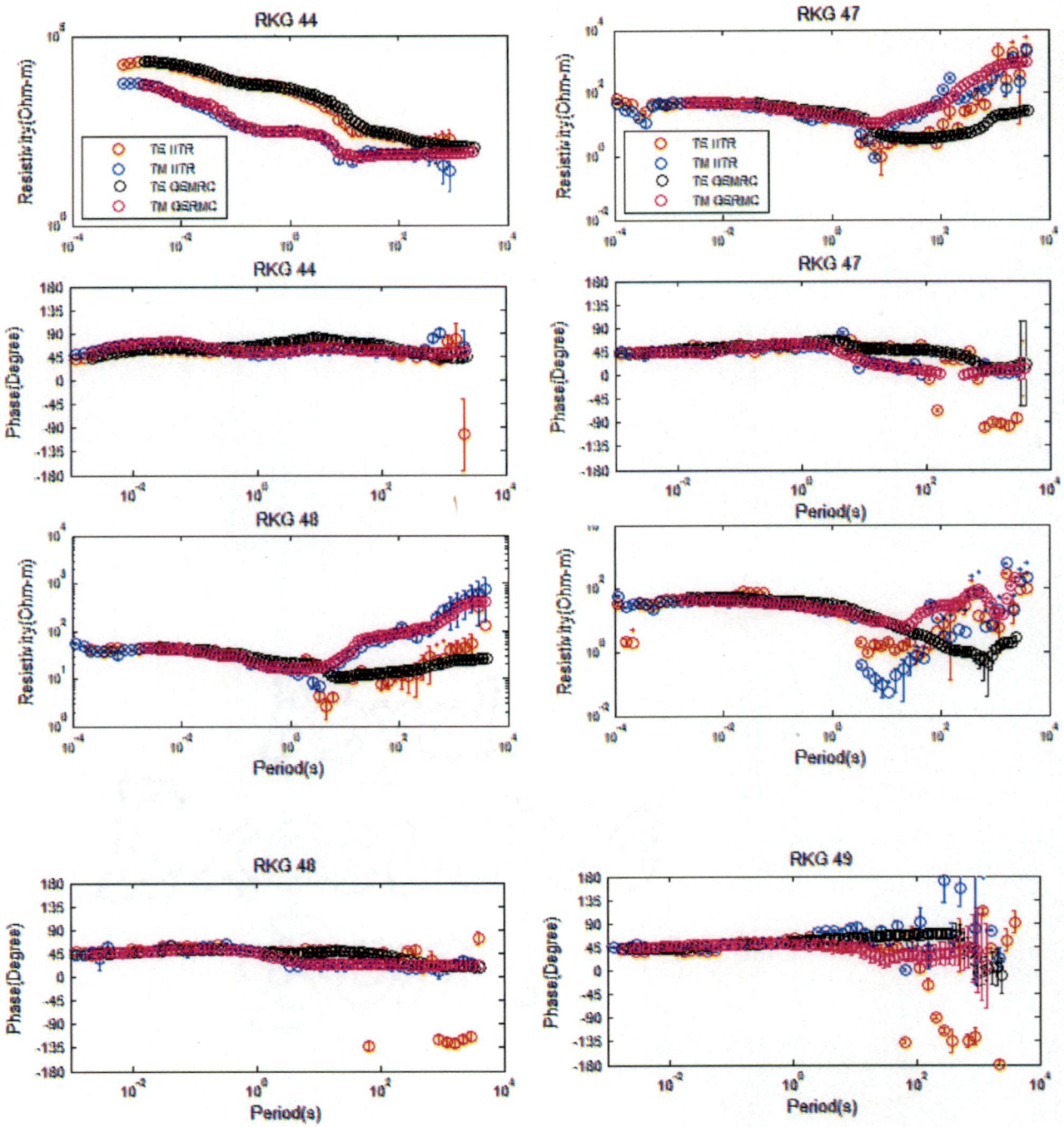

Fig.5.16Shows the comparison plots of the data processed by IITR Group and GERMC Group

The comparison plots of the data processed by IITR and GERMC Group shows that more smooth data value is present in the data processed by GERMC Group

5.7 Averaging of the 33 sites data (Processed by IIT Roorkee Group) using different methods

In order to smooth the data, the averaging has been done over the grouped adjacent sites. The groped sites are (48,50), (47), (1,3,2,4), (6,7,8,9), (10,11,12), (13,14,15,16), (18,19,20), (24,25,26), (27,29,31), (32,34), (35), (37), (43,44).

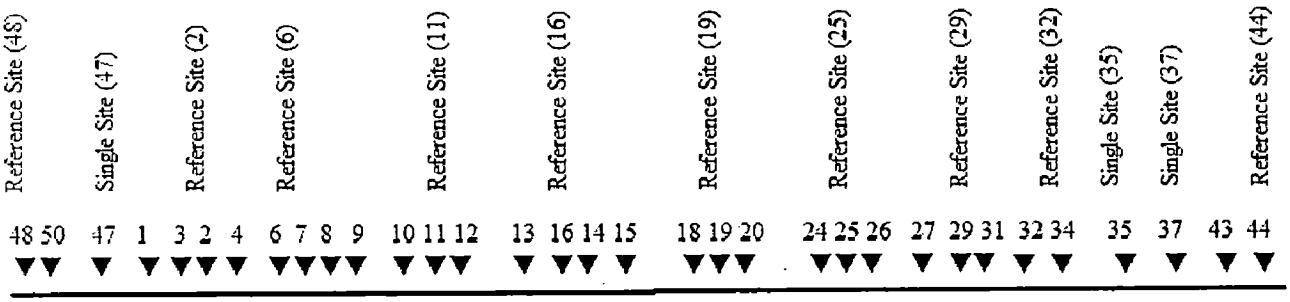

Fig.5.17Showing the 13 grouped sites that have been taken for the averaging purpose and their reference sites

The four following different averaging methods have been used to reduce the spreading of data values.

(a) Weighted average using spacing between sites with respect to reference site as weight

(b) Weighted average using corresponding error as weight

(c) Median

(d) Simple average of the data

5.7.1 Procedures for weighted spacing average

Out of given sites one site which has smoothest trend is taken as reference site. Absolute spacing (weights) of different sites is calculated with respect to the reference site. If the absolute value of the spacing is less than one then it is considered as 1and weight corresponding to reference site is assigned as 1.

Formula used for weighted average of resistivity

$$Rav. = \frac{\sum \frac{\rho i}{wi}}{\sum \frac{1}{wi}} \qquad 5.1$$

Formula used for weighted average of phase

$$Pav. = \frac{\sum \frac{pi}{wi}}{\sum \frac{1}{wi}} \qquad 5.2$$

SR. NO	GROUPED SITES	REFERENCE SITES	SPACING WITH RESPECT TO REFERENCE SITE
1	48,50	48	R1 =1 (weight for reference site) R2 =abs(station location of 48 - station location of 50) = 0.44 (1)
2	47	47	
3	1, 2, 3, 4	2	R1=abs(station location of 2- station location of 1)= 2.9 R2 =1 (weight for reference site) R3 =abs(station location of 2- station location of 3)= 0.23 (1) R4 =abs(station location of 2- station location of 4)= 3.19
4	6, 7, 8, 9	6	R1 =1 (weight for reference site); R2 =abs(station location of 6- station location of 7)= 1.99 R3 =abs(station location of 6- station location of 8)= 2.4 R2 =abs(station location of 6- station location of 9)= 5.2
5	10, 11, 12	11	R1 =abs(station location of 11- station location of 10)= 1.08 R2 =1 (weight for reference site); R3 =abs(station location of 11- station location of 12)= 1.96
6	13, 14, 15, 16	15	R1 =abs(station location of 15- station location of 13)= 4.7 R2 =abs(station location of 15- station location of 14)= 1.3 R3 =1 (weight for reference site) R3 =abs(station location of 15- station location of 16)= 1.5
7	18, 19, 20	18	R1 =1 (weight for reference site); R2 =abs(station location of 18- station location of 19)= 4.31 R3 =abs(station location of 18- station location of 20)= 7.72
8	24, 25, 26	25	R1 =abs(station location of 25- station location of 24)= 6.14 R2 =1 (weight for reference site); R3 =abs(station location of 25- station location of 26)= 33.2
9	27, 29, 31	27	R1 =1 (weight for reference site); R2 =abs(station location of 27- station location of 29)= 5.52 R3 =abs(station location of 27- station location of 31)= 9.84
10	32, 34	34	R2 =1 (weight for reference site); R1 =abs(station location of 32 - station location of 34)= 6.84
11	35	35	
12	37	37	
13	43, 44	44	R1 =abs(station location of 44- station location of 43)= 0.87 (1) R2 =1 (weight for reference site);

Table 5.5 Showing the calculation of spacing of different sites with respect to reference site in each grouped site

5.7.2 Procedures for weighted error average

In this case error corresponding to resistivity and phase is taken as weight for calculation of average resistivity and phase.

Let us consider a grouped site consisting of 3 sites for the averaging purpose. Let ρ1, ρ2, ρ3 are resistivities of three sites at a particular time and e1, e2, e3 are their corresponding errors. So, the formula for the weighted error average will be

$$(\rho 1/e1 + \rho 2/e2 + \rho 3/e3) \,/\, (1/e1 + 1/e2 + 1/e3)$$

Similarly let p1, p2 and p3 are phases of three sites at that same time and e1, e2 and e3 are their corresponding errors. So, the formula for weighted average phase can be written as

$$(p1/e1 + p2/e2 + p3/e3) \,/\, (1/e1 + 1/e2 + 1/e3)$$

So, the generalized formula for weighted average resistivity and phase can be written as

$$Rav. = \sum(\rho i/ei)/\sum(1/ei) \qquad 5.3$$

$$Pav. = \sum(pi/ei)/\sum(1/ei) \qquad 5.4$$

5.7.3 Procedures for median

Median values of grouped site data has been taken

5.7.4 Procedures for simple average

Simple average of grouped site data has been taken

5.7.5 Plotting of 4 sets of grouped averaged data

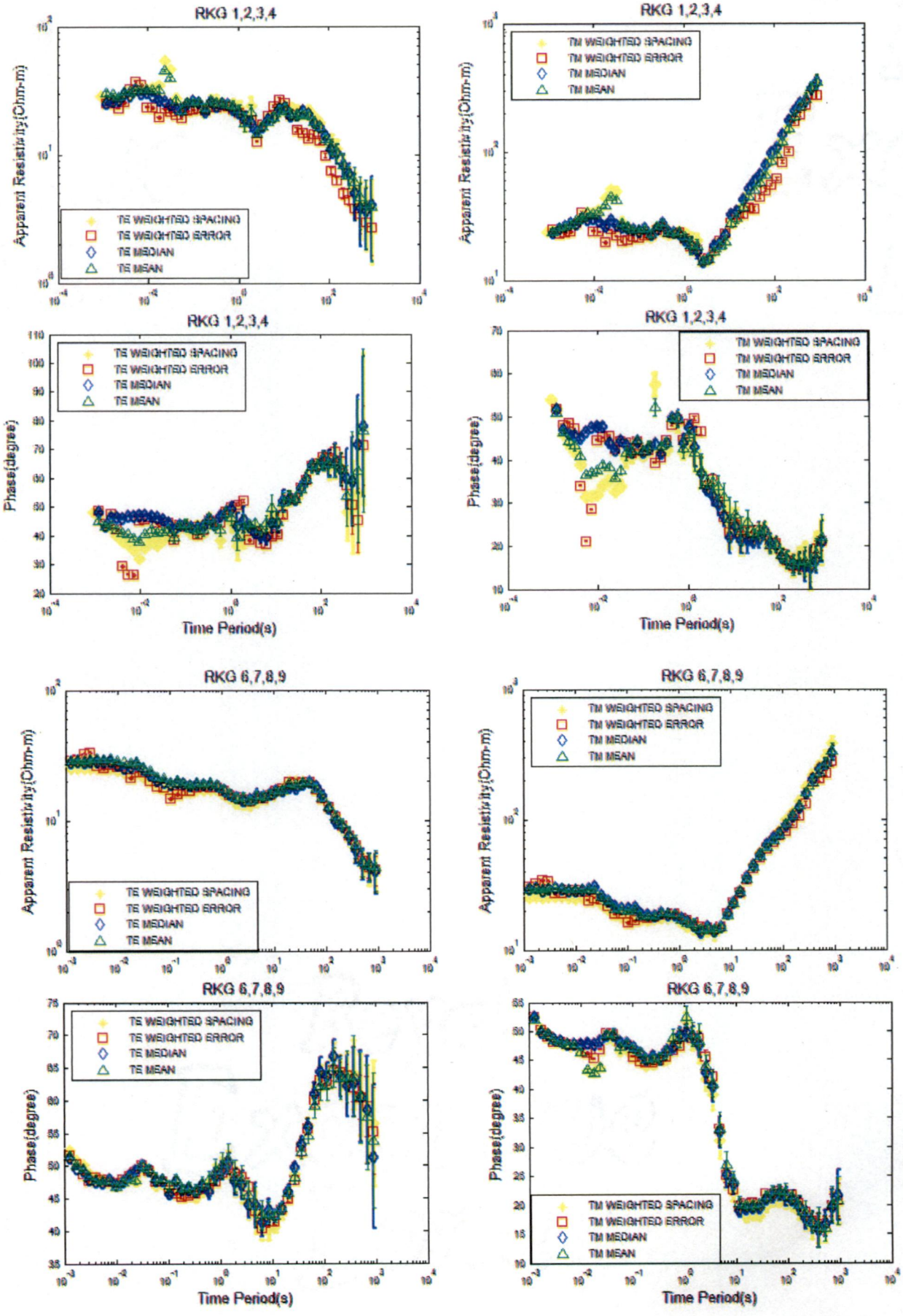

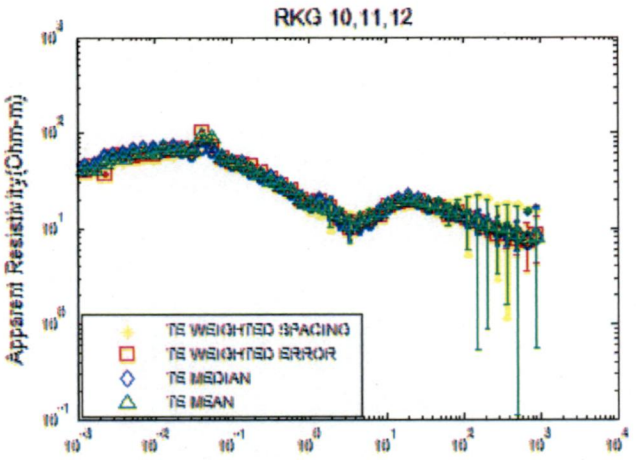
RKG 10,11,12
Apparent Resistivity(Ohm-m)
TE WEIGHTED SPACING
TE WEIGHTED ERROR
TE MEDIAN
TE MEAN

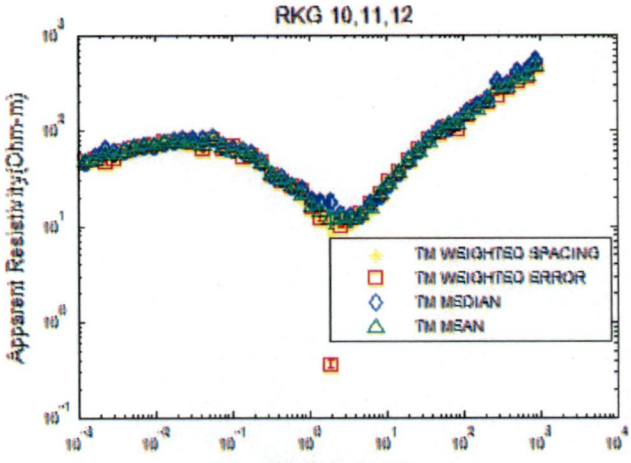
RKG 10,11,12
Apparent Resistivity(Ohm-m)
TM WEIGHTED SPACING
TM WEIGHTED ERROR
TM MEDIAN
TM MEAN

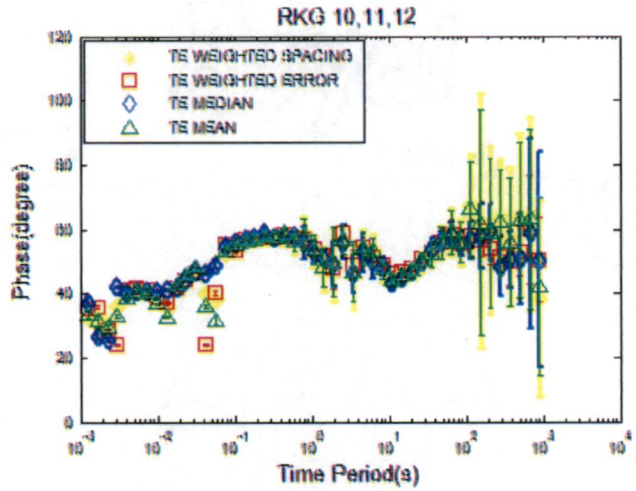
RKG 10,11,12
Phase(degree)
TE WEIGHTED SPACING
TE WEIGHTED ERROR
TE MEDIAN
TE MEAN
Time Period(s)

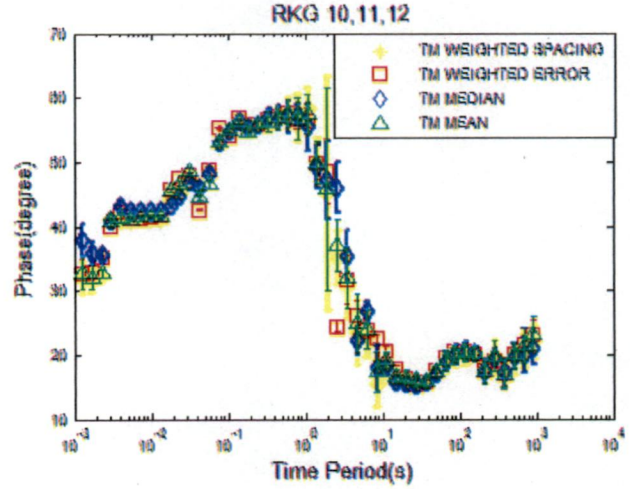
RKG 10,11,12
Phase(degree)
TM WEIGHTED SPACING
TM WEIGHTED ERROR
TM MEDIAN
TM MEAN
Time Period(s)

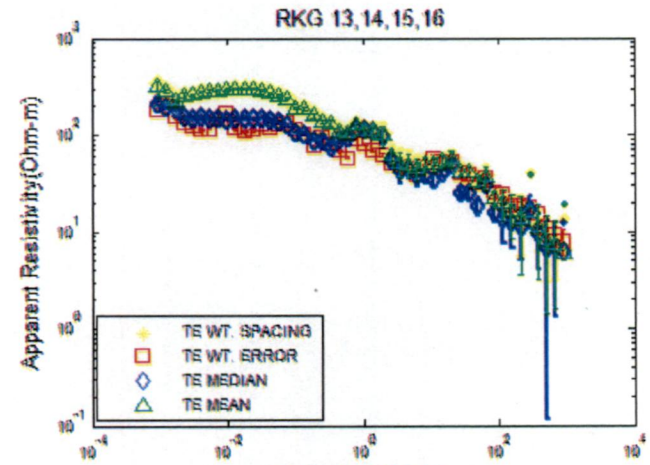
RKG 13,14,15,16
Apparent Resistivity(Ohm-m)
TE WT. SPACING
TE WT. ERROR
TE MEDIAN
TE MEAN

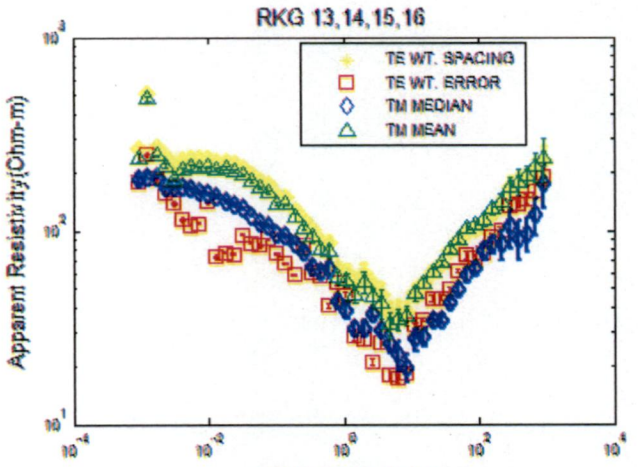
RKG 13,14,15,16
Apparent Resistivity(Ohm-m)
TE WT. SPACING
TE WT. ERROR
TM MEDIAN
TM MEAN

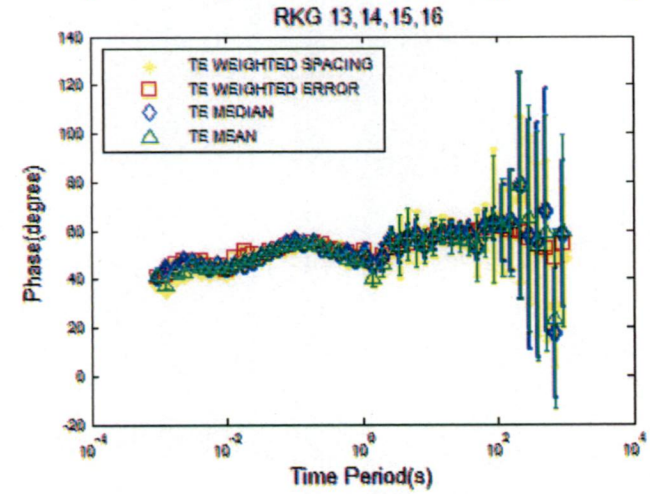
RKG 13,14,15,16
Phase(degree)
TE WEIGHTED SPACING
TE WEIGHTED ERROR
TE MEDIAN
TE MEAN
Time Period(s)

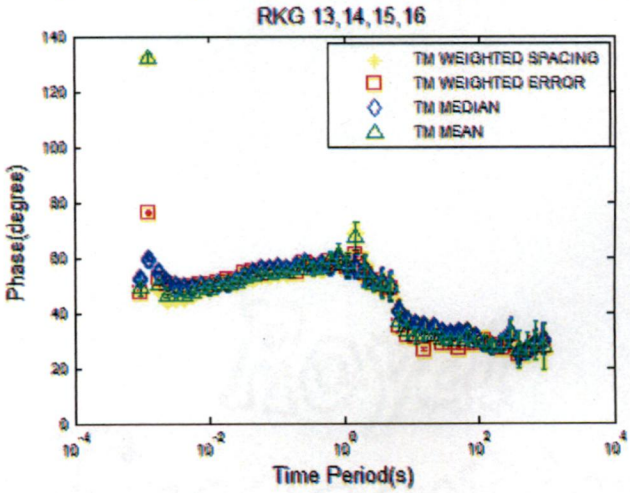
RKG 13,14,15,16
Phase(degree)
TM WEIGHTED SPACING
TM WEIGHTED ERROR
TM MEDIAN
TM MEAN
Time Period(s)

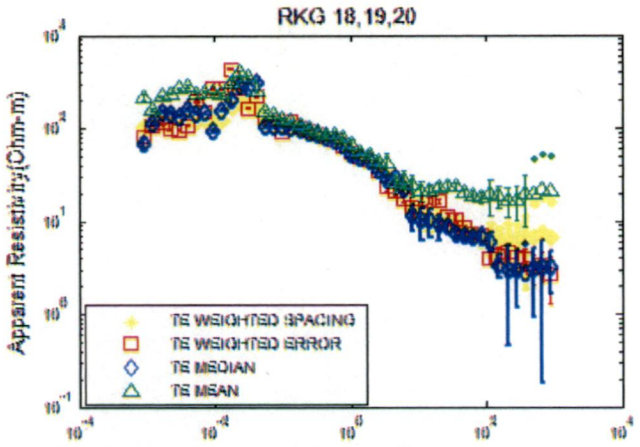
RKG 18,19,20
Apparent Resistivity(Ohm-m)
TE WEIGHTED SPACING
TE WEIGHTED ERROR
TE MEDIAN
TE MEAN

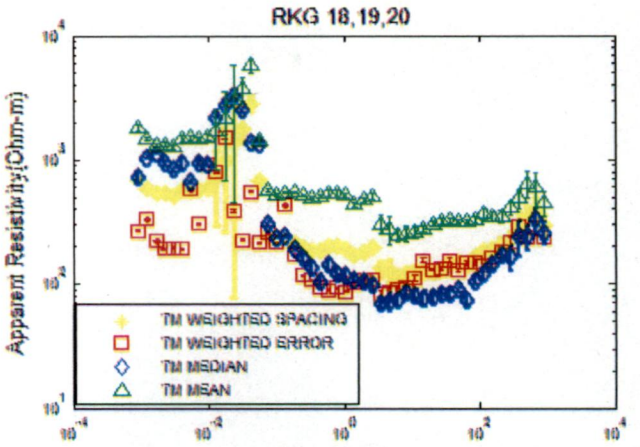
RKG 18,19,20
Apparent Resistivity(Ohm-m)
TM WEIGHTED SPACING
TM WEIGHTED ERROR
TM MEDIAN
TM MEAN

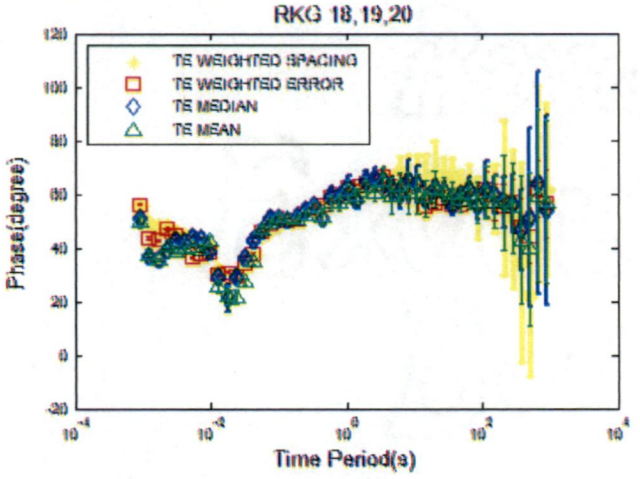
RKG 18,19,20
Phase(degree)
Time Period(s)
TE WEIGHTED SPACING
TE WEIGHTED ERROR
TE MEDIAN
TE MEAN

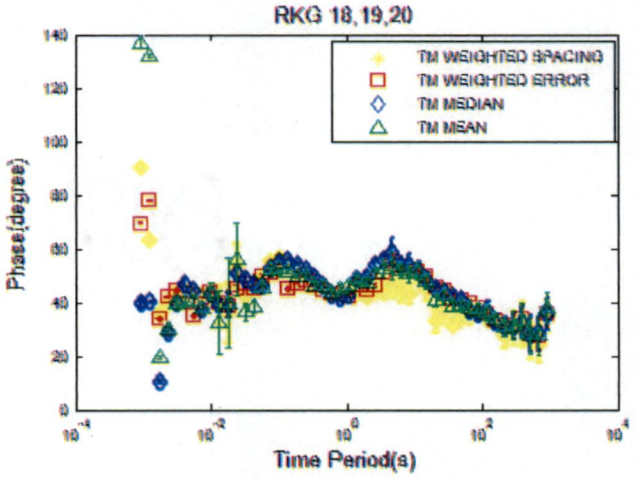
RKG 18,19,20
Phase(degree)
Time Period(s)
TM WEIGHTED SPACING
TM WEIGHTED ERROR
TM MEDIAN
TM MEAN

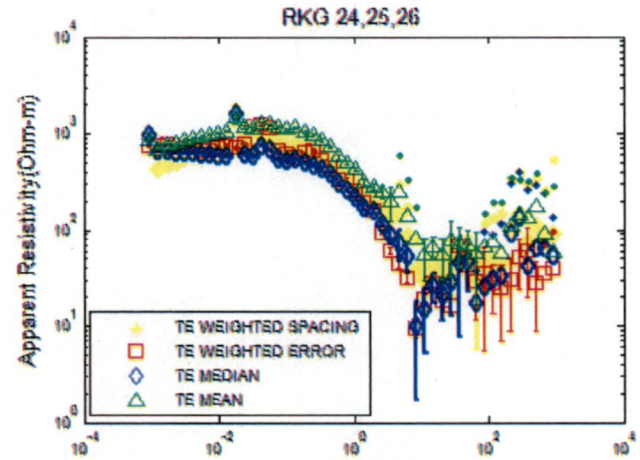
RKG 24,25,26
Apparent Resistivity(Ohm-m)
TE WEIGHTED SPACING
TE WEIGHTED ERROR
TE MEDIAN
TE MEAN

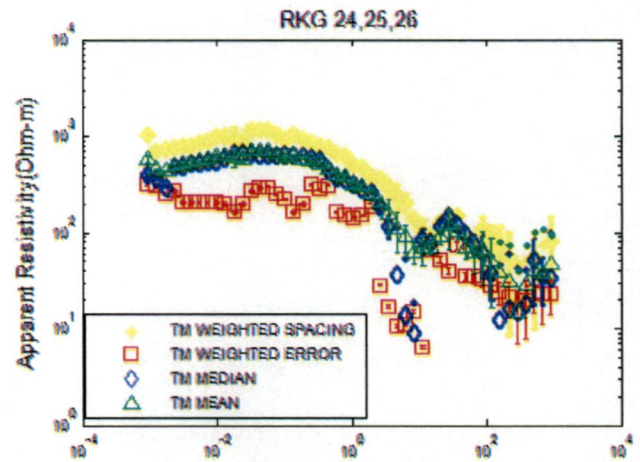
RKG 24,25,26
Apparent Resistivity(Ohm-m)
TM WEIGHTED SPACING
TM WEIGHTED ERROR
TM MEDIAN
TM MEAN

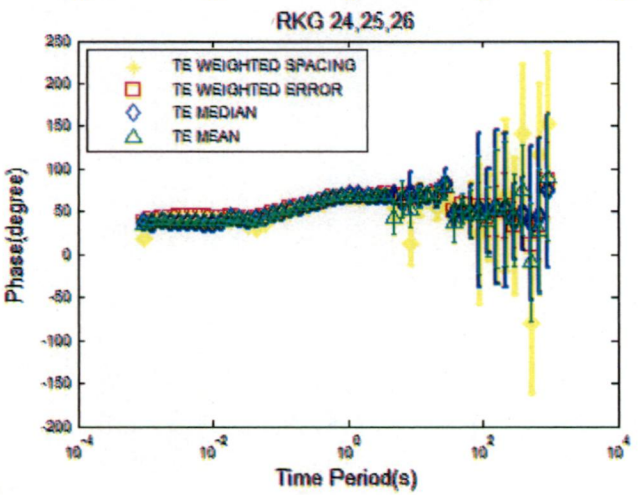
RKG 24,25,26
Phase(degree)
Time Period(s)
TE WEIGHTED SPACING
TE WEIGHTED ERROR
TE MEDIAN
TE MEAN

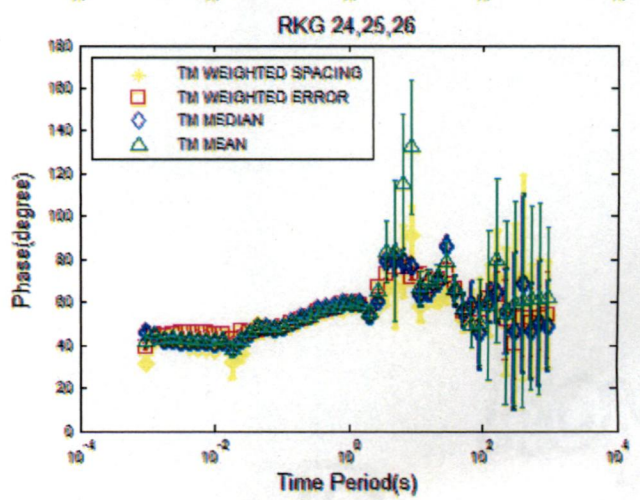
RKG 24,25,26
Phase(degree)
Time Period(s)
TM WEIGHTED SPACING
TM WEIGHTED ERROR
TM MEDIAN
TM MEAN

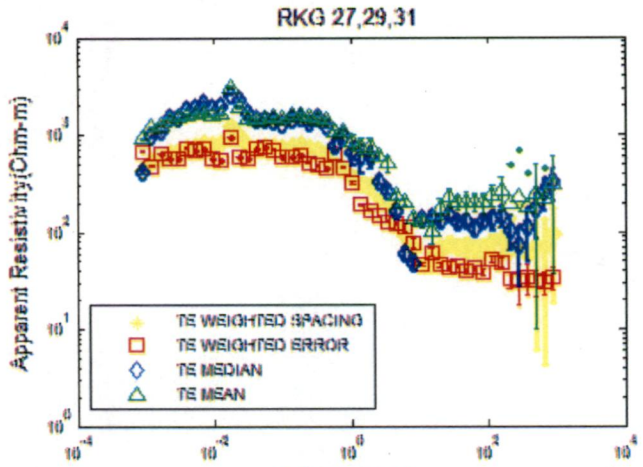
RKG 27,29,31
Apparent Resistivity(Ohm-m)
TE WEIGHTED SPACING
TE WEIGHTED ERROR
TE MEDIAN
TE MEAN

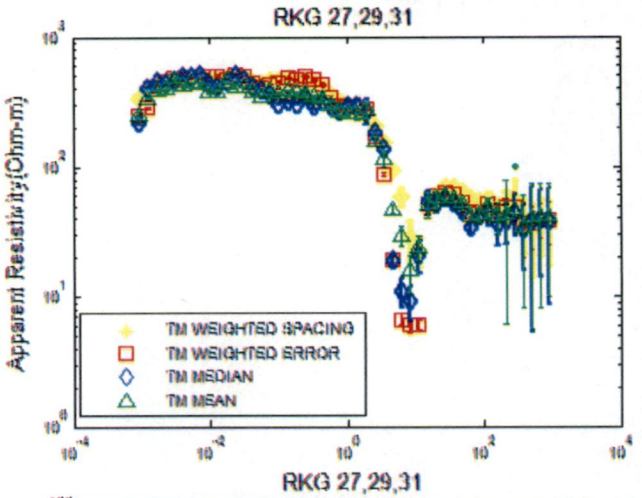
RKG 27,29,31
Apparent Resistivity(Ohm-m)
TM WEIGHTED SPACING
TM WEIGHTED ERROR
TM MEDIAN
TM MEAN

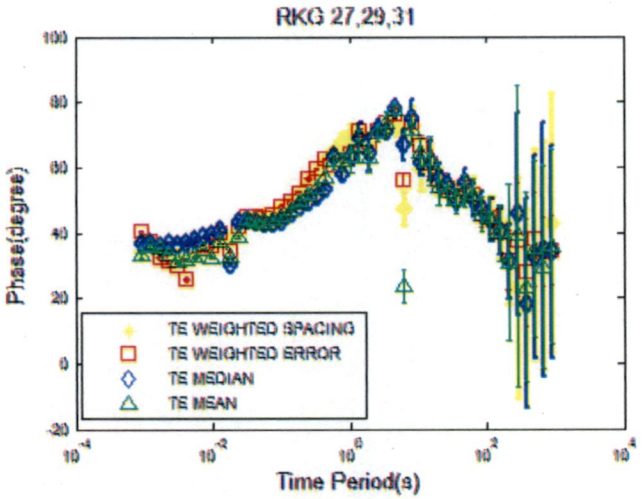
RKG 27,29,31
Phase(degree)
TE WEIGHTED SPACING
TE WEIGHTED ERROR
TE MEDIAN
TE MEAN
Time Period(s)

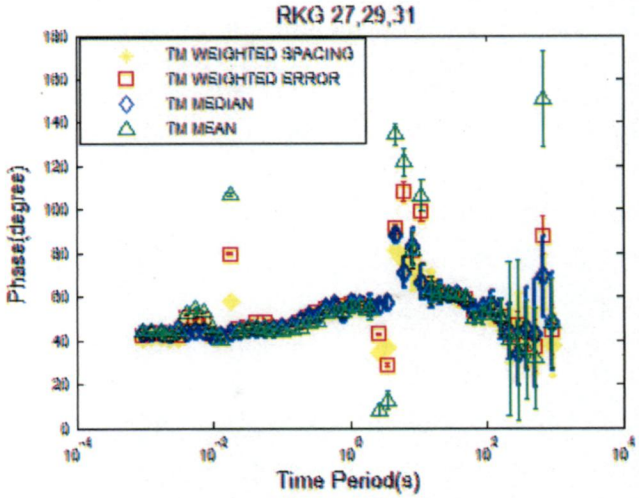
RKG 27,29,31
Phase(degree)
TM WEIGHTED SPACING
TM WEIGHTED ERROR
TM MEDIAN
TM MEAN
Time Period(s)

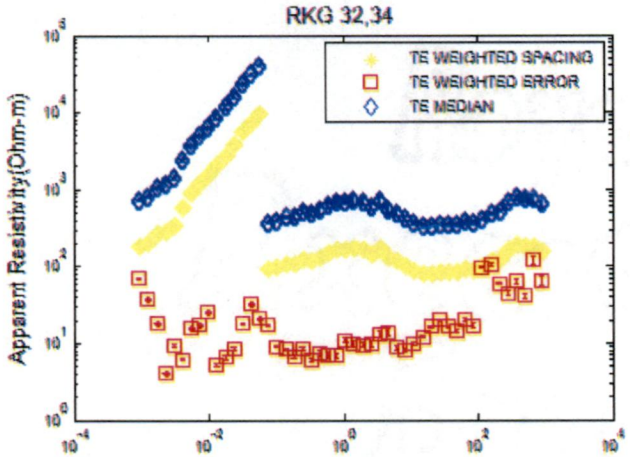
RKG 32,34
Apparent Resistivity(Ohm-m)
TE WEIGHTED SPACING
TE WEIGHTED ERROR
TE MEDIAN

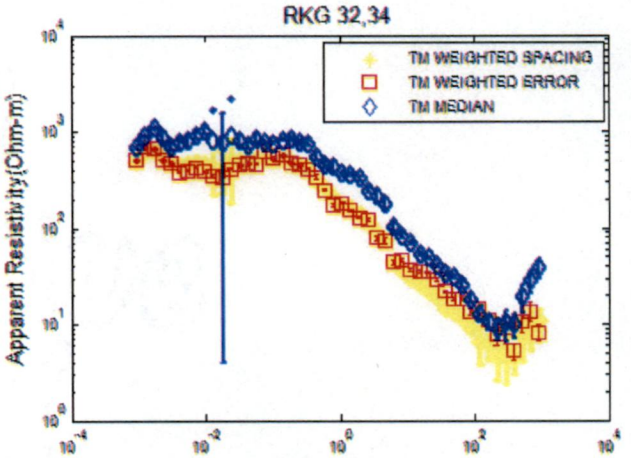
RKG 32,34
Apparent Resistivity(Ohm-m)
TM WEIGHTED SPACING
TM WEIGHTED ERROR
TM MEDIAN

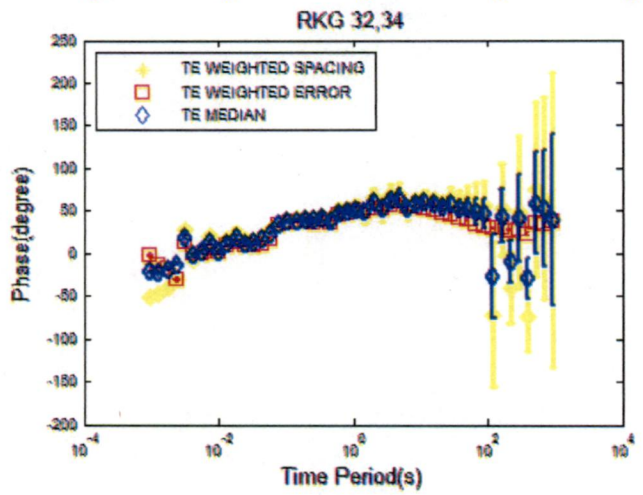
RKG 32,34
Phase(degree)
TE WEIGHTED SPACING
TE WEIGHTED ERROR
TE MEDIAN
Time Period(s)

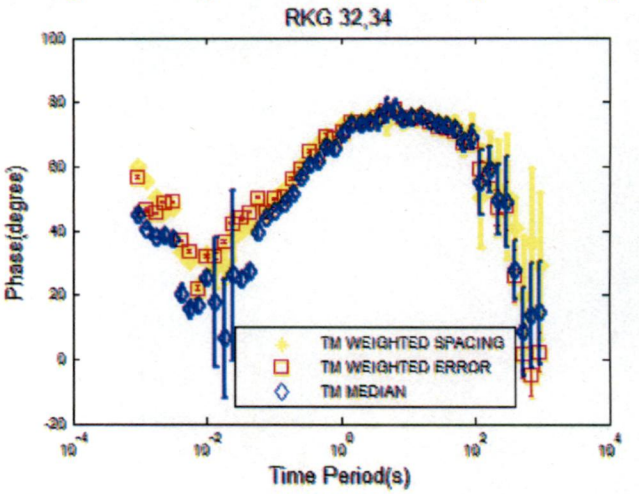
RKG 32,34
Phase(degree)
TM WEIGHTED SPACING
TM WEIGHTED ERROR
TM MEDIAN
Time Period(s)

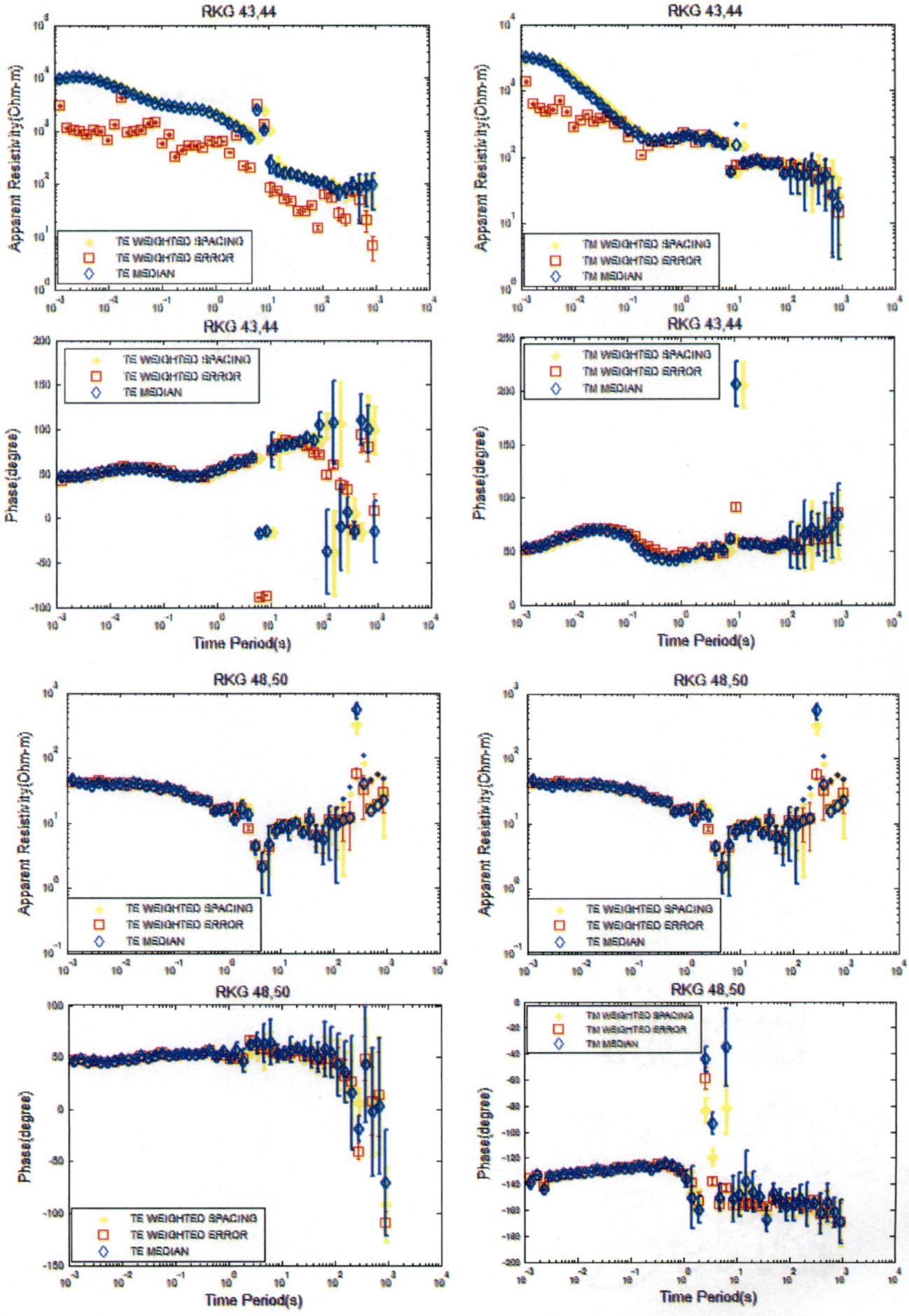

Fig.5.18Plotting of 4 Sets of Grouped Averaged Data

Out of four different averaged methods the above plot shows the maximum smoothness of the data value is achieved from Median method of averaging.

5.8 Creation of EDI files and inversions of 4 sets of averaged data

After averaging the grouped sites, the data obtained was in the dat file format. As for the data reading purpose in WinGlink, the dat file format data has been converted to EDI file format with the help of MATLAB. Then 2D inversion has been applied on the 4 sets of 13 EDI files to study the conductivity structures of the study area. The matlab code that has been used to convert dat file to EDI file format has been given below.

```
clear all
clc
fileID_1 = fopen('rkg29.edi');
load site27mdrkg.txt;
fid = fopen('rkg29n_new.edi', 'w');
cLine = fgets(fileID_1);
fprintf(fid, '%s', cLine);
k = 0;
j = 0;
while(ischar(cLine) )
if (k == 1)
while k <= 134
fprintf(fid, '%s', cLine);
cLine = fgets(fileID_1);
   k = k + 1;
end
end
cLine = fgets(fileID_1);
   k = k + 1;
end
t = site27mdrkg;
a1 =t(1:6,1);
a2 =t(7:12,1);
a3 =t(13:18,1);
a4 =t(19:24,1);
a5 =t(25:30,1);
a6 =t(31:36,1);
a7 =t(37:42,1);
a8 =t(43:48,1);
k1 = [a1';a2';a3';a4';a5';a6';a7';a8'];
fid = fopen('K10.txt','wt');
fprintf(fid, '>FREQ //47\n');
fprintf(fid,' %11.9E %11.9E %11.9E %11.9E %11.9E %11.9E\n',k1');
fprintf(fid, '>RHOXY ROT=RHOROT //47\n');
b1 =t(1:6,2);
```

```
b2 =t(7:12,2);
b3 =t(13:18,2);
b4 =t(19:24,2);
b5 =t(25:30,2);
b6 =t(31:36,2);
b7 =t(37:42,2);
b8 =t(43:48,2);
k2 = [b1';b2';b3';b4';b5';b6';b7';b8'];
fprintf(fid,' %11.9E %11.9E %11.9E %11.9E %11.9E %11.9E\n',k2');

fprintf(fid, '>RHOXY.ERR ROT=RHOROT //47\n');
c1 =t(1:6,3);
c2 =t(7:12,3);
c3 =t(13:18,3);
c4 =t(19:24,3);
c5 =t(25:30,3);
c6 =t(31:36,3);
c7 =t(37:42,3);
c8 =t(43:48,3);
k3 = [c1';c2';c3';c4';c5';c6';c7';c8'];
fprintf(fid,' %11.9E %11.9E %11.9E %11.9E %11.9E %11.9E\n',k3');

fprintf(fid, '>RHOYX ROT=RHOROT //47\n');
d1 =t(1:6,4);
d2 =t(7:12,4);
d3 =t(13:18,4);
d4 =t(19:24,4);
d5 =t(25:30,4);
d6 =t(31:36,4);
d7 =t(37:42,4);
d8 =t(43:48,4);
k4 = [d1';d2';d3';d4';d5';d6';d7';d8'];
fprintf(fid,' %11.9E %11.9E %11.9E %11.9E %11.9E %11.9E\n',k4');

fprintf(fid, '>RHOYX.ERR ROT=RHOROT //47\n');
e1 =t(1:6,5);
e2 =t(7:12,5);
e3 =t(13:18,5);
e4 =t(19:24,5);
e5 =t(25:30,5);
e6 =t(31:36,5);
e7 =t(37:42,5);
e8 =t(43:48,5);
k5 = [e1';e2';e3';e4';e5';e6';e7';e8'];
fprintf(fid,' %11.9E %11.9E %11.9E %11.9E %11.9E %11.9E\n',k5');

fprintf(fid, '>PHSXY ROT=RHOROT //47\n');
f1 =t(1:6,6);
```

```
f2 =t(7:12,6);
f3 =t(13:18,6);
f4 =t(19:24,6);
f5 =t(25:30,6);
f6 =t(31:36,6);
f7 =t(37:42,6);
f8 =t(43:48,6);
k6 = [f1';f2';f3';f4';f5';f6';f7';f8'];
fprintf(fid,' %11.9E %11.9E %11.9E %11.9E %11.9E %11.9E\n',k6');

fprintf(fid, '>PHSXY.ERR ROT=RHOROT //47\n');
g1 =t(1:6,7);
g2 =t(7:12,7);
g3 =t(13:18,7);
g4 =t(19:24,7);
g5 =t(25:30,7);
g6 =t(31:36,7);
g7 =t(37:42,7);
g8 =t(43:48,7);
k7 = [g1';g2';g3';g4';g5';g6';g7';g8'];
fprintf(fid,' %11.9E %11.9E %11.9E %11.9E %11.9E %11.9E\n',k7');

fprintf(fid, '>PHSYX ROT=RHOROT //47\n');
h1 =t(1:6,8);
h2 =t(7:12,8);
h3 =t(13:18,8);
h4 =t(19:24,8);
h5 =t(25:30,8);
h6 =t(31:36,8);
h7 =t(37:42,8);
h8 =t(43:48,8);
k8 = [h1';h2';h3';h4';h5';h6';h7';h8'];
fprintf(fid,' %11.9E %11.9E %11.9E %11.9E %11.9E %11.9E\n',k8');

fprintf(fid, '>PHSYX.ERR ROT=RHOROT //47\n');
j1 =t(1:6,9);
j2 =t(7:12,9);
j3 =t(13:18,9);
j4 =t(19:24,9);
j5 =t(25:30,9);
j6 =t(31:36,9);
j7 =t(37:42,9);
j8 =t(43:48,9);
k9 = [j1';j2';j3';j4';j5';j6';j7';j8'];
fprintf(fid,' %11.9E %11.9E %11.9E %11.9E %11.9E %11.9E\n',k9');
END
```

This matlab code results the EDI file format for the dat file obtained from the averaging (Median) of 27, 29 and 31 sites MT data. The resulted EDI file uses the error and coordinates information (Longitude and latitude) of the reference site 29. The resulted EDI file contains resistivities instead of impedances. The format of EDI file resulted consists of Frequency, RHO XY, RHOXY Error, PHASE XY, PHASE XY Error, RHOYX, RHOYX Error, PHASEYX, PHASEYX Error. The input dat file of individual sites has been extracted from the sounding tab of the WinGlink software. The input file contains 9 columns in the order of frequency, Frequency, RHO XY, RHOXY Error, PHASE XY, PHASE XY Error, RHOYX, RHOYX Error, PHASEYX, PHASEYX Error. The resulted EDI file can not be rotated while using in the WinGlink software as it provides the option for rotating the impendance valuesonly. So to obtain the desired rotated value, the input file is rotated the desired amount from the Sounding tab before averaging.

5.9 2D Inversion of weighted spacing average data

The initial model and the inversion routine used here is same as the inversions of existing data processed by GERMC.

Averaged Sites(Weighted Spacing average (0.001 – 1000s)	Modes	Error Floor		Initial RMS	Final RMS	No. of iterations	Weight Factors α=3, β =1 Minimum Block dimensions 250H, 50V Tau for smoothing operator =10, Data Errors RHO -10, Phase -5
		Resistivity	Phase				
	TE	30	10	7.674	1.7193	150	
	TM	30	10	7.352	1.3665	120	
	TE+TM	TE-30 TM -30	TE-10 TM - 10	3.343	1.7384	90	

Table 5.6Showing information of inversion parameters for the 2D inversion of weighted spacing data

5.9.1 Comparison of all modes of weighted spacing averaged data with reference model

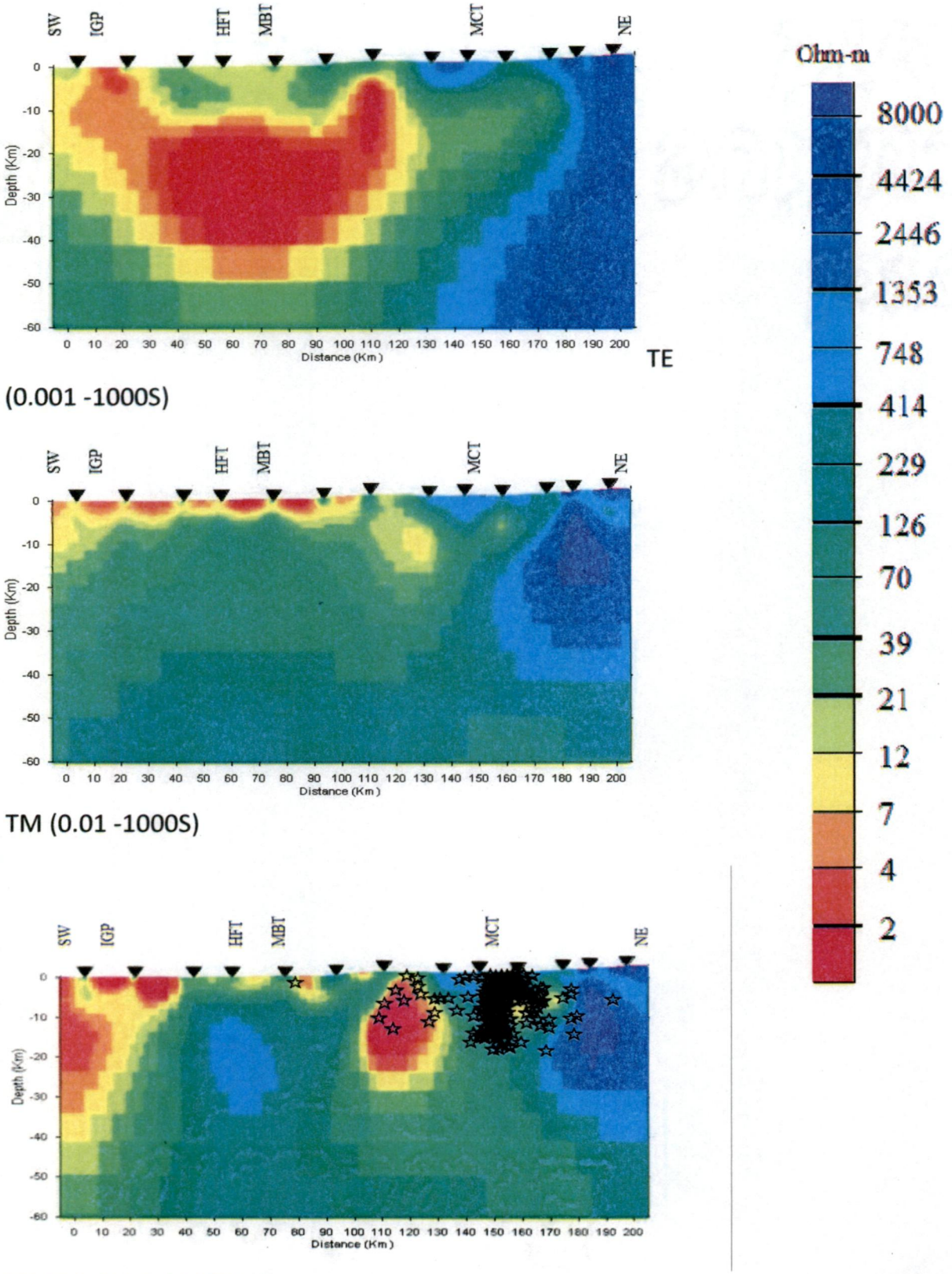

TE (0.001 -1000S)

TM (0.01 -1000S)

TE+TM (0.01 -1000S)

Fig. 5.19 All modes (TE,TM, TE+TM) of weighted spacing data

5.9.2 Fitting of apparent resistivity and phase

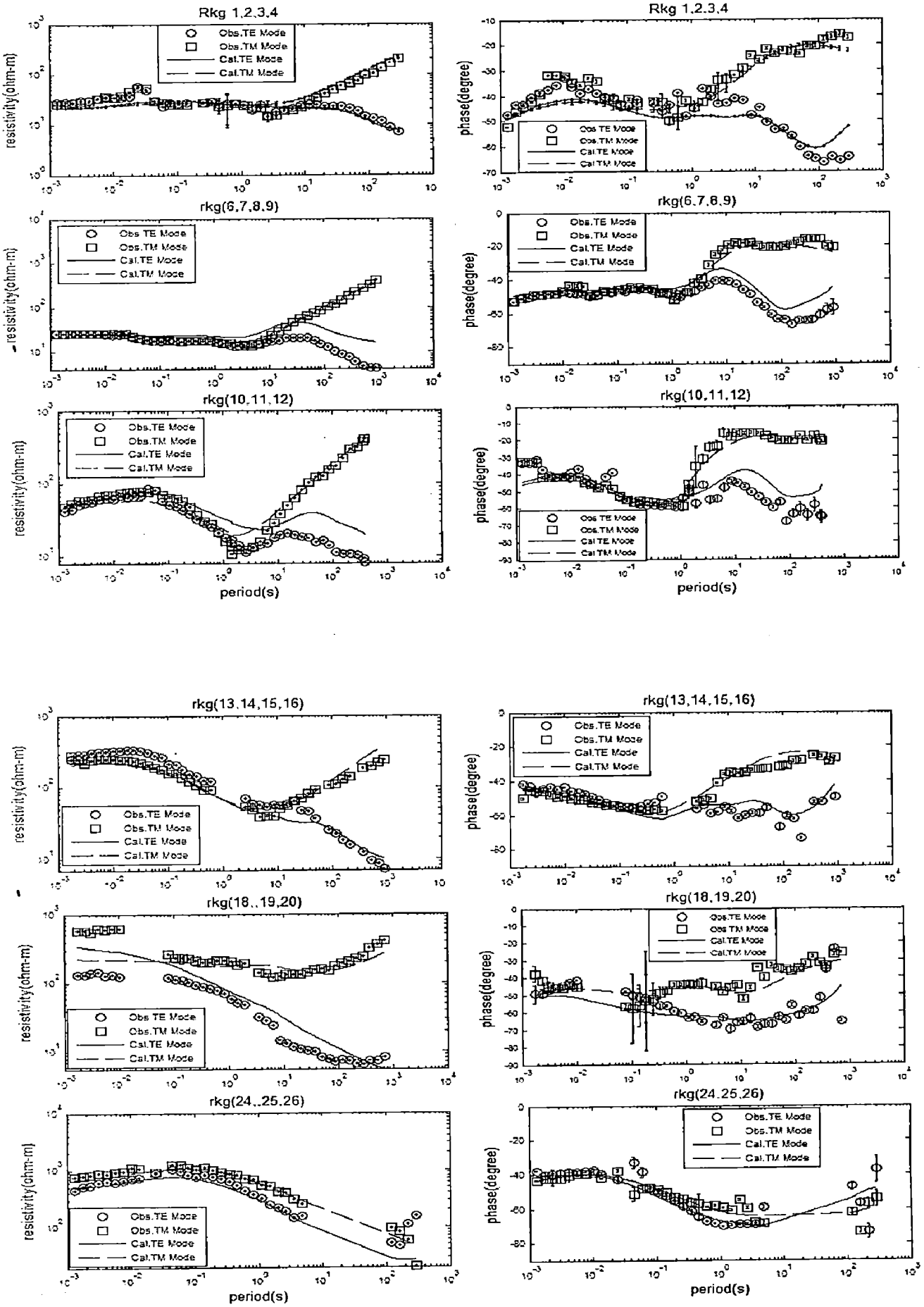

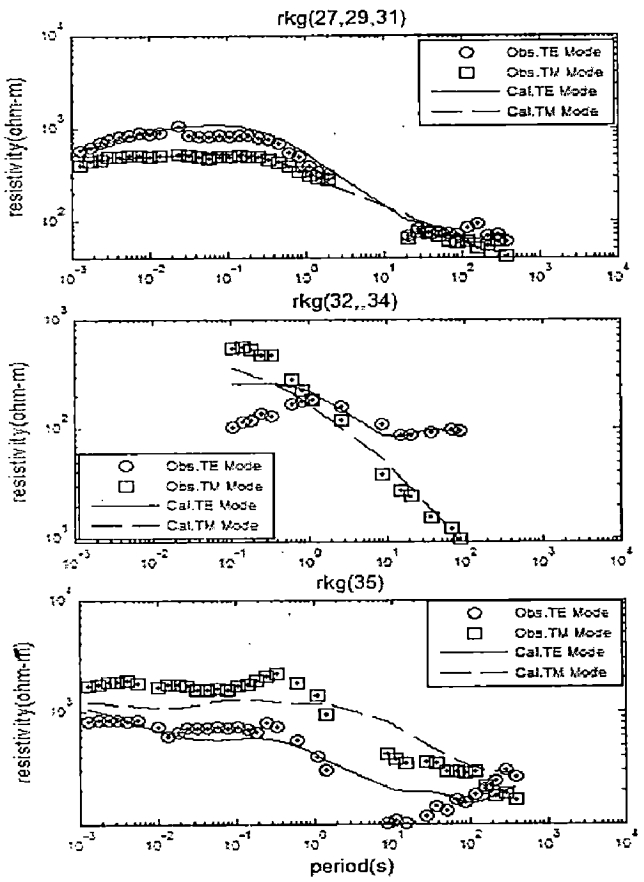
rkg(27,29,31)
rkg(32,,34)
rkg(35)
resistivity(ohm-m)
Obs.TE Mode
Obs.TM Mode
Cal.TE Mode
Cal.TM Mode
period(s)

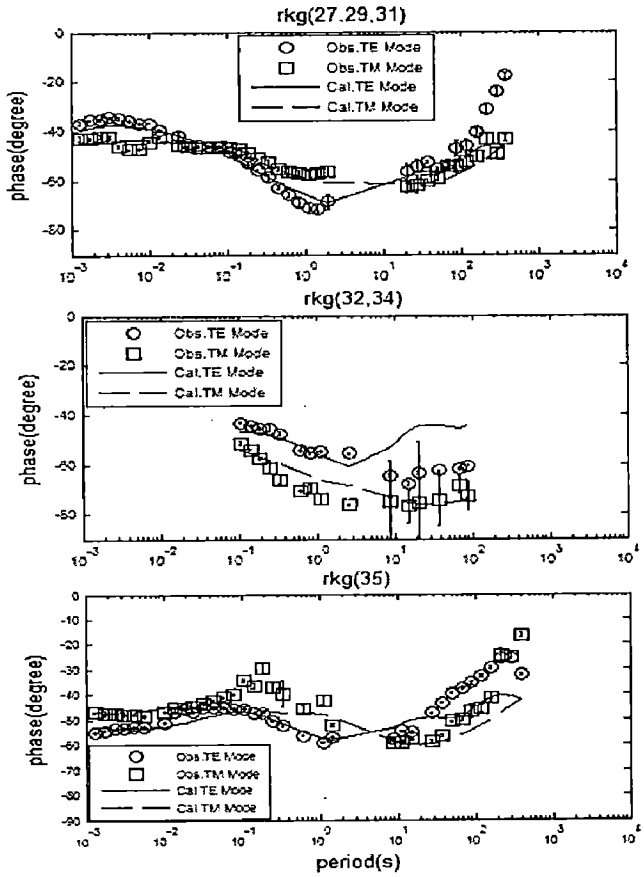
rkg(27,29,31)
rkg(32,34)
rkg(35)
phase(degree)
Obs.TE Mode
Obs.TM Mode
Cal.TE Mode
Cal.TM Mode
period(s)

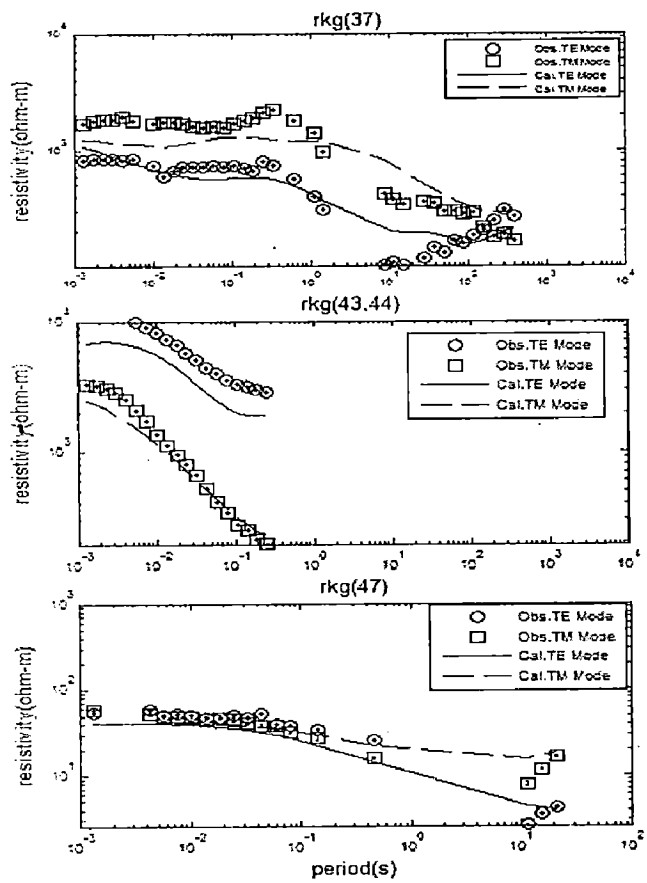
rkg(37)
rkg(43,44)
rkg(47)
resistivity(ohm-m)
Obs.TE Mode
Obs.TM Mode
Cal.TE Mode
Cal.TM Mode
period(s)

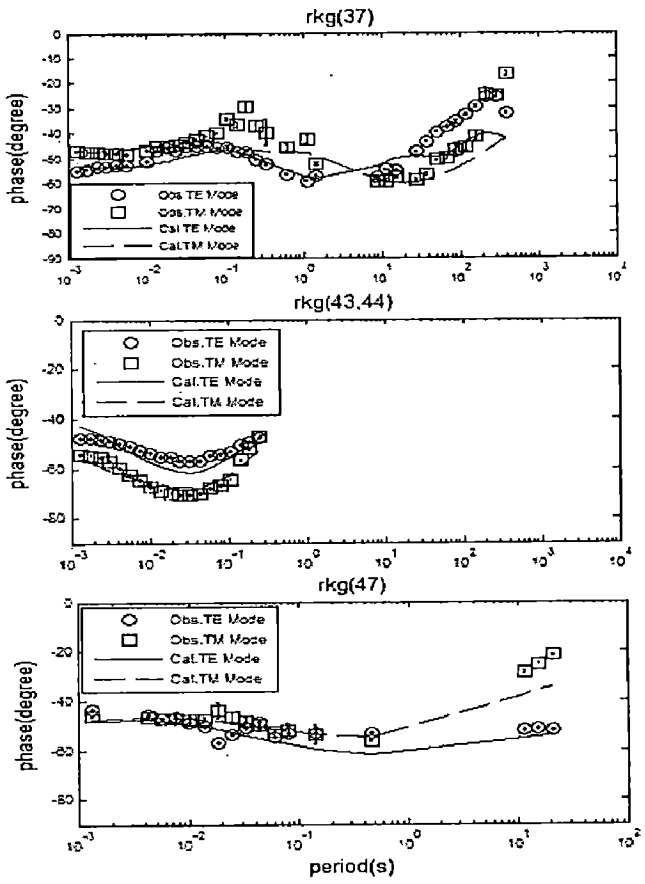
rkg(37)
rkg(43,44)
rkg(47)
phase(degree)
Obs.TE Mode
Obs.TM Mode
Cal.TE Mode
Cal.TM Mode
period(s)

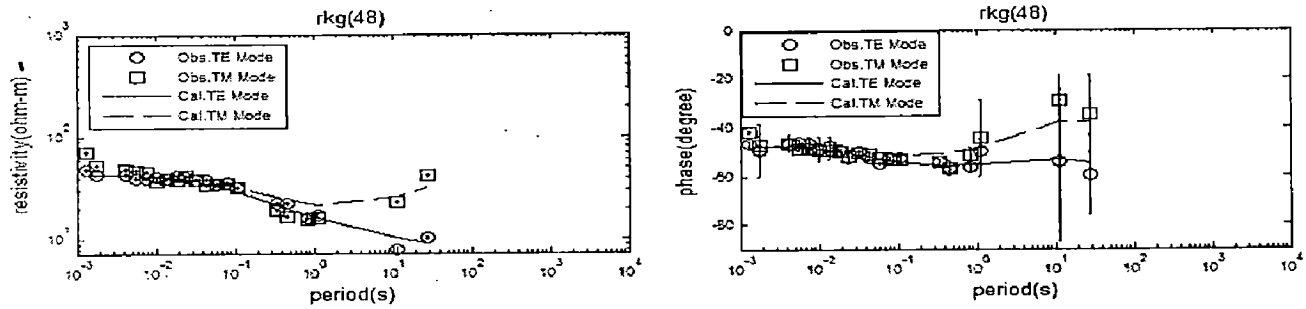

Fig.5.20 Fitting of Apparent resistivity and Phase of weighted spacing averaged data

5.9.3 Results

The TE model is more distorted one with respect to reference model. The near surface conductive features of the IGP are almost missed. It also gives the completely missing of the conductive channels in the Higher Himalayan part. It provides good matching of resistivity structures of the Higher Himalaya. The TM mode slightly matches with reference model. The near surface conductive part is completely detected in the IGP region but the conductivity channel extending from 25 Km to 40 Km depth is not visible and the resistivity structures of the TM model is well matching with the reference model.joint model the conductivity structure has been shifted to left. It is clear that weighted spacing of the grouped data causes loss of information.

5.10 2D Inversion of weighted error data

The initial model and the inversion routine used here is same as the inversions of existing data processed by GERMC.

Averaged Sites(Weighted error average) (0.001 – 1000s	Modes	Error Floor		Initial RMS	Final RMS	No. of iterations	Weight Factors α=3, β =1 Minimum Block dimensions 250H, 50V Tau for smoothing operator =10, Data Errors RHO -10, Phase -5
		Resistivity	Phase				
	TE	30	10	8.053	2.2817	140	
	TM	30	10	6.085	1.9052	115	
	TE+TM	TE-30 TM -30	TE-10 TM -10	3.835	2.2201	95	

Table 5.7Showing information of inversion parameters for the 2D inversion of weighted error data

5.10.1 Comparison of all modes of weighted error averaged data with reference model

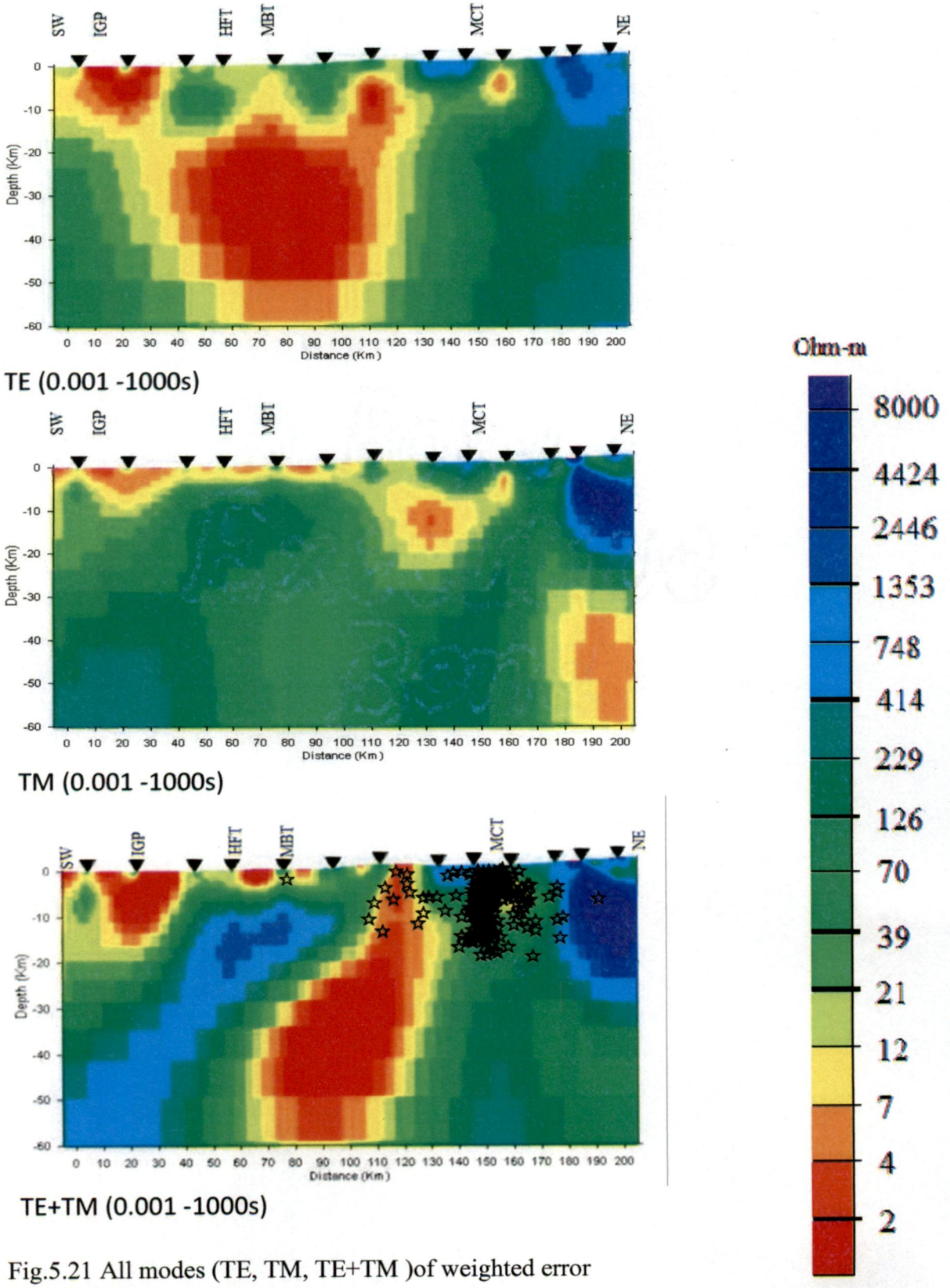

Fig.5.21 All modes (TE, TM, TE+TM)of weighted error averaged data

5.10.2 Fitting of apparent resistivity and phase

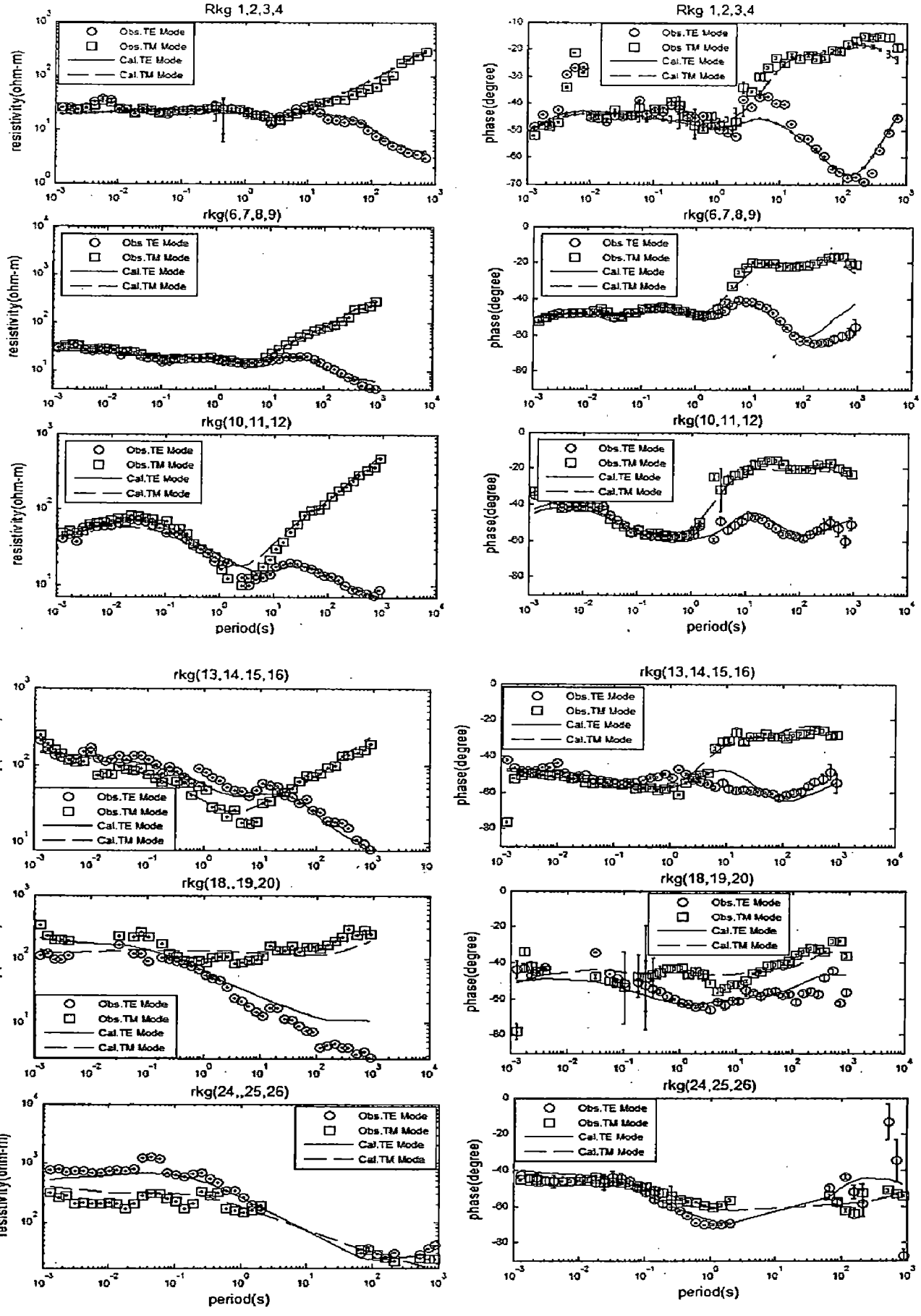

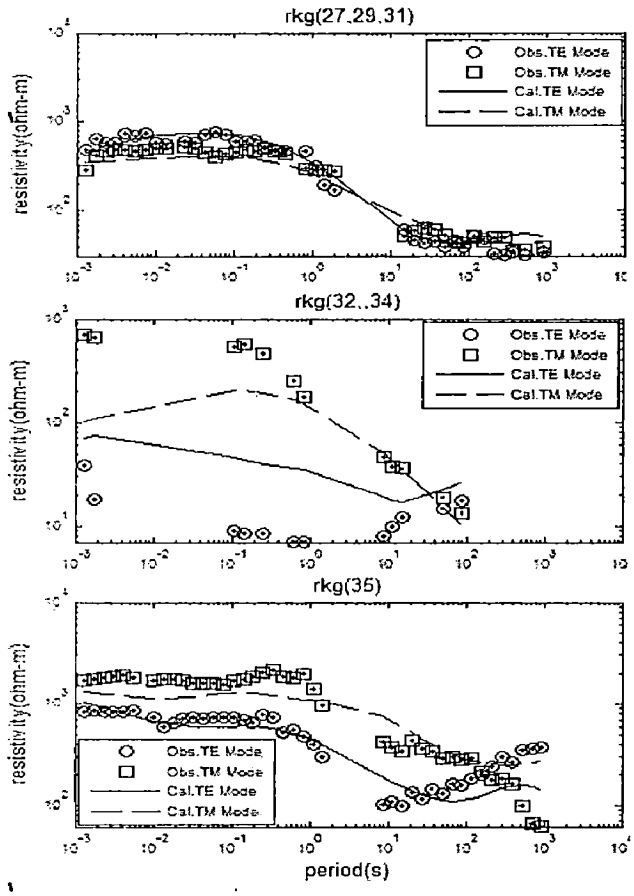
rkg(27,29,31)
resistivity(ohm-m)
Obs.TE Mode
Obs.TM Mode
Cal.TE Mode
Cal.TM Mode
rkg(32,,34)
resistivity(ohm-m)
Obs.TE Mode
Obs.TM Mode
Cal.TE Mode
Cal.TM Mode
rkg(35)
resistivity(ohm-m)
Obs.TE Mode
Obs.TM Mode
Cal.TE Mode
Cal.TM Mode
period(s)

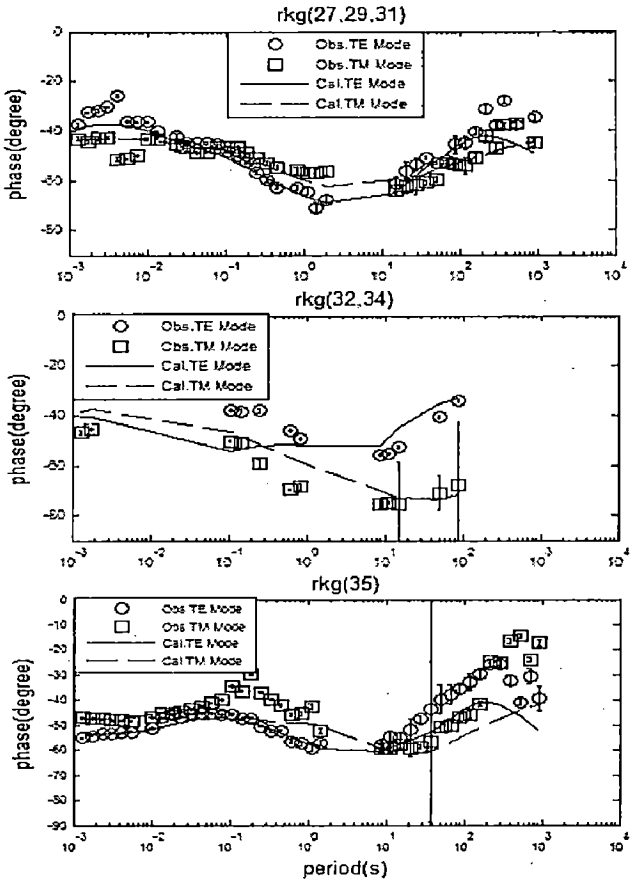
rkg(27,29,31)
phase(degree)
Obs.TE Mode
Obs.TM Mode
Cal.TE Mode
Cal.TM Mode
rkg(32,34)
phase(degree)
Obs.TE Mode
Obs.TM Mode
Cal.TE Mode
Cal.TM Mode
rkg(35)
phase(degree)
Obs.TE Mode
Obs.TM Mode
Cal.TE Mode
Cal.TM Mode
period(s)

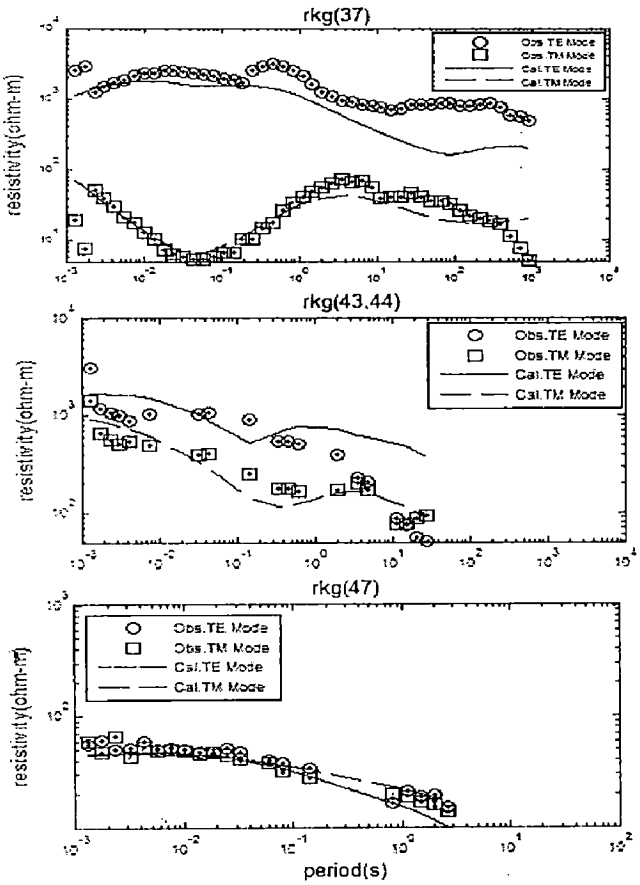
rkg(37)
resistivity(ohm-m)
Obs.TE Mode
Obs.TM Mode
Cal.TE Mode
Cal.TM Mode
rkg(43,44)
resistivity(ohm-m)
Obs.TE Mode
Obs.TM Mode
Cal.TE Mode
Cal.TM Mode
rkg(47)
resistivity(ohm-m)
Obs.TE Mode
Obs.TM Mode
Cal.TE Mode
Cal.TM Mode
period(s)

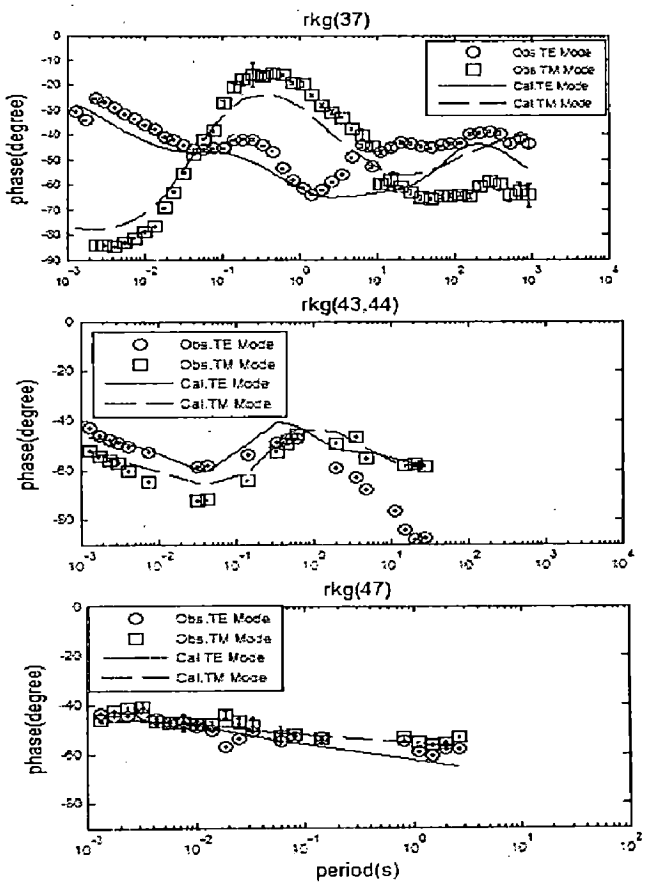
rkg(37)
phase(degree)
Obs.TE Mode
Obs.TM Mode
Cal.TE Mode
Cal.TM Mode
rkg(43,44)
phase(degree)
Obs.TE Mode
Obs.TM Mode
Cal.TE Mode
Cal.TM Mode
rkg(47)
phase(degree)
Obs.TE Mode
Obs.TM Mode
Cal.TE Mode
Cal.TM Mode
period(s)

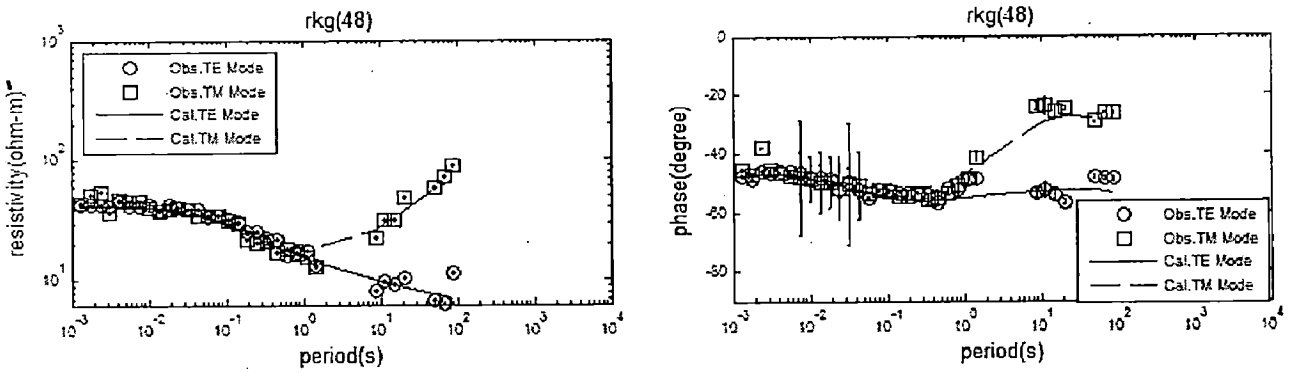

Fig.5.22 Fitting of Apparent resistivity and Phase of weighted error averaged data

5.10.3 Results

The TE model is more distorted one from the reference model. It does not even detect the resistive part of the Higher Himalayan region. Tm model detects the near surface conductive features of IGP region very well and conductive body extends up to depth of 25Km of the Higher Himalaya. The conductive channel of the Higher Himalaya part up to 40 Km depth is not detected by TM mode, whereas TE+TM model shows the conductive part towards left. The result obtained in weighted error average is better than the results obtained in weighted spacing average.

5.11 2D Inversion of simple average data

The initial model and the inversion routine used here is same as the inversions of existing data processed by GERMC.

Averaged Sites(Simple average) (0.001 – 1000s)	Modes	Error Floor		Initial RMS	Final RMS	No. of iterations	Weight Factors α=3, β =1 Minimum Block dimensions 250H, 50V Tau for smoothing operator =10, Data Errors RHO -10, Phase -5
		Resistivity	Phase				
	TE	30	10	7.801	2.3231	130	
	TM	30	10	7.543	2.2925	100	
	TE+TM	TE-30 TM -30	TE-10 TM -10	3.237	2.2969	85	

Table 5.8 Showing information of inversion parameters for the 2D inversion of Simple average data

5.11.1 Comparison of all modes of Simple averaged data with reference model

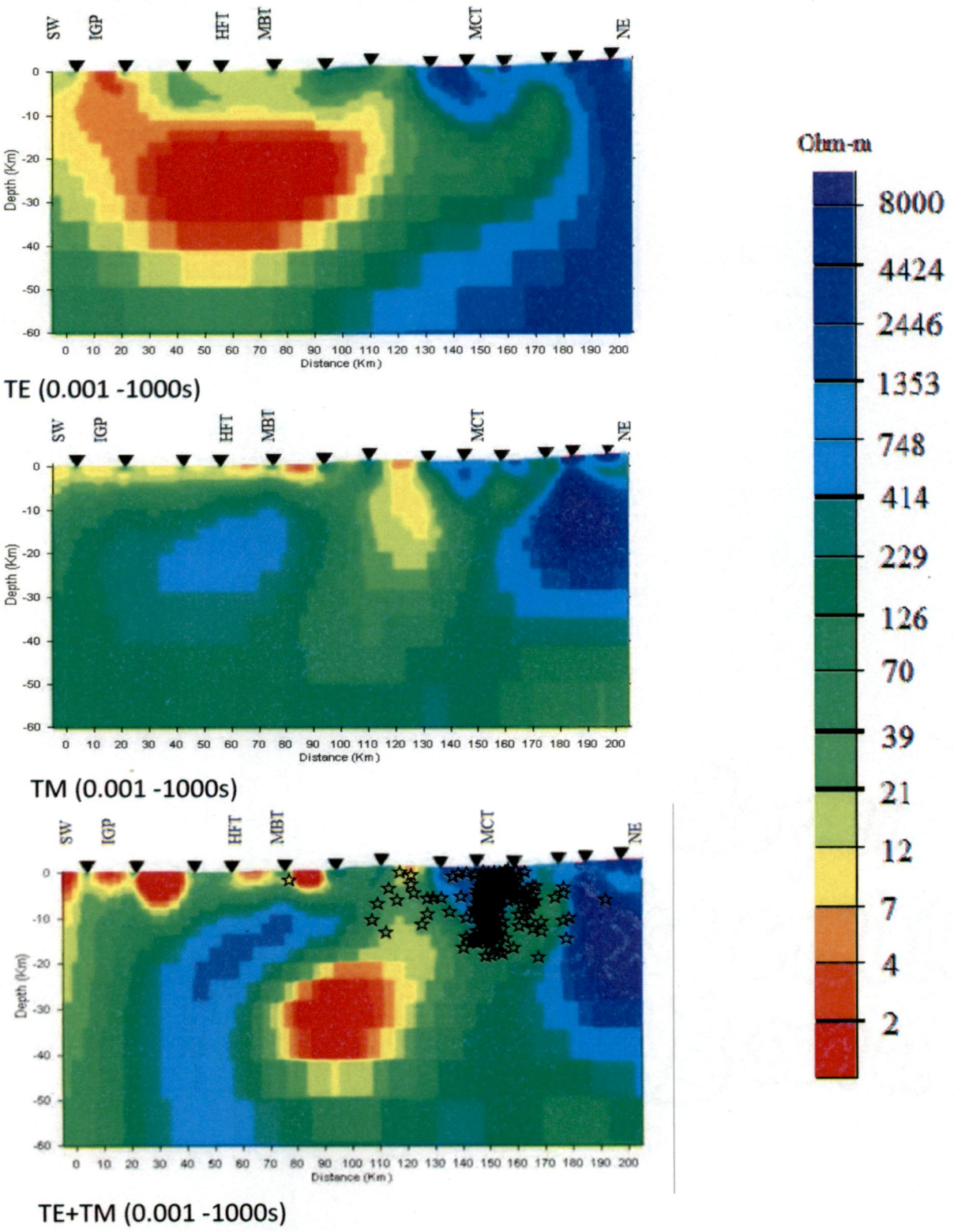

Fig.5.23 All modes (TE, TM, TE+TM) of Simple average data

5.11.2Fitting of apparent resistivity and phase

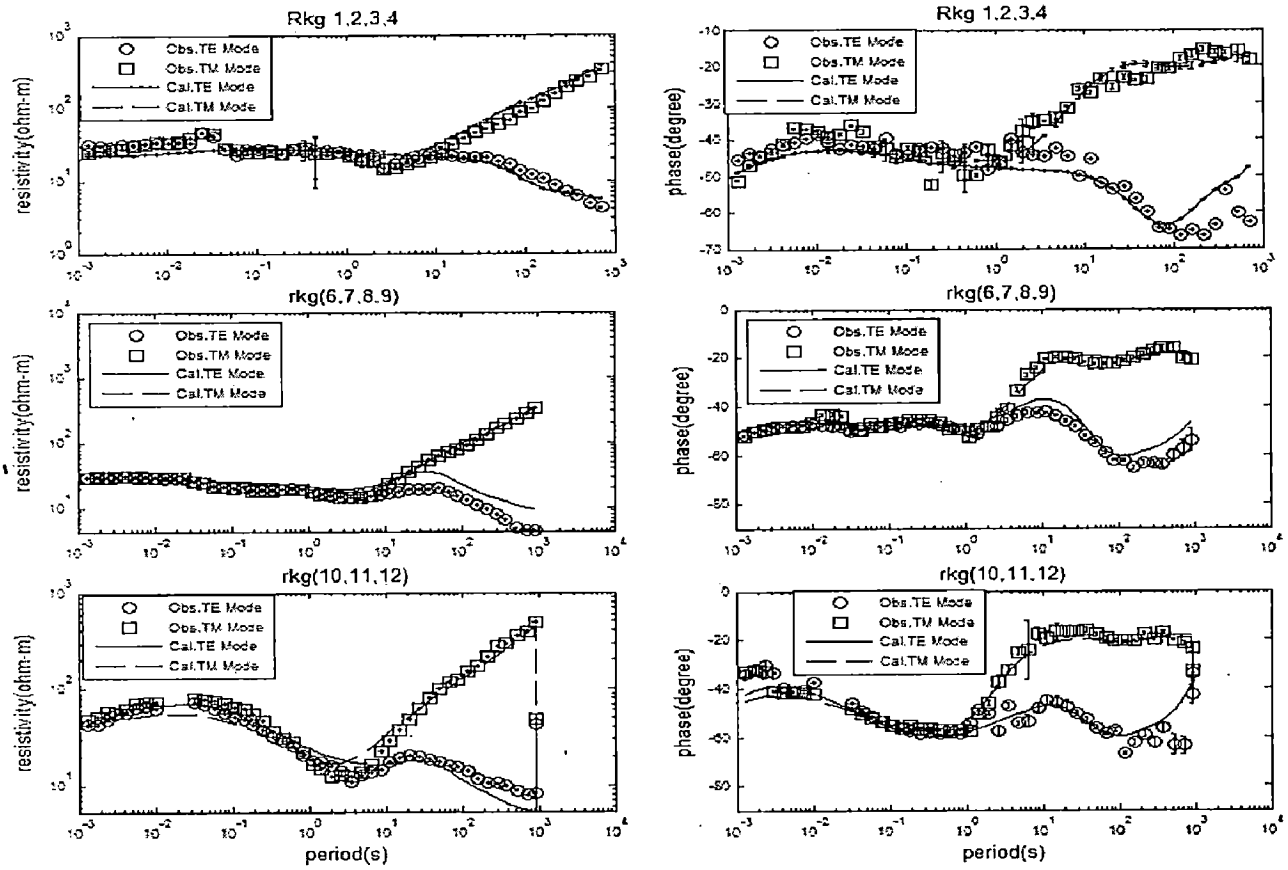

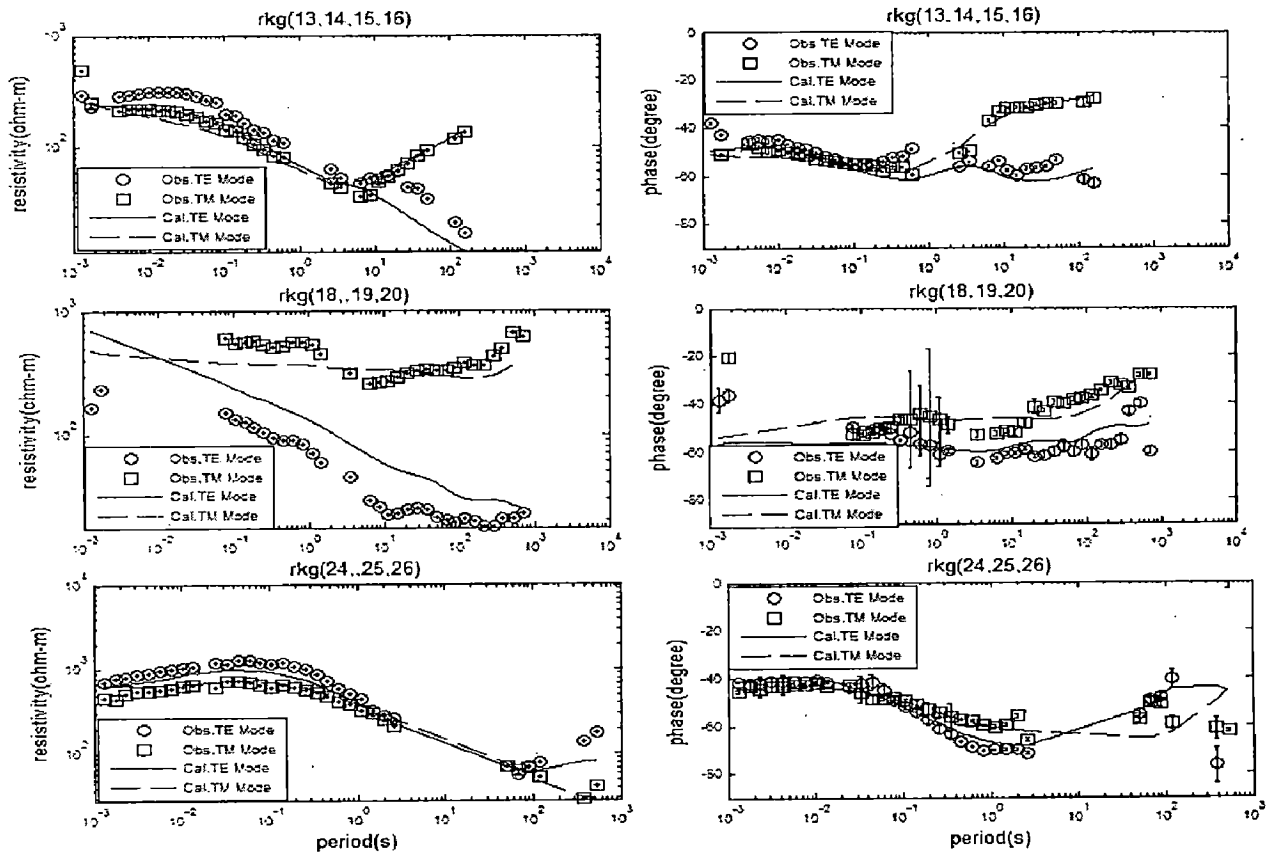

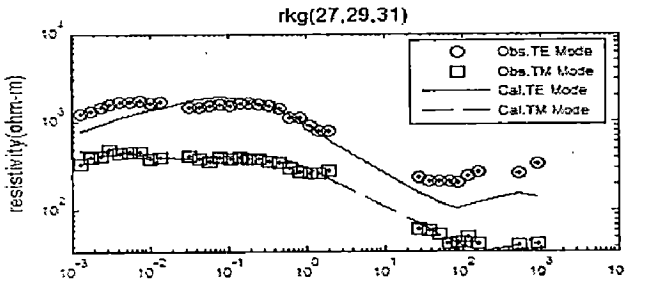
rkg(27,29,31)
resistivity(ohm-m)
Obs.TE Mode
Obs.TM Mode
Cal.TE Mode
Cal.TM Mode

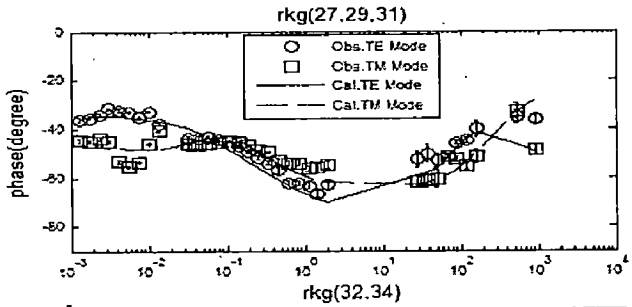
rkg(27,29,31)
phase(degree)
Obs.TE Mode
Obs.TM Mode
Cal.TE Mode
Cal.TM Mode

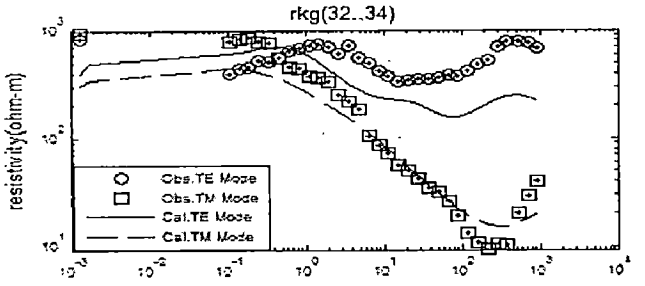
rkg(32..34)
resistivity(ohm-m)
Obs.TE Mode
Obs.TM Mode
Cal.TE Mode
Cal.TM Mode

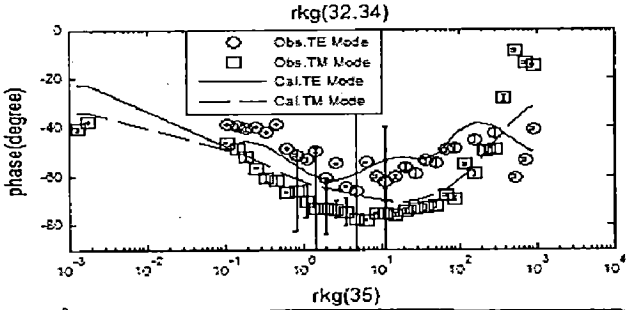
rkg(32,34)
phase(degree)
Obs.TE Mode
Obs.TM Mode
Cal.TE Mode
Cal.TM Mode

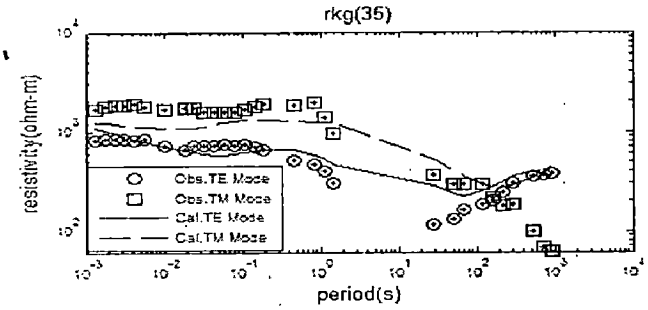
rkg(35)
resistivity(ohm-m)
Obs.TE Mode
Obs.TM Mode
Cal.TE Mode
Cal.TM Mode
period(s)

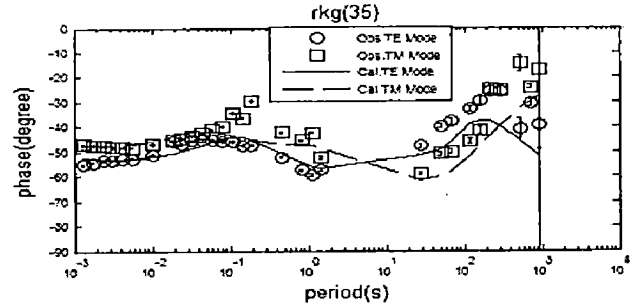
rkg(35)
phase(degree)
Obs.TE Mode
Obs.TM Mode
Cal.TE Mode
Cal.TM Mode
period(s)

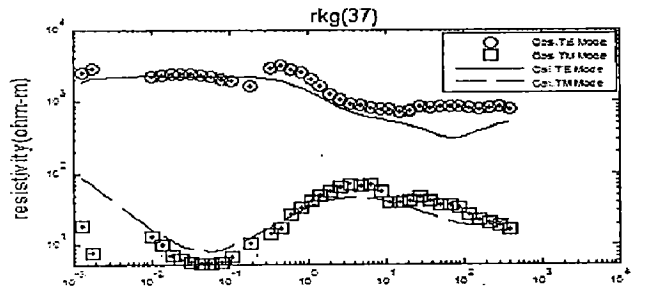
rkg(37)
resistivity(ohm-m)
Obs.TE Mode
Obs.TM Mode
Cal.TE Mode
Cal.TM Mode

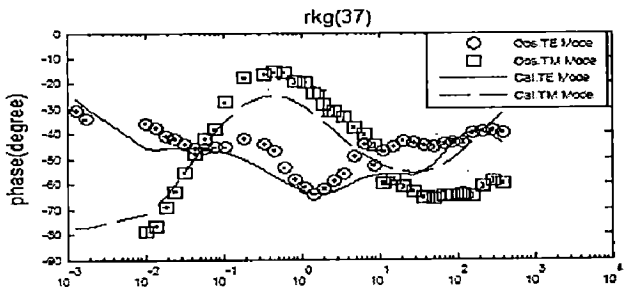
rkg(37)
phase(degree)
Obs.TE Mode
Obs.TM Mode
Cal.TE Mode
Cal.TM Mode

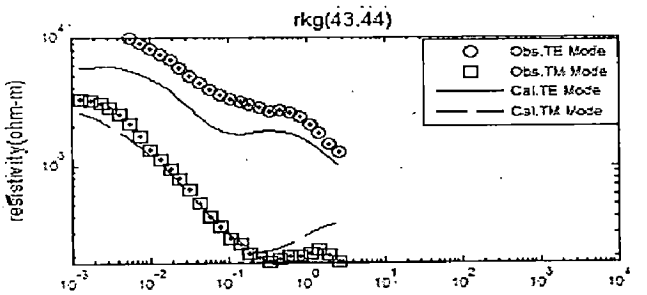
rkg(43.44)
resistivity(ohm-m)
Obs.TE Mode
Obs.TM Mode
Cal.TE Mode
Cal.TM Mode

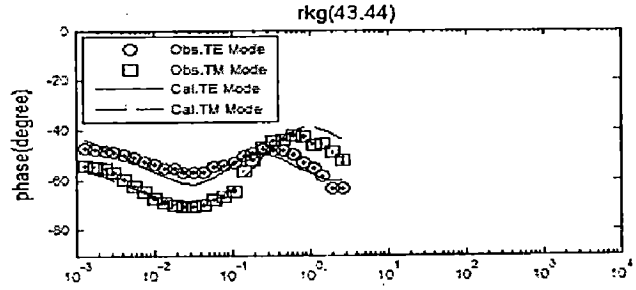
rkg(43.44)
phase(degree)
Obs.TE Mode
Obs.TM Mode
Cal.TE Mode
Cal.TM Mode

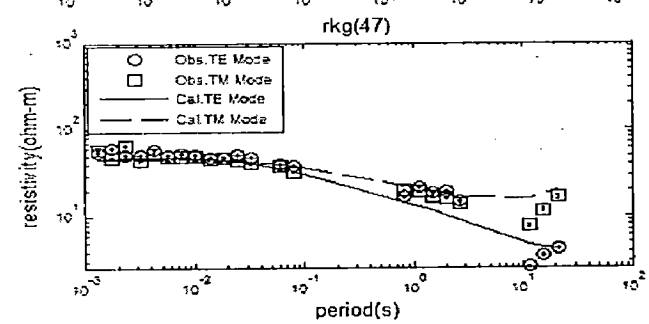
rkg(47)
resistivity(ohm-m)
Obs.TE Mode
Obs.TM Mode
Cal.TE Mode
Cal.TM Mode
period(s)

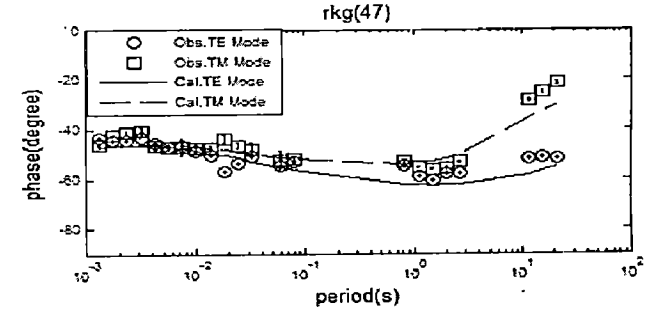
rkg(47)
phase(degree)
Obs.TE Mode
Obs.TM Mode
Cal.TE Mode
Cal.TM Mode
period(s)

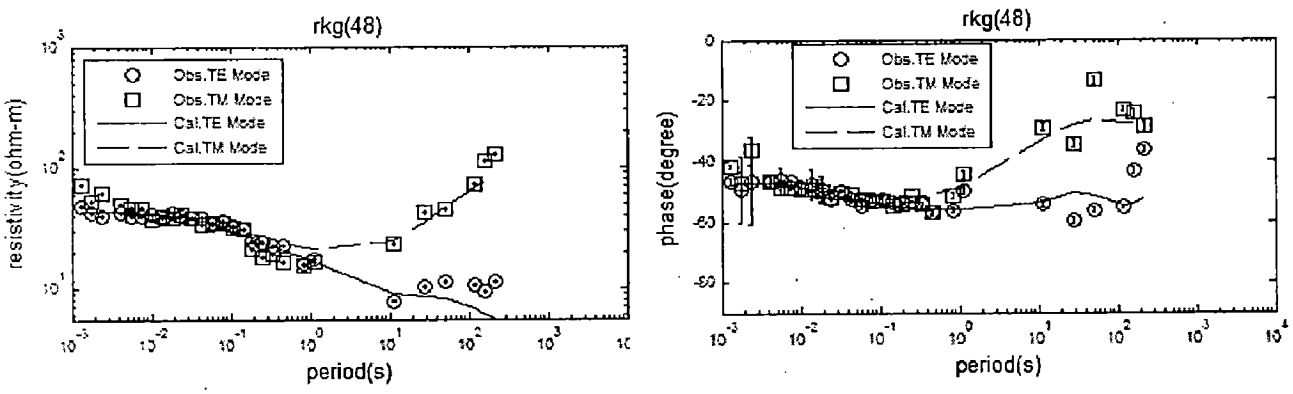

Fig.5.24 Fitting of Apparent resistivity and Phase of simple average data

5.11.3Results

The comparison of TE model with the reference model shows no matching. Here TM mode is also distorted one; the conductive part is not properly visible. But joint model in this case is better than all above cases.

5.12 2D Inversion of median data

The initial model and the inversion routine used here is same as the inversions of existing data processed by GERMC.

Averaged Sites(Median) (0.001 – 1000s)	Modes	Error Floor		Initial RMS	Final RMS	No. of iterations	Weight Factors α=3, β =1 Minimum Block dimensions 250H, 50V Tau for smoothing operator =10, Data Errors RHO -10, Phase -5
		Resistivity	Phase				
	TE	30	10	8.257	2.1365	135	
	TM	30	10	6.132	1.3963	87	
	TE+TM	TE-30 TM -30	TE-10 TM -10	4.489	2.0454	75	

Table 5.9 Showing information of inversion parameters for the 2D inversion of Median data

5.12.1Comparison of all modes of median data with reference model

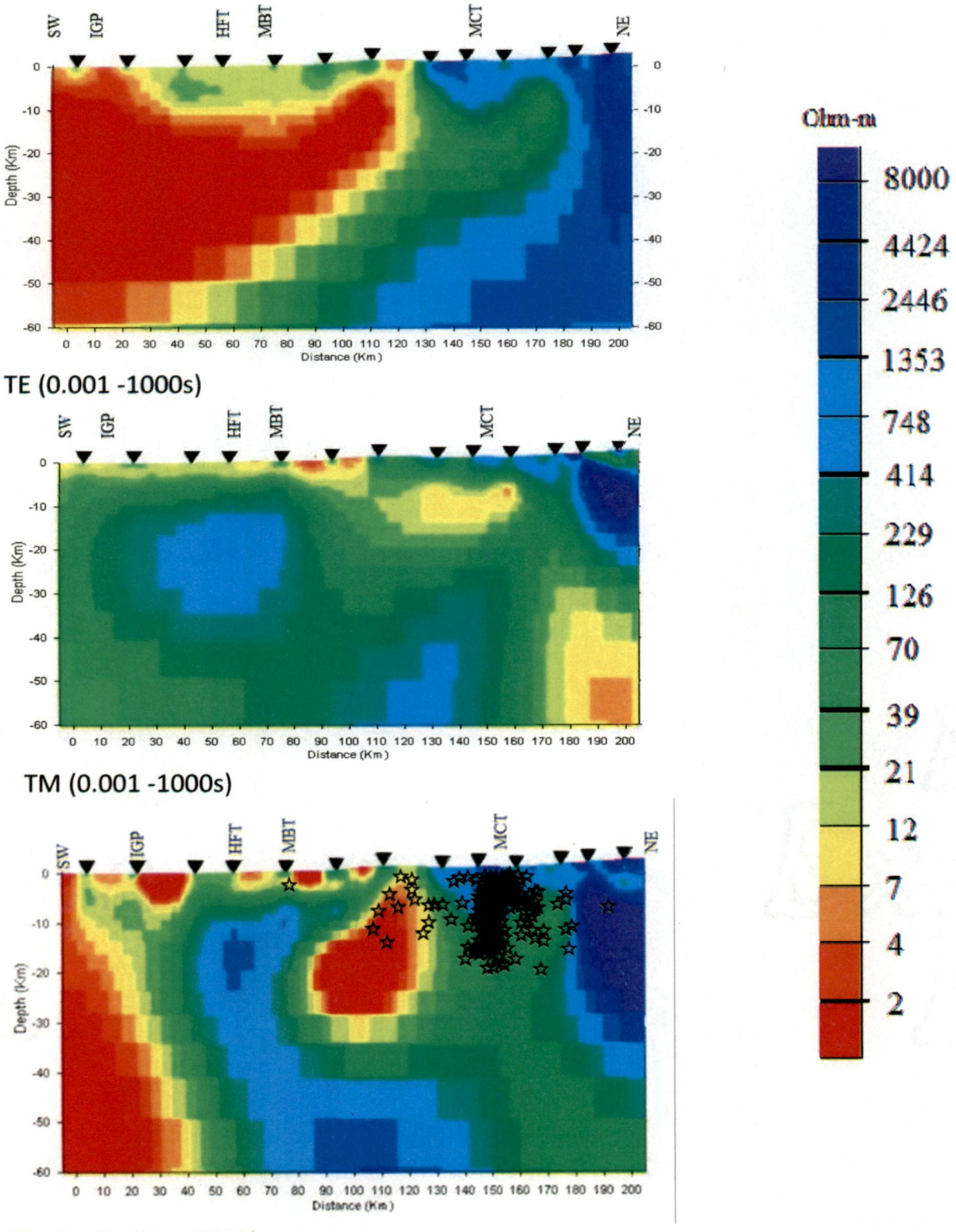

TE (0.001 -1000s)

TM (0.001 -1000s)

TE +TM(0.001 -1000S)

Fig.5.25 All modes (TE, TM, TE+TM) of Median average data

5.12.2Fitting of apparent resistivity and phase

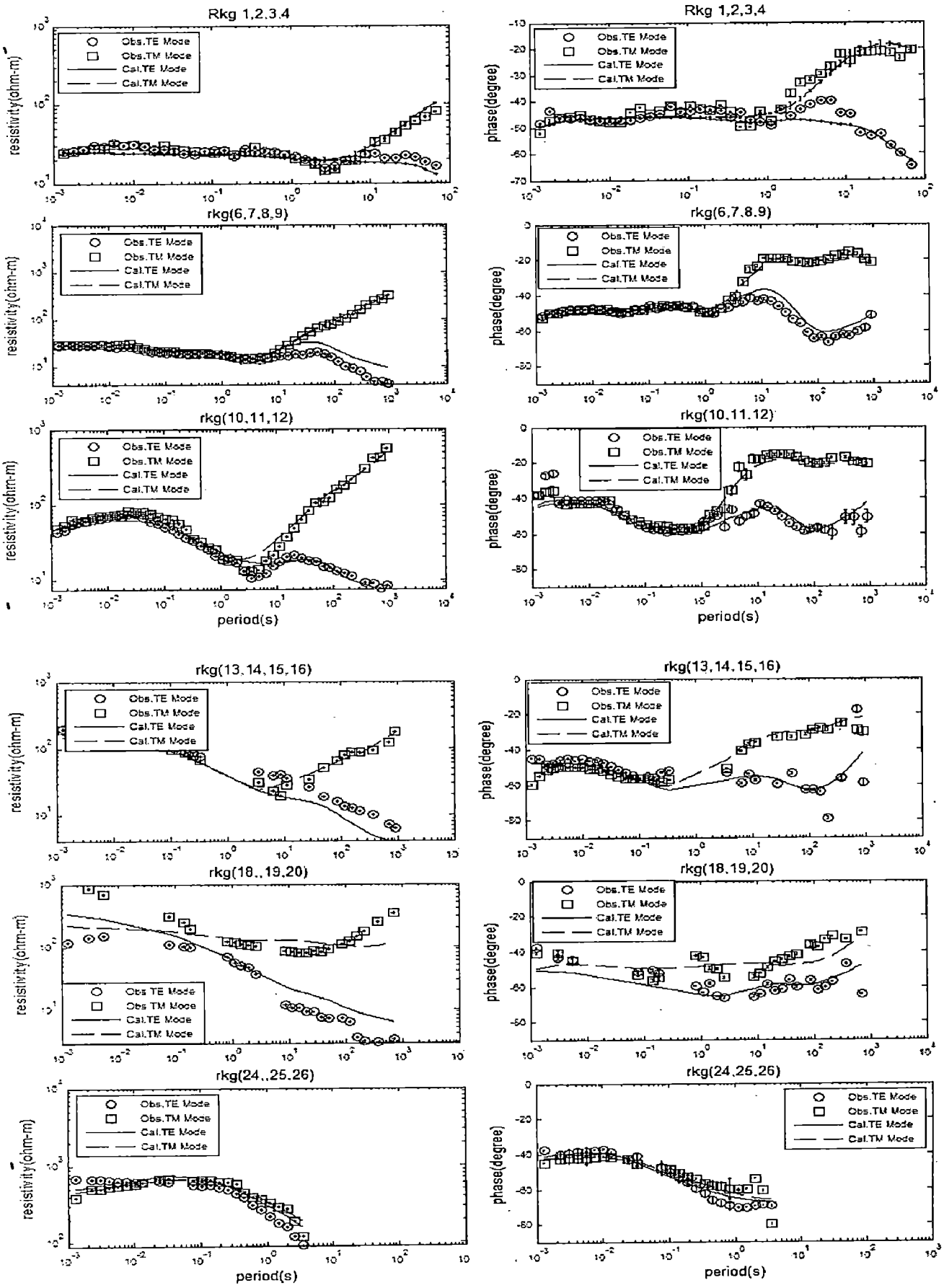

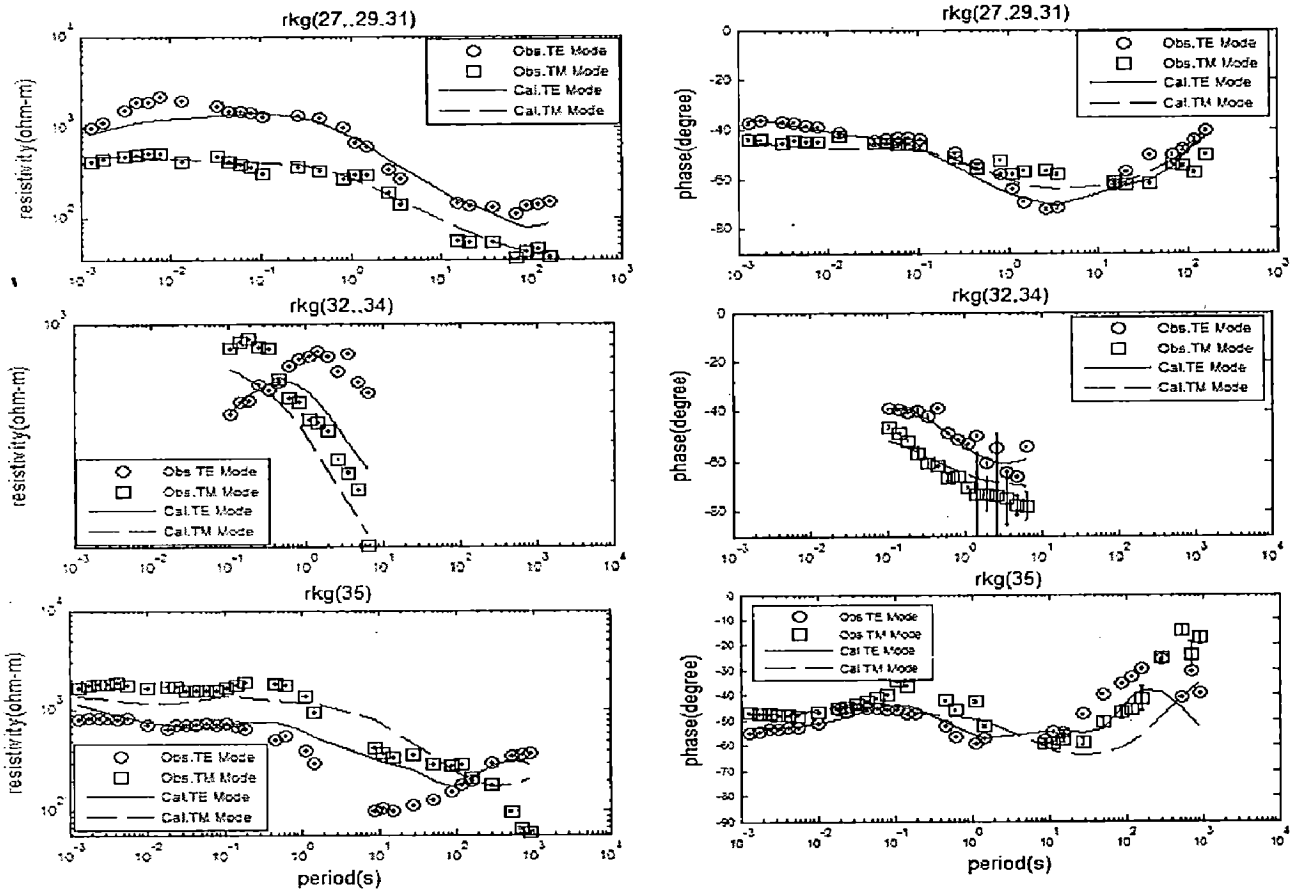
rkg(27,.29.31)
rkg(27.29.31)
rkg(32,.34)
rkg(32,34)
rkg(35)
rkg(35)
rkg(37)
rkg(37)
rkg(43,44)
rkg(43,44)
rkg(47)
rkg(47)
resistivity(ohm-m)
phase(degree)
period(s)
Obs.TE Mode
Obs.TM Mode
Cal.TE Mode
Cal.TM Mode

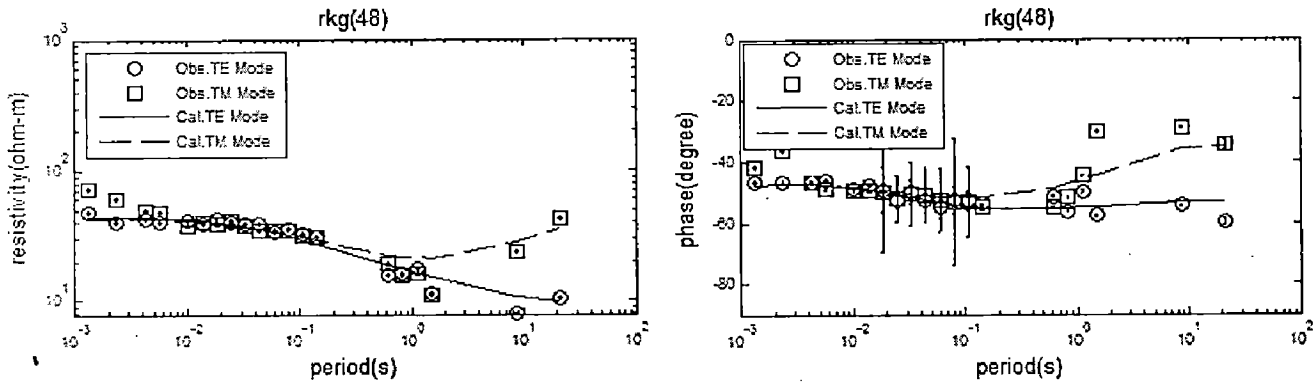

Fig.5.26 Fitting of Apparent resistivity and Phase of weighted error averaged data

5.12.3Results

The TE model is completed distorted one. The most part of the TM model is matching with the reference model except the conductive part from 15Km to 40Km depth. Here Joint model shows better results than joint models of above three methods. The conductive part in joint model is slightly deviated from the reference model. Out of all averaged models, it is clear that TM mode of median averaged method shows well matching with the reference model.

The above study can infer that TM mode is more sensitive to near surface structures and fluid saturated faults (conductive channels) as well as lithosphere resistance but it suffers from the screening effect and may miss the deep structures whereas TE mode is more sensitive to near surface resistive zones and deep conductive zones. TM mode is associated with galvanic distortions due to current gathering whereas TE mode is associated with inductive distortions. But in the presence of superposition of elongated conductive features with 3D small scale conductive feature at the near surface, both TE and TM are associated with galvanic distortions. As the small scale conductive features at the IGP region are delineated by TM mode, it is clear that TM mode is more robust to 3D effects caused by conductive bodies. As TE mode detects the resistive part of the Himalayan region, so it can be inferred that TE mode is more robust to 3D effects caused by resistivity features. From the fitting of TE and TM mode it can be observed that the TE mode resistivity suffers more from static distortions at the left of the curve than TM mode. Hence TM mode is suitable to delineating the small scale conductive features at the near surface of the IGP region properly. The above study shows TM mode 2D inversion is suitable to study up to resistive lithosphere (Crustal depth).

5.13 Averaging of 35 sites data (Processed by GERMC Group)

The comparison plots of the averaging of 33 sites data using four different methods shows the median method is the best method of averaging for reducing the spreading of the data value.

Inorder to smooth the data (Processed by GERMC Group), median method of averaging has been used. The 35 sites data which are in the order of 48, 49,47, 1, 2, 6, 7, 8, 9, B3, 10, 11, P3, 12, 13, 14, 16, 15, 18, 19, 20, 24, 25, 27, 29, 31, 32, 33, 35, 36, 37, 38, 39, 40, 44 have been grouped into 17 sets. Out of 17 sets, 10 sets are grouped and 7sets are single site data. The 17 sets are (48) , (49,47), (1,2), (6,7,8), (9,B3), (10,11,P3,12), (13,14,16,15), (18,19,20), (24,25), (27,29,31), (32,33), (35), (36),(37),(38), (39,40), (40,44).

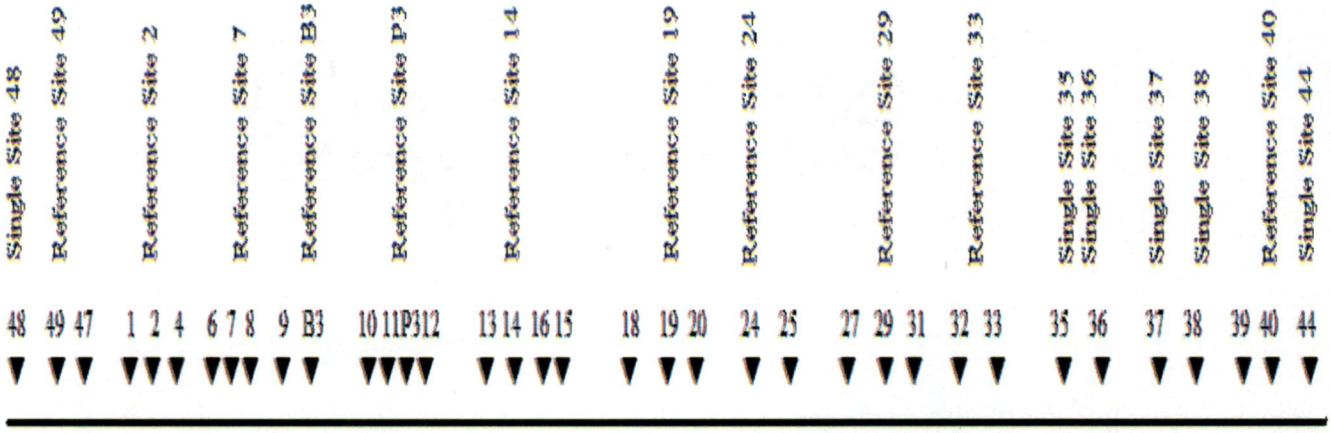

Fig. 5.27Showing the 17 grouped sites that have been taken for the averaging purpose and their reference sites

5.13.1Plotting of Median data with original data

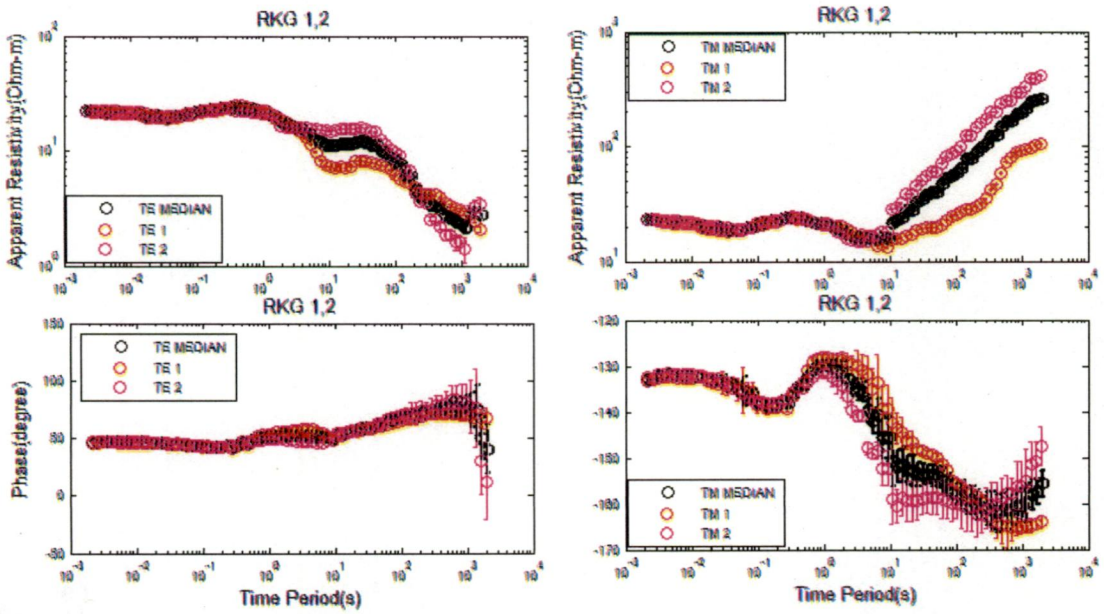

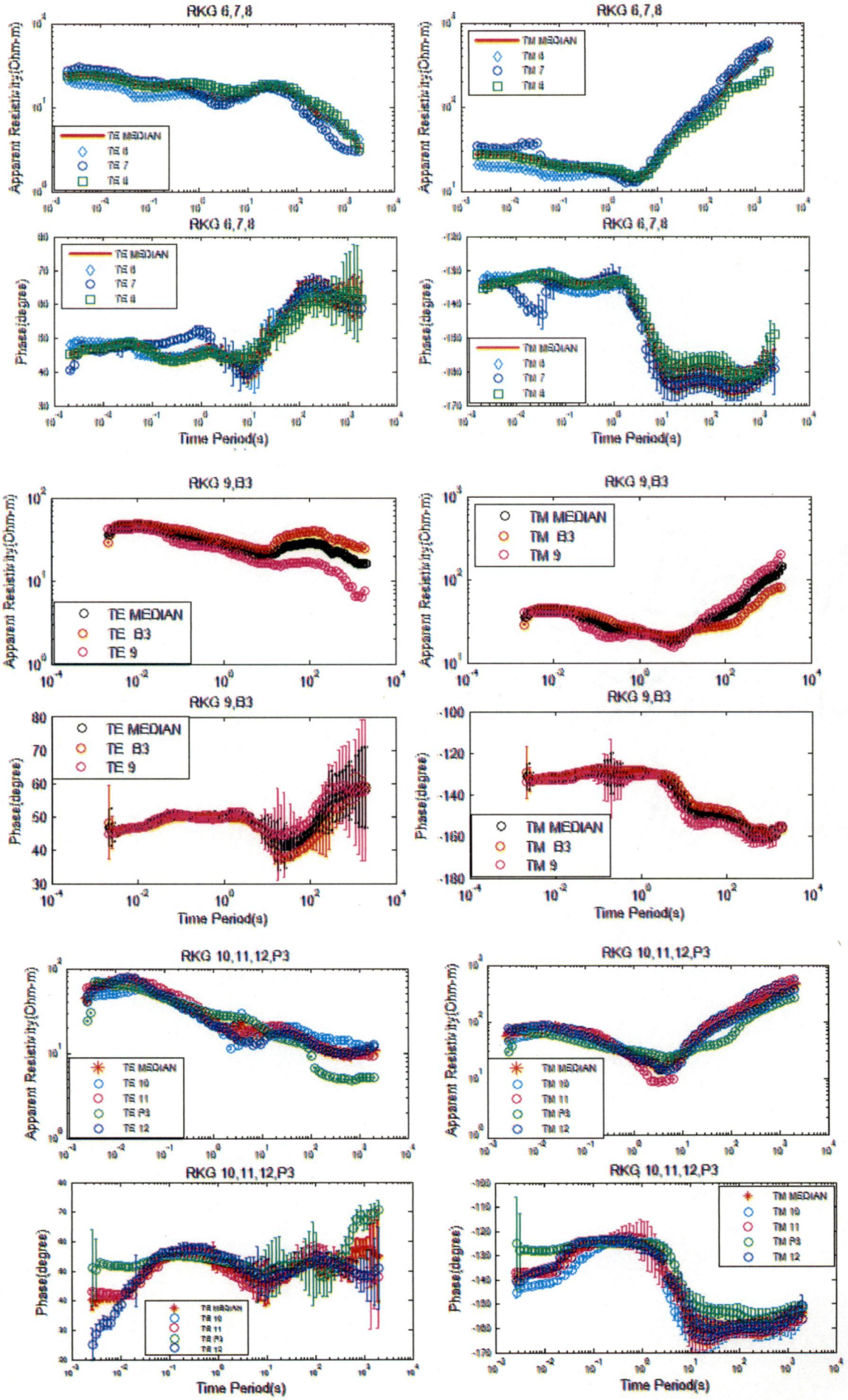
RKG 6,7,8
Apparent Resistivity(Ohm-m)
TE MEDIAN
TE 6
TE 7
TE 8
RKG 6,7,8
TM MEDIAN
TM 6
TM 7
TM 8
RKG 6,7,8
Phase(degree)
Time Period(s)
RKG 6,7,8
RKG 9,B3
TE MEDIAN
TE B3
TE 9
RKG 9,B3
TM MEDIAN
TM B3
TM 9
RKG 9,B3
RKG 9,B3
RKG 10,11,12,P3
TE MEDIAN
TE 10
TE 11
TE P3
TE 12
RKG 10,11,12,P3
TM MEDIAN
TM 10
TM 11
TM P3
TM 12
RKG 10,11,12,P3
RKG 10,11,12,P3

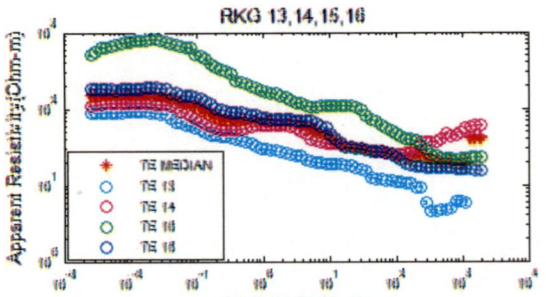
RKG 13,14,15,16
Apparent Resistivity(Ohm-m)
TE MEDIAN
TE 13
TE 14
TE 15
TE 16

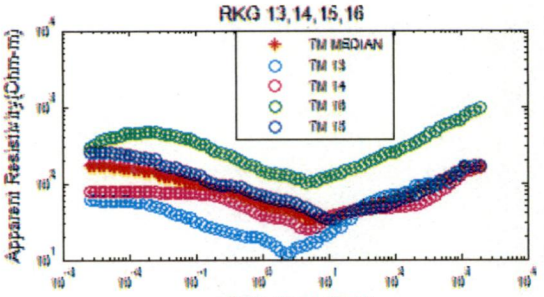
RKG 13,14,15,16
Apparent Resistivity(Ohm-m)
TM MEDIAN
TM 13
TM 14
TM 15
TM 16

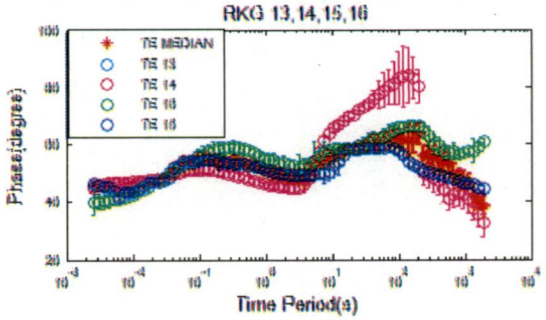
RKG 13,14,15,16
Phase(degree)
TE MEDIAN
TE 13
TE 14
TE 15
TE 16
Time Period(s)

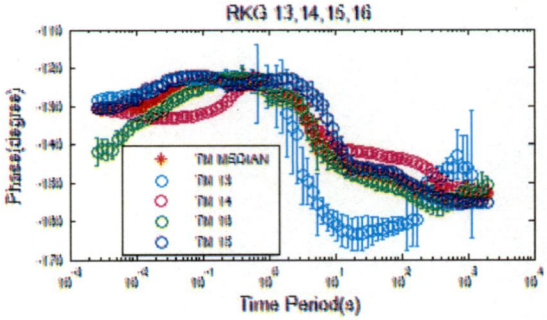
RKG 13,14,15,16
Phase(degree)
TM MEDIAN
TM 13
TM 14
TM 15
TM 16
Time Period(s)

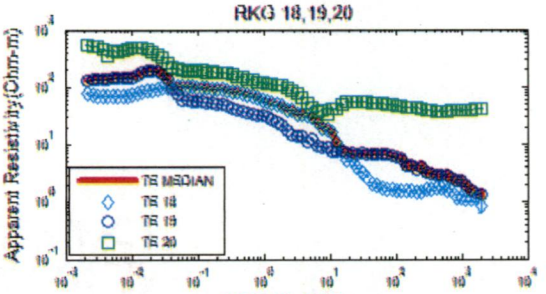
RKG 18,19,20
Apparent Resistivity(Ohm-m)
TE MEDIAN
TE 18
TE 19
TE 20

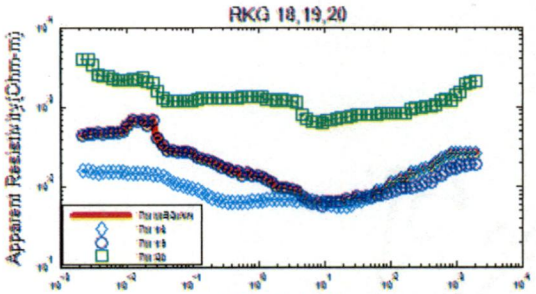
RKG 18,19,20
Apparent Resistivity(Ohm-m)

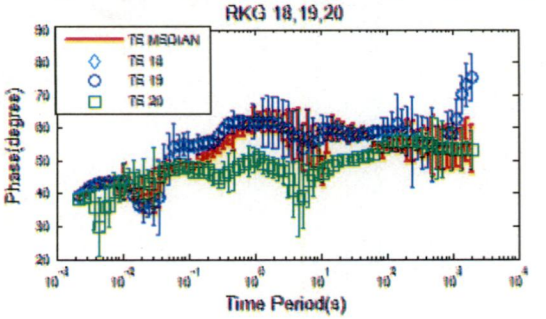
RKG 18,19,20
Phase(degree)
TE MEDIAN
TE 18
TE 19
TE 20
Time Period(s)

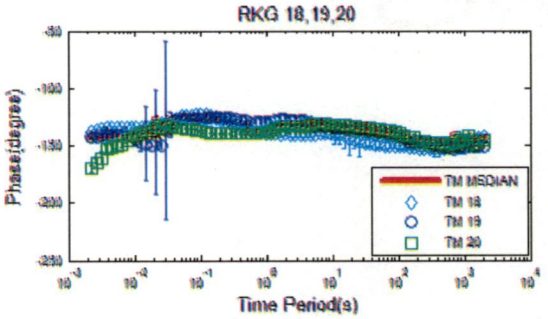
RKG 18,19,20
Phase(degree)
TM MEDIAN
TM 18
TM 19
TM 20
Time Period(s)

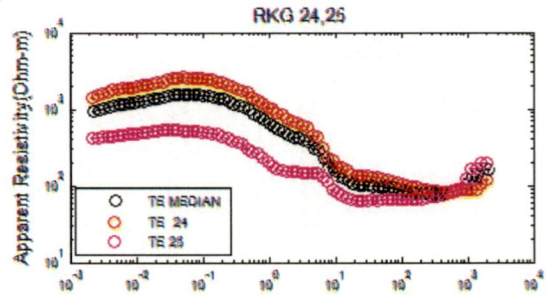
RKG 24,25
Apparent Resistivity(Ohm-m)
TE MEDIAN
TE 24
TE 25

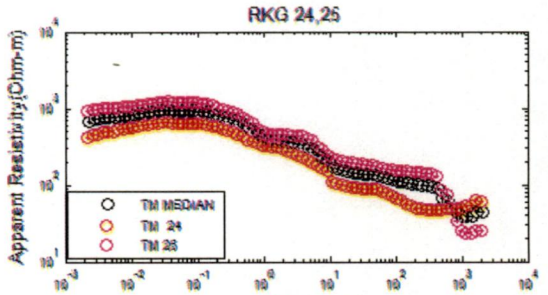
RKG 24,25
Apparent Resistivity(Ohm-m)
TM MEDIAN
TM 24
TM 25

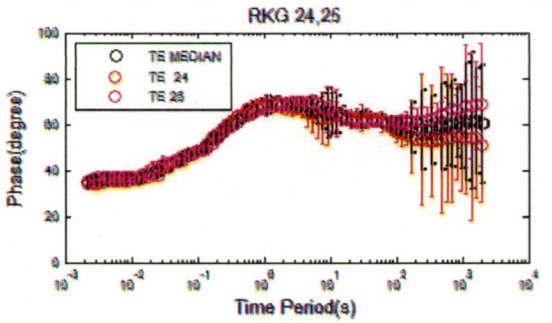
RKG 24,25
Phase(degree)
TE MEDIAN
TE 24
TE 25
Time Period(s)

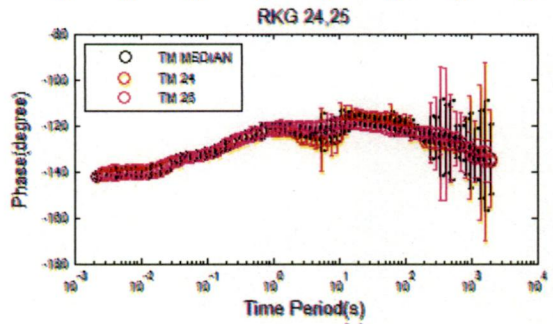
RKG 24,25
Phase(degree)
TM MEDIAN
TM 24
TM 25
Time Period(s)

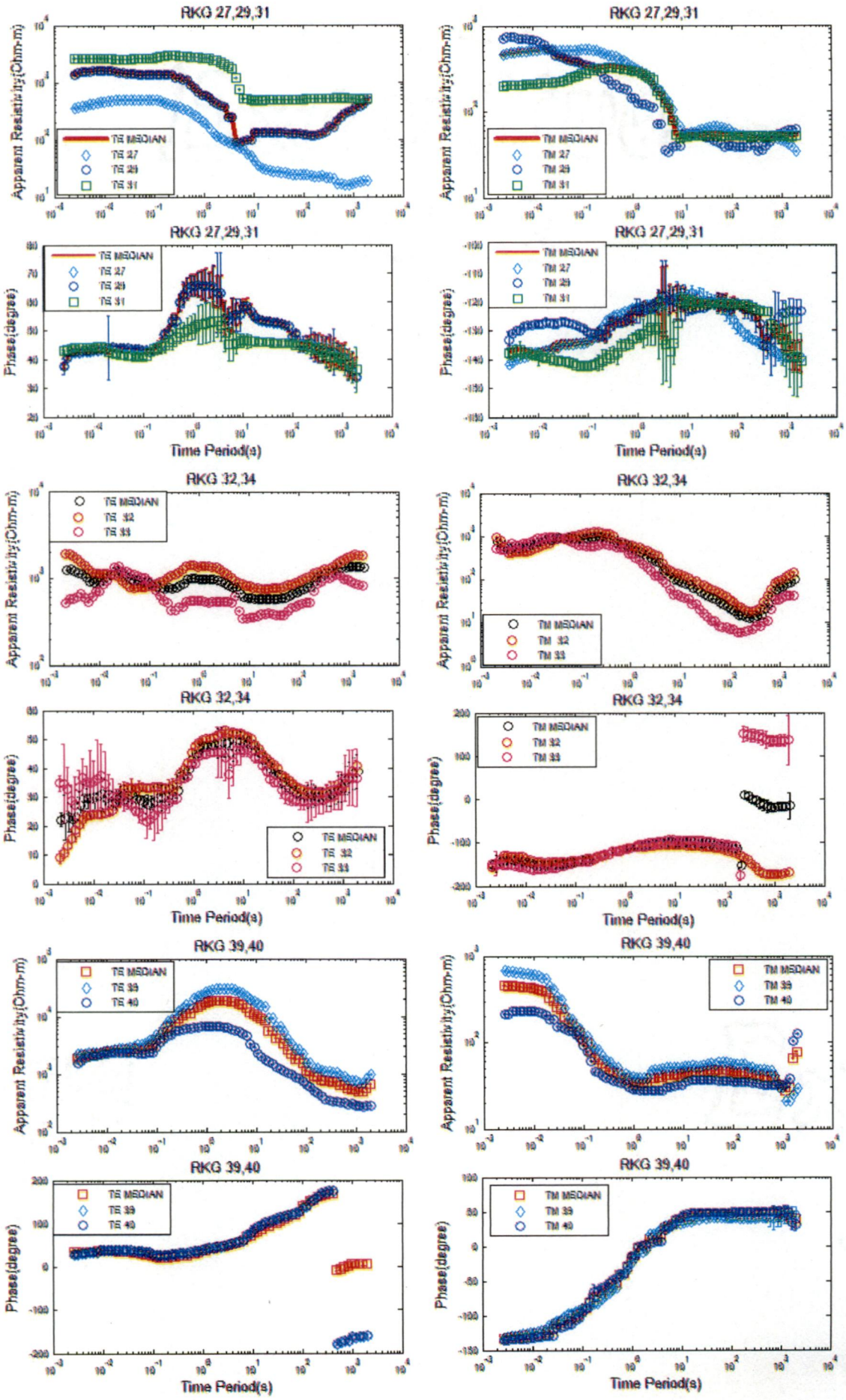
RKG 27,29,31
Apparent Resistivity(Ohm-m)
TE MEDIAN
TE 27
TE 29
TE 31
RKG 27,29,31
Apparent Resistivity(Ohm-m)
TM MEDIAN
TM 27
TM 29
TM 31
RKG 27,29,31
Phase(degree)
TE MEDIAN
TE 27
TE 29
TE 31
Time Period(s)
RKG 27,29,31
Phase(degree)
TM MEDIAN
TM 27
TM 29
TM 31
Time Period(s)
RKG 32,34
Apparent Resistivity(Ohm-m)
TE MEDIAN
TE 32
TE 33
RKG 32,34
Apparent Resistivity(Ohm-m)
TM MEDIAN
TM 32
TM 33
RKG 32,34
Phase(degree)
TE MEDIAN
TE 32
TE 33
Time Period(s)
RKG 32,34
Phase(degree)
TM MEDIAN
TM 32
TM 33
Time Period(s)
RKG 39,40
Apparent Resistivity(Ohm-m)
TE MEDIAN
TE 39
TE 40
RKG 39,40
Apparent Resistivity(Ohm-m)
TM MEDIAN
TM 39
TM 40
RKG 39,40
Phase(degree)
TE MEDIAN
TE 39
TE 40
Time Period(s)
RKG 39,40
Phase(degree)
TM MEDIAN
TM 39
TM 40
Time Period(s)

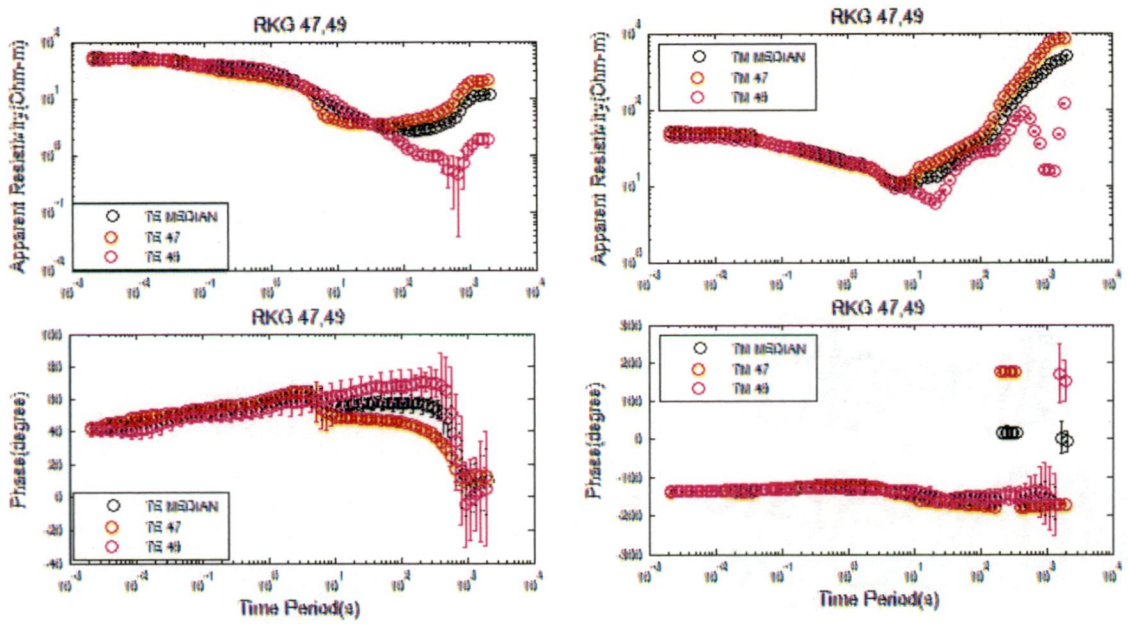

Fig.5. 28 Plotting of Median data with original data

5.13.22D Inversion of 35 sites median averaged data

All the 2D inversions carried out for 33 sites data (Processed by IIT Roorkee Group) , four sets of averaged data and 36 sites data (Processed by GERMC) were non-rotated ones. Inorder to match the co-ordinates of the measurement with the strike direction of the geoelectric structures, the data has been rotated N60^{0}W. This angle of rotation has been found out from the strike code software.

Inversion Parameters

17 Averaged (Median)Sites (0.01 – 2048s)	Modes	Error Floor		Initial RMS	Final RMS	No. of iterations	Weight Factors α=3, β =1
		Resistivity	Phase				
	TE	25	10	7.823	1.4316	80	Minimum Block dimensions 250H, 50V Tau for smoothing operator =10, Data Errors RHO -10, Phase -5
	TM	25	10	6.347	1.140	80	
	TE+TM	TE-25 TM -25	TE-10 TM -10	4.326	1.733	95	

Table 5.10 Showing information of inversion parameters for the 2D inversion of Median data (Processed by GERMC Group)

5.13.3Comparison of all modes of median data with reference model

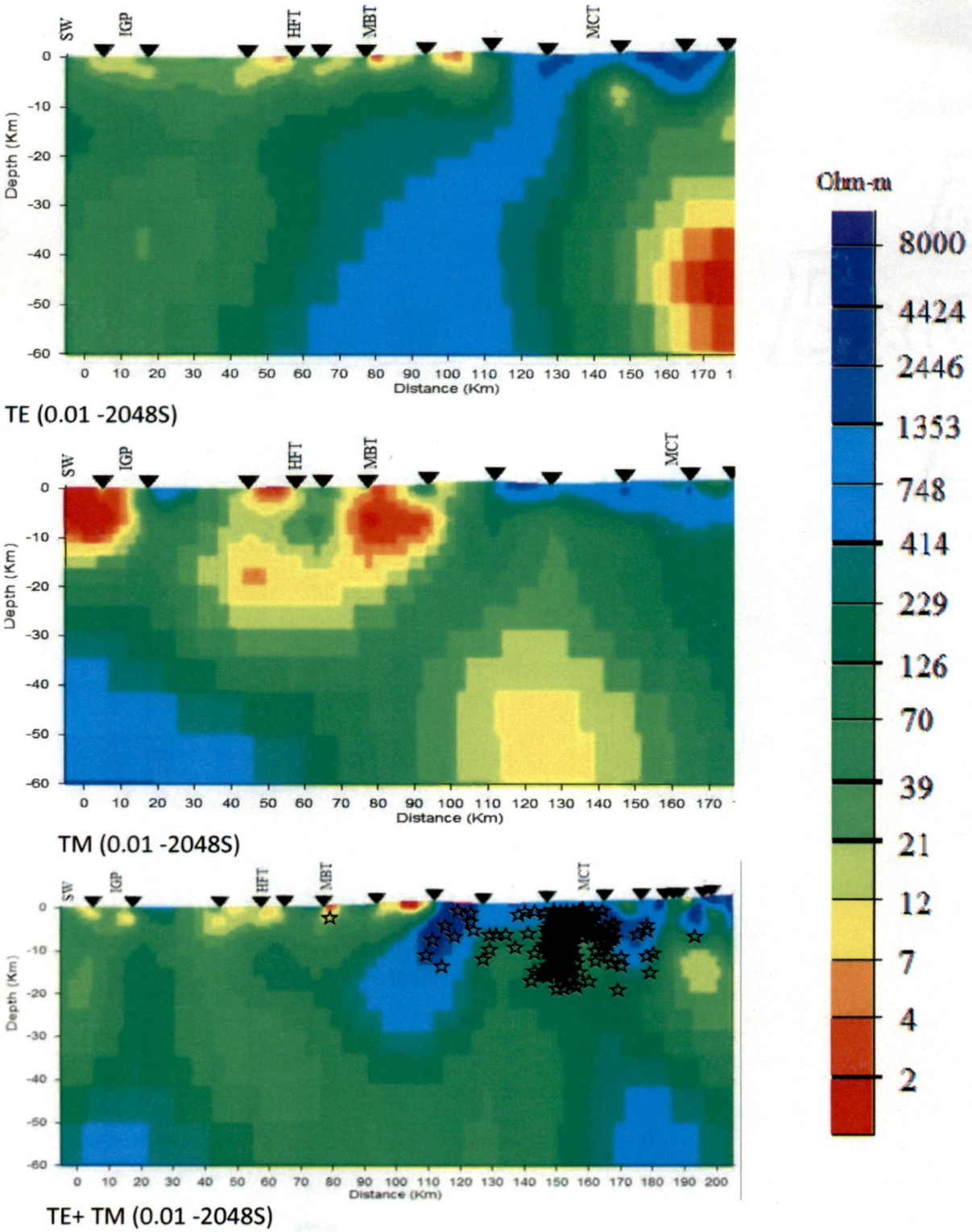

Fig.5.29 All rotated modes (TE, TM, TE+TM) of Median average data of 35 sites data processes by GERMC Group

5.13.4Results

The rotated TE mode model resolves the upper crustal resistivity information and very small scale conductive features close to the surface of the earth at the HFT and MBT region. But it is unable to resolve the conductive vertical channels in the resistive lithosphere and 3D small scale conductive structures and conductive elongated features of the IGP region. The difference between rotated and non-rotated TE model is in the case of non-rotated TE model, the TE model disturbs the conductive part of the IGP region more and provides the wrong position of the conductive features at the scaled depth. In the case of rotated TE model, no 3D small scale conductive features have been resolved but only 2 dimensional conductive small scale features has been clearly resolved at HFTand MBT without any distortions.

The rotated TM model detects both 2D elongated conductive features at HFT and MBT as well as 3D small scale features at the near surface of the IGP region. But the conductive features below the HFT and MBT have been shifted downwards as compared to reference model and non-rotated TM mode. The TM mode also resolves the conductive channels in the resistive part of the lithosphere at the depth of 40 t0 60 Km below the Higher Himalayan part. But in case of non-rotated TM model the vertical channel has been found at the depth 10 to 30Km. The comparison of rotated TM model with reference model shows there is a shift of the conductive channels downwards due to increase in galvanic distortions with depth.

The rotated Joint (TE+TM) Model resolves the small scale conductive features at the near surface of the earth but not well developed. It also does not give any information regarding the presence of conductive channels in the resistive lithosphere. But in the case of non-rotated Joint model we find the distortions of conductive features below the HFT and MBT region. This distortion has been removed by the rotated joint model.

The overall inversion results concludes that TE model resolves the near surface resistive features but it can not stop the distortion caused by 3D small scale conductive features and it can not resolve the conductive channel in the resistive lithosphere. But TM mode is robust to distortions effects caused by 3D small scale features at near surface earth. It also resolves the presence of conductivechannels in the resistive part. But it is not resistant to 3D effects caused by near surface resistive structures. Due to this complementary characteristics of TE and TMmode. the TE mode can be used to obtain the near surface resistive information and the TM mode can be used to obtain the conductive features at near surface as well as conductive channels in the resistive lithosphere.

(1) The analysis of models shows TM model provides better results than TE and Joint mode.
(2) The processing method used by GERMC has improved the data response.
(3) The averaging method helps in reducing the spreading of the data values. The analysis of different averaging method indicates that median method provides better results than all other methods used in this work.
(4) The analysis reveals the conductive structure lies in between 27 and 32 sites with depth 40km.
(5) Due to distortion the Joint mode shows shifting of the conductivity anomaly towards left.
(6) TE mode yields worst results due to inductive distortions at near surface structure.
(7) The TM mode is the suitable mode to produce models for the upper crustal part of the earth's subsurface.

REFERNCES

- Bahr, K., and Simpson,F., 2005, Practical magnetotellurics. In: Basic theoretical concepts, Planning a field campaign, Cambridge press. pp. 15 – 34,37 – 54.

- Berdichevsky, M.N., and Dmitriev, V.i., 2008, Models and methods of magnetotellurics.Geophysics. In: The magnetotelluricresponse function. Springer publisher, Muscow.pp. 3 -24.

- Berdichevsky, M.N., and Zhandov, M.S., 1984, Advanced theory of deep geomagnetic sounding, Elsevier, Amsterdam –Oxford –New York – Tokyo.
- Cagniard, L., 1953, Basic theory of the magnetotelluric method of geophysical prospecting. Geophysics 18: 605–645.

- Constable, S. C., Parker, R. L., and Constable, C. G., 1987, Occam's inversion: A practical algorithm for generating smooth models from EM sounding data. Geophysics 52: 289–300.

- DeGroot-Hedlin, C., and Constable, C.G., 1990, Occam's inversion: a practical algoritm for generating smooth models from electromagnetic sounding data, Geophysics 55, 1613–1624.

- Dosso, H. W., and Oldenburg, D. W., 1991,The similitude equation in magnetotelluric inversion. Geophys. J. Int. 106: 507–509.
- Egbert, G. D., and Booker, J. R., 1986,Robust estimation of geomagnetic transfer functions. Geophys. J. R. Astr. Soc. 87: 173–194.

- Filloux, J. H., 1973, Techniques and instrumentation for studies of natural electromagnetic induction at sea.Phys. Earth Planet. Inter. 7: 323–338.

- Filloux, J. H., 1987, Instrumentation and experimental methods for oceanic studies. In Geomagnetism, Volume 1, ed. J. A. Jacobs. London: Academic Press, pp. 143–248.

- Junge, A., 1990, A new telluric KCl probe using Filloux's Ag–AgCl electrode.Pure and Applied Geophysics 134: 589–598.

- Keller, G. V., and Frischknecht, F. C., 1966, Electrical methods in geophysical prospecting. In International Series ofMonographs in ElectromagneticWaves, 10, eds. A.L. Cullen, V. A. Fock, and J. R. Wait. Oxford: Pergammon Press.

- Parker, E. N., 1958, Dynamics of the interplanetary gas and magnetic field.Astrophys. J. 128: 664–676.

- Simpson, F., 2001b, Resistance to mantle flow inferred from the electromagnetic strike of the Australian upper mantle. Nature 412: 632–635.

- Smith, J.T., and Booker, J.R., 1991, Rapid Inversion of Two- and Three-dimensional MagnetotelluricData, J. Geophys.Res. **96**, 3905–3922.
- Tikhonov, A. N., 1950,The determination of the electrical properties of deep layers of the Earth's crust. Dokl. Acad. Nauk. SSR 73: 295–297 (in Russian).
- Tipler, P. A., 1991, Physics for Scientists and Engineers. New York: Worth Publishers.
- http://digital.library.adelaide.edu.au/dspace/bitstream/2440/48492/6/02chapters1-3.pdfDate of visit 15 April 2012
- http://en.wikipedia.org/wiki/Magnetotellurics Date of visit 14 April 2012
- http://oak.ucc.nau.edu/wittke/Tibet/Himalaya.html Date of visit 15 April 2012
- http://www.searchanddiscovery.com/documents/geophysical/christopherson/images/fig01.htm Date of visit 17 April 2012
- http://88.198.212.158/mtxweb/uploads/media/flyerADU-06_v1.pdfDate of visit 18 April 2012
- mtxgeo/images/brochures/FlyerEFP-06_v33.pdf Date of visit 18 April 2012
- http://178.63.62.205/mtxgeo/index.php/sensors/mfs-06e Date of visit 18 April 2012

A.1 Descriptions of Inversion parameters in WinGlink software

On the **inversion** menu, after selecting **setting,** we will get seven tabs. These are given below

(1) Main inversion parameters (2) Data select (3) Smooth inversion parameters (4) Error floor (5) Static shift (6) Data errors (7) Fixed parameters

A.1.1 Main inversion Parameters

In inversion algorithm, input data may be any combination of TE mode, TM mode or vertical transfer function. Before inverting the data masking is done to remove the unwanted data in the Pseudo-Section program.

In main parameters tab, we will find three options for the inversion

(i) Invert TM rho and phase data

(ii) Invert TE rho and phase data

(iii)Invert Hz transfer function

For sharp boundary inversion routine an error value is entered to terminate the inversion.

A.1.2 Data Select

Min Frequency – The lower frequency range of the observed curve is filled

Decades – It specifies the upper bound of the observed curve's frequency range on which fitting is tried. It is equal to Min Frequency.10^(Decades). In this work Decade 6 has been used.

Use Station Data – It compels the program to use the observed curve data samples. It takes long time for the calculation if the data points of the observed curves are not ordered in the frequency domain. In this case to cut the inversion time use interpolated data option is used.

Use Smoothed Curves - This forces the program to use the smoothed curves instead of edited curves.

A.1.3 Smooth inversion parameters

The Nonlinear conjugate gradient algorithm attempts to minimize an objective function that is the sum of the normalized data misfits and the smoothness of the model. The trade-off between data misfits and model smoothness is controlled by the regularization parameter tau. The NCLG algorithm does not try to automatically determine tau to reach a target misfit. Many experiments are made to run several inversions using different values of tau and the algorithm is run until convergence to determine what value of tau will give the smoothest model and the target misfit. It is possible with real field data that one would never be able to

reach the desired target misfit. In this case, one would want the tau that gives the smaller RMS error and the smoothest model. The following parameters are available to the user for inversion control.

Smoothest model or variations – The program solves for the smoothest model or the smoothest variations away from a starting model. Choosing smoothest variations is a useful way to do hypothesis testing for different model parameters or features.
Regularization Laplacian- It consists of two options (1) Uniform grid Laplacian (2) Standard Laplacian. The uniform grid Laplacian produces smoother model at the expense of smearing features both vertically and horizontally. The standard Laplacian may produce a rougher looking model but the definition of smoothness is consistent with the model dimensions.
Regularization Order – This option is used to minimize the gradients of the model or the Laplacian of the model. Variations of this parameter, equal or unequal grid Laplacian, and the smoothest model or the smoothest variations give the user a great deal of flexibility for generating different types of constraints on the inversion. Inthis work Laplacian smoothing option has been used.

Tau for smoothing operators - This is the regularization parameter which controls the trade-off between fitting the data and adhering to the model constraint. Larger values cause a smoother model at the expense of a worse data fit. Several experiments are run with changing the values of tau to find which provides good fitting as well as smoothest model. Values between 3 and 300 seem to be typical for most MT inversions and are good starting points. In this work tau value 10 has been chosen.

Weighting function - The first option specifies the αfactor to multiply horizontal derivatives. Recommended value is one if horizontal smoothness is not required. In this work α value 3 has been used.The second line specifies β value in weighting function. Recommended value is 3 for minimizing the Laplacian of the model and 1 for minimizing the gradient of the model. Zero value of β indicates no weightage to the regularization term. In this work β value 3 has been used. The third line specifies the minimum block dimensions to be used for computing the weightage function. These are specified in meters. These are useful for setting a transition from a depth-independent regularization in the shallow part of the model to a depth-dependent regularization in the deeper part of the model. Recommended values of block dimension lie in between 500 -1000. For zero value of block dimension, we get overly

rough in the shallow part for standard grid Laplacian, or overly smooth for uniform grid Laplacian.

Output sensitivity map – By selecting this option, the sensitivity map is obtained as output by the inversion routine at the final iteration, regardless of the preconditioner used. The diagonal part of $A^T R_{dd} A$ is output for each model parameter. This information can be used to determine those parts of the model that have the greatest sensitivity to that data and which parts of the model are relatively unimportant.

Save intermediate models – When this option is selected, the resistivity values calculated for each model iteration by the inversion code are stored in the database. The meshes can be viewed for any iteration after completion of the inversion. After that the mesh can be saved as a model at a given iteration number using save option.

A.1.4 Error floor

By selecting the Error floor tab, we will get the option for filling up the resistivity and phase error values for any combination of TE, TM and tipper mode. Recommended ration of resistivity and phase error is 1:0.29. For tipper data, the Error floor is an absolute magnitude that should optimally be chosen relative to the quality of the Hz estimates. A reasonable starting point is recommended as 0.01.

A.1.5 Static shift

Static shift is a galvanic distortion which is caused by charge accumulation at the conductive discontinuity. Due to static shift, we find the parallel shift of observed resistivity and phase value from the calculated value. This can be removed by clicking on the static shift tab. Static shift is associated with all modes. If all data is to be inverted with static shift then we have to select the invert for static shift check box. If selected stations are to be inverted with static shift, then we have to click on edit static shift tab.

Static shift applied to selected stations change their colours on the basis of any combination of TE, TM or joint mode.

None – Black

TE – Red

TM – Blue

TE and TM – Purple

Static shift settings

Invert for static shift – The program can optionally invert for static shifts of the TM and TE mode apparent resistivity. The static shift values are included as parameters in the inversion, and the datum is that the sum of the logarithmic of the static shifts should be zero.

Variance for constraint – The variance is the variance in the requirement that the log of the static shifts sum to zero. Values are entered in percentage, like 5 or 10. Larger values mean the zero sum constraint is less important.

Damping for constraint – The damping parameters damps the inversion so that large changes are not made to the static shifts on the first few numbers of iterations. This is mainly to fit the data as good as possible before allowing changes to the static shifts. After every three inversion iterations, the program reduces the damping value by a third. Thus static shift parameters gain in influence as the inversion progresses. In order to keep statics to remain fixed till later iterations, a large value like 1000 or 10000 is chosen. To keep the statics be changeable, a small value is entered. A value of zero for damping means that the statics are completely free to be changed.

A.1.6 Data errors

Use data errors if existing - This option is used to take the errors of the observed curves.

(TE/TM) Rho, Phase – If the above option is not checked or the observed curves have no errors, these are the default standard deviation errors to use.

A.1.7 Fixed Parameters

If the resistivities of some model cells have been blocked, the options are used in the fixed parameters to specify whether or not cell locking is to be used, and the parameter which specifies the amount which the fixed parameters may change over the course of the inversion.

Fixed Parameters – Model parameters can optionally be forced to remain fixed through the inversion.

For clamping fixed parameters – If the above option is chosen, then a tau value for the parameters fixed must be input.